Virtual Compton Scattering in Baryon Chiral Perturbation Theory

Dissertation
zur Erlangung des Grades
„Doktor der Naturwissenschaften"

am Fachbereich Physik, Mathematik und Informatik
der Johannes Gutenberg-Universität
in Mainz

Dalibor Djukanovic,
geboren in Mainz

Mainz, Juni 2008

Tag der mündlichen Prüfung: 11.07.2008

Abstract

This thesis is concerned with the calculation of virtual Compton scattering (VCS) in manifestly Lorentz-invariant baryon chiral perturbation theory to fourth order in the momentum and quark-mass expansion. In the one-photon-exchange approximation, the VCS process is experimentally accessible in photon electro-production $ep \to e'p'\gamma$ and has been measured at the MAMI facility in Mainz, at MIT-Bates, and at Jefferson Lab. Through VCS one gains new information on the nucleon structure beyond its static properties, such as charge, magnetic moments, or form factors. The nucleon response to an incident electromagnetic field is parameterized in terms of 2 spin-independent (scalar) and 4 spin-dependent (vector) generalized polarizabilities (GP). In analogy to classical electrodynamics the two scalar GPs represent the induced electric and magnetic dipole polarizability of a medium. For the vector GPs, a classical interpretation is less straightforward. They are derived from a multipole expansion of the VCS amplitude.

This thesis describes the first calculation of all GPs within the framework of manifestly Lorentz-invariant baryon chiral perturbation theory. Because of the comparatively large number of diagrams—100 one-loop diagrams need to be calculated—several computer programs were developed dealing with different aspects of Feynman diagram calculations. One can distinguish between two areas of development, the first concerning the algebraic manipulations of large expressions, and the second dealing with numerical instabilities in the calculation of one-loop integrals. In this thesis we describe our approach using Mathematica and FORM for algebraic tasks, and C for the numerical evaluations.

We use our results for real Compton scattering to fix the two unknown low-energy constants emerging at fourth order. Furthermore, we present the results for the differential cross sections and the generalized polarizabilities of VCS off the proton.

Zusammenfassung

Die vorliegende Dissertation befasst sich mit der Berechnung der virtuellen Compton-Streuung (VCS) in manifest Lorentz-invarianter baryonischer chiraler Störungstheorie bis zur vierten Ordnung in der Impuls- und Quarkmassenentwicklung. In der Einphotonaustauschnäherung ist der VCS-Prozess experimentell in der Photonelektroproduktion $ep \to e'p'\gamma$ zugänglich und wurde am Beschleuniger MAMI in Mainz, sowie am MIT-Bates und am Jefferson Lab gemessen. Durch VCS erhält man neue Informationen über die Struktur des Nukleons jenseits seiner statischen Eigenschaften wie Ladung, magnetisches Moment oder Formfaktoren. Das Verhalten des Nukleons unter dem Einfluss elektromagnetischer Felder wird durch 2 spinunabhängige (skalare) und 4 spinabhängige (vektorielle) generalisierte Polarisierbarkeiten (GP) parametrisiert. In Analogie zur klassischen Elektrodynamik lassen sich die 2 skalaren GPs als induzierte elektrische und magnetische Dipole deuten. Für die vektoriellen GPs ist eine klassische Interpretation deutlich schwieriger. Sie werden über eine Multipolentwicklung der VCS-Amplitude hergeleitet.
Diese Arbeit stellt die erste Berechnung aller GPs in manifest Lorentz-invarianter baryonischer chiraler Störungstheorie dar. Hierfür müssen 100 Einschleifendiagramme berechnet werden. Aufgrund der vergleichsweise großen Anzahl an Einschleifendiagrammen wurden im Rahmen dieser Arbeit verschiedene Computerprogramme zur Berechnung von Feynmandiagrammen entwickelt. Man kann hier zwei Entwicklungsstränge unterscheiden. Zum einen benötigen wir Computerprogramme zur algebraischen Manipulation großer Ausdrücke, zum anderen stellt sich das Problem von numerischen Instabilitäten bei der Berechnung der Einschleifenintegrale. Wir stellen in dieser Arbeit unsere Vorgehensweise dar, wobei für den algebraischen Teil Mathematica und FORM verwendet wurden, und der numerische Teil durch C-Programme realisiert wurde.
Wir benutzen unsere Ergebnisse für die reelle Compton-Streuung, um die beiden unbekannten Niederenergiekonstanten der vierten Ordnung zu bestimmen. Schließlich präsentieren wir unsere Resultate für die differentiellen Wirkungsquerschnitte und die generalisierten Polarisierbarkeiten für VCS am Proton.

Contents

Chapter 1

Introduction

There is a rich history of analyzing the nucleon structure by means of an electromagnetic probe. The deviation of the nucleon magnetic moment from the theoretical predictions of a point-like spin-$\frac{1}{2}$ particle, as seen in early experiments by Frisch and Stern [FS 33], indicates the composite nature of the nucleon. In later experiments by Hofstadter et al. [HBY 58] the internal structure of nucleons was investigated using electron-nucleon scattering. From the experiments one could deduce the electromagnetic form factors which, in the nonrelativistic limit, allow for an interpretation as the spatial distribution of charge and the magnetic moments inside the nucleon. In recent years the investigation of the nucleon structure at low energies has drawn much attention on the experimental as well as the theoretical side [DW 07].

Quantum chromodynamics (QCD) is by now the established gauge theory of the strong interactions and a lot of effort has been put forth in the quest of understanding the implications of QCD at very low energies. QCD itself is a remarkably beautiful theory, given its simplicity compared to the large variety of phenomena it ought to describe. There is, however, a caveat concerning the low-energy domain of QCD. Because the coupling constant of QCD grows with decreasing energy [GW 73, Pol 73] a perturbative treatment in terms of an expansion in the strong coupling is not possible. This led to an increasing activity in the field of effective field theories (EFT). Starting from the pioneering work by Weinberg [Wei 79], Gasser and Leutwyler introduced a consistent framework for the effective theory of QCD at very low energies [GL 84, GL 85] called chiral perturbation theory (χPT). The main ingredients in the construction of χPT are the underlying global symmetries of the strong interactions. QCD exhibits a chiral symmetry in the limit of massless quarks. Assuming this symmetry to be approximately realized in nature, one further analyzes the hadronic spectrum in the low-energy domain. The crucial observation here is that the pions have comparatively small masses. This can be explained by the assumption that the chiral symmetry of QCD is spontaneously broken, thus giving rise to *nearly* massless Goldstone bosons, the pions. Given the symmetry properties, the effective action is constructed in such a way that the symmetries of the effective and fundamental theory coincide. However the knowledge of global symmetries of QCD does not suffice to completely fix the low-energy EFT. The physical matrix elements are encoded in the Green functions calculable from

the Lagrangian of the EFT. Symmetries of the Lagrangian manifest themselves in terms of identities among different Green functions, which are called Ward identities. Thus the sum of all Ward identities represent the complete restrictions coming from symmetries. In χPT the Ward identities imply a promotion of the global symmetries of QCD to local ones, enhancing the restrictions of symmetries on the low-energy structure of the theory. Since χPT is an EFT the Lagrangian contains an infinite number of interaction terms. Weinberg proposed a method to ascribe the degree of importance to certain diagrams contributing to a given physical matrix element, the so called Weinberg power counting. In contrast to the strong coupling constant of QCD the interaction between pions becomes weaker at low energies, therefore the perturbation series is organized as an expansion in small momenta of pions and the quark masses. The formulation of Gasser and Leutwyler was first applied to the sector of pseudoscalar mesons and later extended to the case of meson-baryon interactions [GSS 88]. The extensions to the baryonic sector proved to be rather involved, as the straightforward generalization of the power counting did not work as expected. Subsequently different methods were developed for the description of meson-baryon reactions. Among the first formulations, heavy-baryon chiral perturbation theory (HBχPT) gained most success as a consistent framework for the description of meson-baryon interactions [JM 91, Ber+ 92, EM 96]. HBχPT is constructed similarly to heavy-quark effective theory. The nucleon field is divided into heavy and light components, where the heavy components are integrated out. Subsequently the nonlocal contributions generated by integrating out the heavy components are expanded in local interaction terms suppressed with powers of the nucleon mass. This essentially amounts to an expansion of the relativistic Lagrangian in inverse powers of the nucleon mass. In the late 90's new manifestly Lorentz-invariant formulations of baryonic chiral perturbation theory (BχPT) have been developed [ET 98, BL 99, GJ 99, Goi+ 01, Fuc+ 03, SGS 04]. These formulations use appropriate renormalization schemes to restore the power counting in the baryonic sector. In this thesis we use the infrared regularization scheme by Becher and Leutwyler [BL 99] in its reformulated version of [SGS 04].

We use χPT to investigate the low-energy structure of QCD in electromagnetic reactions of nucleons. Electromagnetic interactions are particularly useful for the examination of QCD, since we use the cleanest possible probe, the electron. The interactions of electrons are described by QED, which is by far the best-tested quantum field theory. Because the electron is a point-like particle it does not exhibit any internal structure effects. The nucleon is, in contrast to the electron, a composite object. This composite structure manifests itself in an excitation spectrum, and we can describe nucleons by their response to electromagnetic probes, parameterized by form factors or polarizabilities. These observables are intimately connected to the dynamics of the constituents making up the nucleon, the quarks. Therefore the measurement of quantities such as form factors or polarizabilities reveals the properties of QCD at low energies. Particularly we are interested in information on the structure of the nucleon, beyond the information gained by form factor measurements. With the advent of coincidence techniques Compton scattering off the proton became an experimentally feasible tool for the investigation of the nucleon structure.

In Compton scattering the nucleon response is parameterized by the nucleon polarizabilities. In classical electrodynamics a medium containing freely moving charges acquires a polarization if exposed to an external electromagnetic field. The degree of polarizability is a measure of the rigidity. The induced electric dipole moment $\vec{P}$ is due to a deformation of the charge distribution and is proportional to the strength of the applied electric field

$$\vec{P} = \alpha \vec{E}. \tag{1.1}$$

The constant of proportionality is called electric polarizability. Correspondingly, the induced magnetic dipole moment is related via the magnetic polarizability β to the strength of the magnetic field $\vec{B}$. Since the nucleon has spin degrees of freedom the Compton scattering amplitude is parameterized by 6 invariant amplitudes. In addition to the two spin-independent (scalar) polarizabilities α and β, four more polarizabilities exist [Rag 93, Rag 94]. These vector polarizabilities characterize the spin-flip transition amplitudes, and in the classical analogy describe the interactions of an electromagnetic field with a permanent magnetic dipole that has internal structure. The polarizabilities attributed to different types of interactions of the nucleon with the electromagnetic field can be written in an effective phenomenological Hamiltonian illustrating the classical interpretation. For example the electric and magnetic polarizabilities correspond to the following effective Hamiltonian

$$H = \frac{1}{2}\alpha \vec{E}^2 + \frac{1}{2}\beta \vec{B}^2. \tag{1.2}$$

Making the incoming photon virtual, one gains information about the spatial distribution of polarization, very similar to the situation for the form factors. In analogy to the real Compton scattering (RCS) case, one can introduce polarizabilities parameterizing the structure information of the nucleon. In [GLT 95] the virtual Compton scattering (VCS) process was parameterized using generalized polarizabilities (GP). The VCS process is experimentally accessible in the photon electro-production process $ep \to e'p'\gamma$. The most recent data from laboratories in Mainz (MAMI), MIT-Bates and Newport News (Jefferson Lab) are of high quality and allow for a test of theoretical predictions.

There are a lot of theoretical predictions for Compton scattering including a wide variety of approaches, e.g. constituent quark model [DR 84] , the MIT bag model [Sch+ 84], the Skyrme model [SM 92], linear sigma model [MD 96], dispersion theory [Pas+ 00], and heavy-baryon chiral perturbation theory [Ber+ 93, Hem+ 97a, Hem+ 97b, Hem+ 98, Hem+ 00, GHM 00, VKMB 00, BHM 03]. The leading-order HBχPT calculations in [Hem+ 97a] indicated a good description of the scalar electric and magnetic polarizability, nearly reproducing the experimental values. Subsequent calculations of the next-to-leading order effects yielded large corrections, casting serious doubts about the convergence of the chiral expansion. This work provides the first complete fourth-order calculation of all GPs in the framework of relativistic BχPT.

This thesis is organized as follows. In Chapter 2 we give a short introduction to chiral perturbation theory. To that end we introduce the QCD Lagrangian and

discuss its symmetry properties. Furthermore we present the Lagrangians necessary for the calculations in this work. Chapter 3 discusses details of the VCS process. This concerns in particular the kinematics, the definition of the genuine VCS process and the definition of physical observables. A short introduction to the concept of GPs is also given in this chapter. Moreover we give the definitions of all quantities, which have been calculated in this thesis. Technical details of the calculation are discussed in Chapter 4. Here we summarize the most problematic parts of our calculation, concerning in particular the problems arising for the 100 one-loop diagrams. We outline our approach, with the emphasis on a discussion of the use of computer programs. To that end we describe our implementations as well as modifications to existing programs. The results are collected in Chapter 5. We compare our theoretical predictions with experimental data and previous calculations in the framework of HBχPT. Finally, in Chapter 6 we give a conclusion and an outlook for future investigations.

Chapter 2

QCD and chiral perturbation theory

Within the Standard Model of particle physics the strong interactions between quarks and gluons is described by quantum chromodynamics (QCD). The low-energy properties of QCD are governed by a chiral symmetry and the effective field theory describing the physics of these degrees of freedom that are relevant in this domain is called chiral perturbation theory (χPT).

Effective field theories (EFT) have become a successful tool in quantum field theoretical calculations. In the construction of EFTs one takes advantage of the often present separation of scales, thus if one is interested in physics taking place well below a certain scale Λ one constructs a theory well suited for processes below this scale only. There are two approaches in the construction of an EFT. The first one could be called a top down approach, where we know the fundamental theory but calculations turn out to be cumbersome. In this case we can cast the contributions of particles much heavier than the scale of the problem we are interested in, into local effective interactions. This amounts to a modification of the high-energy behavior of the fundamental theory. In technical terms we integrate out the heavy modes and perform an operator product expansion (OPE), so that we end up with a local field theory containing only the relevant degrees of freedom and additional local effective interaction terms generated by the OPE. The additional interaction terms are suppressed with powers of the large scale Λ, therefore for processes much below this scale one needs only a limited number of additional effective interactions. The expansion coefficients of the OPE can be calculated from the fundamental theory, which amounts to a matching of both theories at some intermediate scale, where one can expect both descriptions to work reasonably well. There are a lot of examples of EFT's employing the above reasoning such as Fermi-theory or heavy quark effective theory.

The second method of constructing an EFT relies solely on the symmetry properties of the fundamental theory. In this approach one constructs an effective action such that all symmetries of the effective action coincide with the symmetries of the fundamental theory. The particle content and the dynamics of the fields of the fundamental theory is not invoked in the construction of the EFT. χPT is an example

of an EFT constructed in this way, i.e. based only on the symmetry properties of QCD.

In light of the above discussion this chapter introduces the Lagrangian of QCD and its symmetries. Furthermore we present the Lagrangians of the mesonic and baryonic sectors of χPT relevant for this work. We closely follow the extensive introduction to χPT in [Sch 03].

2.1 QCD

QCD is a non-Abelian gauge theory with a color SU(3) gauge group describing the interactions of quarks and gluons. In addition the quarks come in six different flavors called up (u), down (d), strange (s), charm (c), bottom (b) and top (t). Besides the different masses associated with each flavor, the dynamics of QCD is not affected by flavor.

The QCD Lagrangian is given by

$$\mathcal{L}_{\mathrm{QCD}} = \sum_f \bar{q}_f (i \not{D} - m_f) q_f - \frac{1}{4} \mathcal{G}_{\mu\nu,a} \mathcal{G}_a^{\mu\nu}. \tag{2.1}$$

The quark fields q_f are color triplets (r(ed), g(reen) and b(lue))

$$q_f = \begin{pmatrix} q_{f,r} \\ q_{f,g} \\ q_{f,b} \end{pmatrix}, \tag{2.2}$$

where f denotes the flavor index. The covariant derivative containing the gauge potential $\mathcal{A}_{\mu,a}$ describing the gluons is given by

$$D_\mu \begin{pmatrix} q_{f,r} \\ q_{f,g} \\ q_{f,b} \end{pmatrix} = \partial_\mu \begin{pmatrix} q_{f,r} \\ q_{f,g} \\ q_{f,b} \end{pmatrix} - ig \sum_{a=1}^{8} \frac{\lambda_a}{2} \mathcal{A}_{\mu,a} \begin{pmatrix} q_{f,r} \\ q_{f,g} \\ q_{f,b} \end{pmatrix}, \tag{2.3}$$

where λ_a are the Gell-Mann matrices obeying the commutation relations

$$\left[\lambda_a, \lambda_b\right] = 2i f_{abc} \lambda_c, \quad (a,\, b,\, c = 1, \ldots, 8).$$

Finally the field strength tensor reads

$$\mathcal{G}_{\mu\nu,a} = \partial_\mu \mathcal{A}_{\nu,a} - \partial_\nu \mathcal{A}_{\mu,a} + g f_{abc} \mathcal{A}_{\mu,b} \mathcal{A}_{\nu,c}. \tag{2.4}$$

The only free parameters in the Lagrangian of Eq. (2.1) are the six quark masses m_f and the strong coupling constant g. The quark masses exhibit a hierarchy pattern with the masses of u, d, and s being much smaller than the ones of c, b and t [Yao+ 06],

$$\begin{pmatrix} m_u = (0.0015 - 0.003)\,\mathrm{GeV} \\ m_d = (0.003 - 0.007)\,\mathrm{GeV} \\ m_s = (0.95 \pm 0.25)\,\mathrm{GeV} \end{pmatrix} \ll 1\,\mathrm{GeV} \leq \begin{pmatrix} m_c = 1.25\,\mathrm{GeV} \\ m_b = (4.2 - 4.7)\,\mathrm{GeV} \\ m_t = 174\,\mathrm{GeV} \end{pmatrix}. \tag{2.5}$$

In contrast to the Abelian case of QED the squared field strength tensor of the QCD Lagrangian in Eq. (2.1) gives rise to self interactions among gluons involving vertices of three gluons with strength g and a four gluon vertex with strength g^2.

From the point of view of gauge invariance the strong-interaction Lagrangian could also involve a term of the type

$$\mathcal{L}_\theta = \frac{g^2\bar{\theta}}{64\pi^2}\epsilon^{\mu\nu\rho\sigma}\sum_{a=1}^{8}\mathcal{G}^a_{\mu\nu}\mathcal{G}^a_{\rho\sigma}, \tag{2.6}$$

where $\epsilon_{\mu\nu\rho\sigma}$ denotes the totally antisymmetric Levi-Cività tensor. This so-called θ-term violates P and CP symmetry, however since experiments indicate that contributions violating P and CP are negligible, i.e. $\bar{\theta}$ is very small, we use the P- and CP- invariant Lagrangian of Eq. (2.1) in this work.

2.1.1 Massless QCD

Bearing the hierarchy of the quark masses in Eq. (2.5) in mind let us consider, as a first approximation, the theoretical limit in which the masses of u, d and s are sent to zero[1] and the masses of c, b and t are sent to infinity. In Leutwyler' s terminology this limit represents a *theoretical paradise*, as there are no dimensionless couplings and all transition probabilities of physical interest are unambiguously determined by the Lagrangian[2]. The QCD Lagrangian in this limit reads

$$\mathcal{L}^0_{\mathrm{QCD}} = \sum_{l=u,d,s}\bar{q}_l i\not{D}\, q_l - \frac{1}{4}\mathcal{G}_{\mu\nu,a}\mathcal{G}^{\mu\nu}_a. \tag{2.7}$$

Note that the covariant derivative $\not{D}\, q_l$ acts on color and Dirac indices only, but is independent of flavor. In order to see the symmetry properties of $\mathcal{L}^0_{\mathrm{QCD}}$ let us first define the chirality projectors $P_{R/L}$

$$P_R = \frac{1}{2}(1+\gamma_5) = P_R^\dagger, \quad P_L = \frac{1}{2}(1-\gamma_5) = P_L^\dagger, \tag{2.8}$$

where the indices R and L refer to right-handed and left-handed, respectively. The following properties are easily verified using the definitions in Eq. (2.8)

$$\begin{aligned} P_R + P_L &= 1, \\ P_R^2 = P_R, \quad P_L^2 &= P_L, \\ P_R P_L = P_L P_R &= 0. \end{aligned} \tag{2.9}$$

The projectors acting on the quark fields single out the right-handed and left-handed components of the quark fields, respectively,

$$q_R = P_R\, q, \quad q_L = P_L\, q. \tag{2.10}$$

[1] For reasons that will be obvious later this limit is referred to as the chiral limit.

[2] This is true since the strong coupling g can be related to an intrinsic scale (Λ_{QCD}) and all momenta can be expressed within units of this scale.

Using the properties of $P_{R/L}$ in Eq. (2.9) the Lagrangian in Eq. (2.7) can be written as

$$\mathcal{L}^0_{\rm QCD} = \sum_{l=u,d,s} (\bar{q}_{R,l} i\not{D}\, q_{R,l} + \bar{q}_{L,l} i\not{D}\, q_{L,l}) - \frac{1}{4}\mathcal{G}_{\mu\nu,a}\mathcal{G}^{\mu\nu}_a. \tag{2.11}$$

One clearly sees that the right-handed and left-handed components of the quark fields decouple in the massless limit of QCD. The Lagrangian $\mathcal{L}^0_{\rm QCD}$ is invariant under independent U(3) global transformations of the left-handed and right-handed components,

$$\begin{aligned}
\begin{pmatrix} u_L \\ d_L \\ s_L \end{pmatrix} &\mapsto U_L \begin{pmatrix} u_L \\ d_L \\ s_L \end{pmatrix} = \exp\left(-i\sum_{a=1}^{8}\Theta^L_a \frac{\lambda_a}{2}\right) e^{-i\Theta^L} \begin{pmatrix} u_L \\ d_L \\ s_L \end{pmatrix}, \\
\begin{pmatrix} u_R \\ d_R \\ s_R \end{pmatrix} &\mapsto U_R \begin{pmatrix} u_R \\ d_R \\ s_R \end{pmatrix} = \exp\left(-i\sum_{a=1}^{8}\Theta^R_a \frac{\lambda_a}{2}\right) e^{-i\Theta^R} \begin{pmatrix} u_R \\ d_R \\ s_R \end{pmatrix}.
\end{aligned} \tag{2.12}$$

The full symmetry group of the Lagrangian is $\mathrm{U}(3)_L \times \mathrm{U}(3)_R$, which can be decomposed as the product of

$$S = \mathrm{SU}(3)_L \times \mathrm{SU}(3)_R \times \mathrm{U}(1)_V \times \mathrm{U}(1)_A. \tag{2.13}$$

Using Noether's theorem one can derive conserved currents associated to the above transformations

$$\begin{aligned}
L^{\mu,a} &= \bar{q}_L \gamma^\mu \frac{\lambda^a}{2} q_L, \quad \partial_\mu L^{\mu,a} = 0, \\
R^{\mu,a} &= \bar{q}_R \gamma^\mu \frac{\lambda^a}{2} q_R, \quad \partial_\mu R^{\mu,a} = 0.
\end{aligned} \tag{2.14}$$

Instead of these chiral currents one often uses linear combinations,

$$V^{\mu,a} = R^{\mu,a} + L^{\mu,a} = \bar{q}\gamma^\mu \frac{\lambda^a}{2} q, \tag{2.15}$$

$$A^{\mu,a} = R^{\mu,a} - L^{\mu,a} = \bar{q}\gamma^\mu\gamma_5 \frac{\lambda^a}{2} q, \tag{2.16}$$

transforming under parity as vector and axial-vector current densities, respectively,

$$P : V^{\mu,a}(\vec{x},t) \mapsto V^a_\mu(-\vec{x},t), \tag{2.17}$$

$$P : A^{\mu,a}(\vec{x},t) \mapsto -A^a_\mu(-\vec{x},t). \tag{2.18}$$

One also obtains a conserved singlet vector current resulting from a transformation of all left-handed and right-handed quark fields by the *same* phase,

$$V^\mu = \bar{q}_R\gamma^\mu q_R + \bar{q}_L\gamma^\mu q_L = \bar{q}\gamma^\mu q, \quad \partial_\mu V^\mu = 0. \tag{2.19}$$

The singlet axial-vector current,

$$A^\mu = \bar{q}_R\gamma^\mu q_R - \bar{q}_L\gamma^\mu q_L = \bar{q}\gamma^\mu\gamma_5 q, \tag{2.20}$$

originates from a transformation of all left-handed quark fields with one phase and all right-handed with the *opposite* phase. From the conserved currents one easily derives conserved charges $Q^a_{V/A}$ which generate the symmetry group S.

The symmetry with respect to $\mathrm{SU}(3)_L \times \mathrm{SU}(3)_R$ is called chiral symmetry, this explains why the massless limit of QCD is referred to as the chiral limit. The $\mathrm{U}(1)_V$ is related to baryon number conservation. At the quantum level the Abelian anomaly is responsible for the $\mathrm{U}(1)_A$ not being a symmetry of $\mathcal{L}^0_{\mathrm{QCD}}$. This can be seen by explicitly calculating the divergence of the corresponding axial singlet current

$$\partial_\mu A^\mu = \frac{3g^2}{32\pi^2}\epsilon_{\mu\nu\rho\sigma}\mathcal{G}^{\mu\nu}_a\mathcal{G}^{\rho\sigma}_a.$$

Taking these considerations into account we have 9 conserved vector charges Q^0_V, $\ldots$, Q^8_V and 8 conserved axial charges $Q^1_A, \ldots, Q^8_A$ generating the group

$$G = \mathrm{SU(3)_R} \times \mathrm{SU(3)_L} \times \mathrm{U(1)_V}. \tag{2.21}$$

As was shown by Vafa and Witten [VW 84], the ground state of QCD is necessarily invariant under the subgroup generated by the vector charges. For the axial charges, however, there are two possibilities:

1. $Q^a_A|0\rangle = 0$: The ground state is invariant under chiral rotations, and the symmetry is realized in the so-called Wigner-Weyl mode. The spectrum consists of degenerate multiplets that transform irreducibly under the full symmetry group S and thus contain degenerate states of opposite parity.

2. $Q^a_A|0\rangle \neq 0$: The ground state is not invariant under the full symmetry group. S is realized in the so-called Nambu-Goldstone mode. This phenomenon is called spontaneous breakdown of a symmetry and the spectrum of the theory consists of the multiplets of the subgroup $H = \mathrm{SU(3)_V} \times \mathrm{U(1)_V}$ which leaves the vacuum invariant. In this case the axial charges acting on the ground state $Q_A|0\rangle$ generate multiplets, which carry the same energy and momentum as the ground state, giving rise to a multiplet of massless particles, the so-called Goldstone bosons.

The experimental situation strongly implies that the second case is realized. Therefore we conclude that QCD in the massless limit is, on the classical level, invariant under the symmetry group $S = \mathrm{SU(3)_R} \times \mathrm{SU(3)_L} \times \mathrm{U(1)_V} \times \mathrm{U(1)_A}$, where the $\mathrm{U(1)_A}$ is subject to an anomaly and does not survive quantization and the chiral symmetry $C = \mathrm{SU(3)_R} \times \mathrm{SU(3)_L}$ is spontaneously broken to the subgroup $C' = \mathrm{SU(3)_V}$. The number of generators of the chiral symmetry is $n_C = 16$ whereas the number of the generators of the group C' is $n_{C'} = 8$. Therefore, according to the Goldstone theorem, we expect $n_C - n_{C'} = 8$ massless Goldstone bosons. In fact the spectrum of QCD contains eight pseudoscalar mesons having comparatively small, but non-vanishing masses, namely kaons, pions, and etas.

2.1.2 Explicit symmetry breaking in QCD

So far we have considered the massless limit of QCD. Of course in nature the quarks have non-vanishing masses, which break the chiral symmetry explicitly as the Lagrangian contains a term

$$\mathcal{L}_M = -\bar{q}Mq = -(\bar{q}_R M q_L + \bar{q}_L M q_R), \tag{2.22}$$

where M is the quark mass matrix given by

$$M = \begin{pmatrix} m_u & 0 & 0 \\ 0 & m_d & 0 \\ 0 & 0 & m_s \end{pmatrix}. \tag{2.23}$$

This gives rise to additional contributions to the divergences of the vector and axial-vector currents

$$\begin{aligned} \partial_\mu V^{\mu,a} &= i\bar{q}\big[M, \frac{\lambda_a}{2}\big]q, \\ \partial_\mu A^{\mu,a} &= i\left(\bar{q}_L\{\frac{\lambda_a}{2}, M\}q_R - \bar{q}_R\{\frac{\lambda_a}{2}, M\}q_L\right) = i\bar{q}\{\frac{\lambda_a}{2}, M\}\gamma_5 q, \\ \partial_\mu V^{\mu} &= 0, \\ \partial_\mu A^{\mu} &= 2i\bar{q}M\gamma_5 q + \frac{3g^2}{32\pi^2}\epsilon_{\mu\nu\rho\sigma}\mathcal{G}_a^{\mu\nu}\mathcal{G}_a^{\rho\sigma}, \end{aligned} \tag{2.24}$$

where the axial anomaly is taken into account as well. As the divergences are proportional to the quark masses, we conclude that for small quark masses chiral symmetry is an approximate symmetry of QCD. Note that in the case of equal quark masses for u,d and s the quark mass matrix is proportional to the identity matrix, thus the eight vector currents are still conserved in accordance with the eightfold way introduced by Gell-Mann and Ne'eman [GMN 64].

2.2 Chiral Ward identities

In quantum field theory the objects we are mostly concerned with are vacuum expectation values of time ordered products of operators, the so-called Green functions. The Green functions are related to physical transition amplitudes via the Lehmann-Symanzik-Zimmermann formalsim (LSZ) [LSZ 55]. As will be shown below the symmetry properties of the theory impose relations among different Green functions.

As an example of a Green function and the consequences emerging from symmetries let us first take a look at the vacuum expectation value involving an axial-vector current and a pseudoscalar density

$$\begin{aligned} G_{AP}^{\mu,ab}(x,y) &= \langle 0|T[A_a^\mu(x)P_b(y)]|0\rangle \\ &= \Theta(x_0-y_0)\langle 0|A_a^\mu(x)P_b(y)|0\rangle + \Theta(y_0-x_0)\langle 0|P_b(y)A_a^\mu(x)|0\rangle, \end{aligned}$$

(2.25)

where the axial-vector current (see Eq. (2.16)) and the pseudoscalar density are defined as

$$A^{\mu,a} = \bar{q}\gamma^\mu\gamma_5\frac{\lambda^a}{2}q,$$
$$P_a = i\bar{q}\gamma_5\lambda_a q.$$

The time ordering has been made explicit using the Heavyside function Θ with the properties

$$\Theta(x) = \begin{cases} 1 & \text{, for } x > 0 \\ 0 & \text{, for } x \leq 0 \end{cases}.$$

Let us take the divergence of the above Green function

$$\begin{aligned}
&\partial_\mu^x G_{AP}^{\mu,ab}(x,y) \\
&= \delta(x_0-y_0)\langle 0|A_0^a(x)P_b(y)|0\rangle - \delta(x_0-y_0)\langle 0|P_b(y)A_0^a(x)|0\rangle \\
&\quad +\Theta(x_0-y_0)\langle 0|\partial_\mu^x A_a^\mu(x)P_b(y)|0\rangle + \Theta(y_0-x_0)\langle 0|P_b(y)\partial_\mu^x A_a^\mu(x)|0\rangle \\
&= \delta(x_0-y_0)\langle 0|[A_0^a(x),P_b(y)]|0\rangle + \langle 0|T[\partial_\mu^x A_a^\mu(x)P_b(y)]|0\rangle,
\end{aligned}$$

where we made use of $\partial_\mu^x\Theta(x_0-y_0) = \delta(x_0-y_0)g_{0\mu} = -\partial_\mu^x\Theta(y_0-x_0)$. Note that the derivative acting on Θ generates an equal-time commutator. The divergence of the axial-vector current vanishes in the case of an exact symmetry, whereas the equal time commutator in the first part is in general different from zero and depends on the underlying symmetries. The equal-time commutation relations of the quark fields in the Heisenberg picture are given by

$$\{q_{\alpha,r}(\vec{x},t), q_{\beta,s}^\dagger(\vec{y},t)\} = \delta^3(\vec{x}-\vec{y})\delta_{\alpha\beta}\delta_{rs}, \tag{2.26}$$
$$\{q_{\alpha,r}(\vec{x},t), q_{\beta,s}(\vec{y},t)\} = 0, \tag{2.27}$$
$$\{q_{\alpha,r}^\dagger(\vec{x},t), q_{\beta,s}^\dagger(\vec{y},t)\} = 0, \tag{2.28}$$

where α and β are Dirac indices and r and s flavor indices, respectively. Using these relations and the explicit expression for $A_0^a(x)$ and $P_b(y)$ the commutator reads

$$[A_0^a(\vec{x},t), P_b(\vec{y},t)] = \delta^3(\vec{x}-\vec{y})if_{abc}S_c(\vec{x},t),$$

where

$$S_a(x) = \bar{q}(x)\lambda_a q(x).$$

As the symmetry in our case is only approximate the divergence of the axial-vector current gives a non vanishing contribution and for the considered Green function we obtain

$$\partial_\mu^x G_{AP}^{\mu,ab}(x,y) = \delta^4(x-y)if_{abc}\langle 0|S_c(x)|0\rangle$$

$$+i\langle 0|T[\bar{q}(x)\{\frac{\lambda_a}{2},M\}\gamma_5 q(x)P_b(y)]|0\rangle. \tag{2.29}$$

In the above derivation we have made use of a naive time ordering T which is not covariant, however in the calculation of the commutator we have omitted the so-called Schwinger term containing an additional derivative on the δ function. Both effects cancel in our case, thus leading to a correct result. We have seen that symmetry arguments relate the divergence of a Green function containing an axial-vector current to some linear combination of other Green functions. This was first realized in the context of the U(1) gauge invariance of QED, where the vector current is exactly conserved and gives rise to the identity [War 50]

$$\Gamma^\mu(p,p) = -\frac{\partial}{\partial p_\mu}\Sigma(p), \tag{2.30}$$

which relates the electromagnetic vertex of an electron at zero momentum transfer, $\gamma^\mu + \Gamma^\mu(p,p)$, to the electron self energy, $\Sigma(p)$. Such symmetry relations among Green functions are called Ward identities[3]. The Ward identity for our example is called a chiral Ward identity, as the underlying symmetry is the chiral symmetry $\mathrm{SU}(3)_L \times \mathrm{SU}(3)_R$.

Chiral Ward identities are crucial to the construction of χPT, as the global symmetries we have established so far are not sufficient to fully determine the low-energy structure of our theory. Working out all possible Ward identities in the above way is a tedious task, fortunately there is a compact and more elegant way of obtaining all Green functions of a theory using the path integral. Having the Lagrangian of a theory all possible Green functions are encoded in the so-called generating functional. For the Green functions involving currents one introduces auxiliary fields, called sources or external fields.

Following the procedure of Gasser and Leutwyler [GL 84, GL 85], we introduce into the Lagrangian of QCD the couplings of the nine vector currents and the eight axial-vector currents as well as the scalar and pseudoscalar quark densities to external c-number fields $v^\mu(x)$, $v^\mu_{(s)}$, $a^\mu(x)$, $s(x)$, and $p(x)$,

$$\mathcal{L} = \mathcal{L}^0_{\mathrm{QCD}} + \mathcal{L}_{\mathrm{ext}} = \mathcal{L}^0_{\mathrm{QCD}} + \bar{q}\gamma_\mu(v^\mu + \frac{1}{3}v^\mu_{(s)} + \gamma_5 a^\mu)q - \bar{q}(s - i\gamma_5 p)q. \tag{2.31}$$

The external fields are given by

$$v^\mu = \sum_{a=1}^{8}\frac{\lambda_a}{2}v^\mu_a, \quad a^\mu = \sum_{a=1}^{8}\frac{\lambda_a}{2}a^\mu_a, \quad s = \sum_{a=0}^{8}\lambda_a s_a, \quad p = \sum_{a=0}^{8}\lambda_a p_a \tag{2.32}$$

and the isoscalar vector current $v^\mu_{(s)}$ is proportional to the unit matrix. The ordinary three flavor QCD Lagrangian is recovered by setting $v^\mu = v^\mu_{(s)} = a^\mu = p = 0$ and $s = \mathrm{diag}(m_u, m_d, m_s)$ in Eq. (2.31). We define the generating functional as

$$\exp(iZ[v,a,s,p]) = \langle 0|T\exp\left[i\int d^4x\mathcal{L}_{\mathrm{ext}}(x)\right]|0\rangle, \tag{2.33}$$

[3]The generalization to non-vanishing momentum transfer and more complicated groups is called Ward-Fradkin-Takahashi identities [War 50, Fra 55, Tak 57].

where all Green functions are obtained by functional derivatives with respect to the external fields. The generating functional is related to the vacuum-to-vacuum transition amplitude in the presence of external fields [GL 84, GL 85],

$$\exp[iZ(v,a,s,p)] = \langle 0_{\text{out}}|0_{\text{in}}\rangle_{v,a,s,p}, \tag{2.34}$$

where the dynamics is determined by the Lagrangian of Eq. (2.31). As an example, let us consider the two-point function of the axial-vector currents of Eq. (2.16) of the "real world," i.e., for $s = \text{diag}(m_u, m_d, m_s)$, and the "true vacuum" $|0\rangle$,

$$\begin{aligned}\langle 0|T[A_\mu^a(x)A_\nu^b(0)]|0\rangle = \\ (-i)^2\frac{\delta^2}{\delta a_a^\mu(x)\delta a_b^\nu(0)}\exp(iZ[v,a,s,p])\Big|_{v=a=p=0,s=\text{diag}(m_u,m_d,m_s)}.\end{aligned} \tag{2.35}$$

An important aspect of the generating functional of Eq. (2.33) is invariance under local gauge transformations of the external fields which ultimately defines the symmetry properties of the Green functions we are interested in[4]. To be more specific the Lagrangian of Eq. (2.31) is invariant under local $\text{SU(3)}_\text{L} \times \text{SU(3)}_\text{R}$ transformations with the external fields transforming according to

$$\begin{aligned}\big(v_\mu + a_\mu\big) &\mapsto V_R r_\mu V_R^\dagger + iV_R\partial_\mu V_R^\dagger,\\ \big(v_\mu - a_\mu\big) &\mapsto V_L l_\mu V_L^\dagger + iV_L\partial_\mu V_L^\dagger,\\ v_\mu^{(s)} &\mapsto v_\mu^{(s)} - \partial_\mu\Theta,\\ s + ip &\mapsto V_R(s+ip)V_L^\dagger,\\ s - ip &\mapsto V_L(s-ip)V_R^\dagger,\end{aligned} \tag{2.36}$$

where

$$\big(V_L, V_R\big) \in \text{SU(3)}_\text{L} \times \text{SU(3)}_\text{R}.$$

Let us stress that the generating functional is the essential link between the underlying theory and the effective theory. We construct our effective theory in accordance to the locally gauge-invariant generating functional of Eq. (2.33).

2.3 Chiral perturbation theory

Having discussed the symmetries of QCD we are now in the position to construct the corresponding effective theory for low-energy hadronic processes, chiral perturbation theory. χPT originates from the pioneering work by Weinberg [Wei 79] and was systematically worked out by Gasser and Leutwyler [GL 84, GL 85]. One of the biggest accomplishments of χPT is to cast previous findings based on current

[4]Note that this is only true in the absence of anomalies.

algebra and the partially conserved axial-vector current (PCAC) hypothesis into a systematic framework allowing for the calculation of corrections.

In χPT the effective degrees of freedom are the experimentally observed hadronic states, rather than the fundamental degrees of freedom of QCD, namely quarks and gluons. Contrary to the implications of the name χPT, it is in fact non-perturbative in the strong coupling constant g. The perturbative series is rather realized as a Taylor series expansion in powers of the momenta over some scale Λ, with Λ typically chosen to be of the order of 1 GeV.

In this work we restrict ourselves to the two flavor case. Moreover we work in the so-called isospin symmetric limit where $m_u = m_d = m$. According to the discussion in the previous section the chiral $\mathrm{SU}(2)_\mathrm{L} \times \mathrm{SU}(2)_\mathrm{R}$ is spontaneously broken to the subgroup $\mathrm{SU}(2)_\mathrm{V}$. Experimental evidence for the spontaneous symmetry breaking can be seen in the hadronic spectrum, where the pion mass is much smaller than the masses of other hadrons and the fact that mass-degenerate states with opposite parity are missing. Applying the Goldstone theorem to the SU(2) case we expect $6 - 3 = 3$ massless Goldstone bosons with spin 0. Taking into account the explicit symmetry breaking due to the small quark mass m one identifies the pions as Goldstone bosons[5]. Even though the symmetries restrict the number of possible terms, the most general Lagrangian still contains an infinite number of terms. Clearly in perturbative calculations a pattern organizing the Lagrangian is required.

2.3.1 Power counting

Let us first set up a scheme for the organization of the infinitely many terms contributing to the most general effective Lagrangian. In constructing such a scheme we exploit the fact that the interaction of Goldstone bosons becomes weak at low energies[6]. We start by organizing the terms in the Lagrangian according to the number of derivatives acting on pion fields and powers of quark masses,

$$\mathcal{L} = \mathcal{L}_2 + \mathcal{L}_4 + \ldots,$$

where the subscript denotes the number of derivatives or powers of the quark mass respectively. Note that derivatives acting on pion fields yield momenta of pions in the corresponding Feynman rule. We are interested in perturbative calculations of physical matrix elements using a Feynman diagrammatic approach. Therefore we need a scheme assessing the importance of an individual diagram generated by the interactions of the above Lagrangian. Weinberg proposed such a scheme, called Weinberg's power counting [Wei 79]. Any Feynman diagram contributing to a physical matrix element $\mathcal{M}$ is a function of the quark masses and the momenta of pions

$$\mathcal{M} = \mathcal{D}_1(m_q, p_i) + \mathcal{D}_2(m_q, p_i) + \ldots \quad .$$

[5]Strictly speaking Goldstone bosons are massless, therefore the pions are referred to as pseudo or would-be Goldstone bosons in the literature.

[6]This is in marked contrast to the underlying theory where the strong coupling of QCD increases at lower energies.

Considering the behavior of a physical matrix element $\mathcal{M}(m_q, p_i)$ under a linear rescaling of the pion momenta $p_i \mapsto t\, p_i$ and a quadratic rescaling of quark masses $m_q \mapsto t^2 m_q$, we write

$$\begin{aligned}\mathcal{M}(m_q, p_i) \mapsto \mathcal{M}(t^2\, m_q, t\, p_i) &= \mathcal{D}_1(t^2\, m_q, t\, p_i) + \mathcal{D}_2(t^2\, m_q, t\, p_i) + \ldots, \\ &= t^{D_1}\, \mathcal{D}_1(m_q, p_i) + t^{D_2} \mathcal{D}_2(m_q, p_i) + \ldots.\end{aligned}$$

In this way one assigns a chiral order D to each individual diagram contributing to $\mathcal{M}$. We obtain the general expression

$$D = 2 + \sum_{n=0}^{\infty} 2\big(n-1\big)\, N_{2n} + 2\, N_L, \tag{2.37}$$

for the chiral order of an individual Feynman diagram. N_{2n} denotes the number of vertices from the Lagrangian $\mathcal{L}_{2n}$ and N_L stands for the number of loops. Obviously for small values of t diagrams with an increasing chiral order D are suppressed and those with smaller D prevail. In this way in a calculation to a fixed order in D only a limited number of diagrams from the most general Lagrangian contribute. We rewrite Eq. (2.37) using the relation

$$N_V = N_I - N_L + 1,$$

where N_V is the total number of vertices[7] and N_I is the number of internal pion lines, and obtain for D

$$D = 4\, N_L - 2\, N_I + \sum_{n=0}^{\infty} 2n\, N_{2n}. \tag{2.38}$$

This definition of the chiral order is convenient, as we assign the following chiral orders to individual components of a Feynman diagram:

1. Integration in 4 dimensions counts as chiral order 4,

2. a pion propagator counts as chiral order -2,

3. a vertex from $\mathcal{L}_{2n}$ counts as chiral order $2n$.

Essentially counting the powers of pion propagators, pion momenta and powers of loop momenta determines the importance of an individual diagram, hence the name power counting. Of course when organizing the most general effective Lagrangian according to the number of derivatives and quark masses we had this power counting in mind.

[7] Note that $N_V = \sum_n N_{2n}$.

2.3.2 Mesonic Lagrangian

Since the essential link between χPT and QCD is the generating functional of Eq. (2.33) the task at hand is to construct an effective Lagrangian invariant under local $C = \mathrm{SU(2)_L} \times \mathrm{SU(2)_R}$ transformations. In [CWZ 69, Cal+ 69] a procedure has been developed how a spontaneously broken symmetry is realized on quantum fields. To that end it is convenient to collect the Goldstone boson fields in a unitary 2×2 matrix U

$$U(x) = \exp\Big(\frac{i\Phi(x)}{F}\Big), \quad \Phi(x) = \sum_{i=1}^{3} \tau_i \Phi_i = \begin{pmatrix} \pi^0 & \sqrt{2}\,\pi^+ \\ \sqrt{2}\,\pi^- & -\pi^0 \end{pmatrix}, \tag{2.39}$$

where the τ_i are the Pauli matrices. U transforms under chiral transformations according to

$$U(x) \mapsto V_R\, U(x) V_L^\dagger, \tag{2.40}$$

where $\big(V_L, V_R\big) \in \mathrm{SU(2)_L} \times \mathrm{SU(2)_R}$ now depend on x. The transformation properties of the external sources are the same as displayed in Eq. (2.36) with the obvious substitution $\big(V_L, V_R\big) \in \mathrm{SU(2)_L} \times \mathrm{SU(2)_R}$. Introducing the definitions

$$r_\mu = v_\mu + a_\mu, \quad l_\mu = v_\mu - a_\mu, \quad \chi = 2B\big(s + ip\big),$$

the covariant derivative acting on U is given by

$$D_\mu U = \partial_\mu U - i r_\mu U + i U l_\mu.$$

For the construction of higher-order terms it is useful to define the field strength tensors of the external fields,

$$\begin{aligned} f^R_{\mu\nu} &= \partial_\mu r_\nu - \partial_\nu r_\mu - i\big[r_\mu, r_\nu\big], \\ f^L_{\mu\nu} &= \partial_\mu l_\nu - \partial_\nu l_\mu - i\big[l_\mu, l_\nu\big], \end{aligned}$$

which under chiral transformations behave as

$$\begin{aligned} f^R_{\mu\nu} &\mapsto V_R f^R_{\mu\nu}\, V_R^\dagger, \\ f^L_{\mu\nu} &\mapsto V_L f^L_{\mu\nu}\, V_L^\dagger. \end{aligned}$$

The construction of the effective Lagrangian uses the above defined quantities as building blocks. They have a well defined behavior with respect to chiral symmetry and the discrete symmetries C and P. The chiral orders of the building blocks are given by

$$U = \mathcal{O}(q^0), \quad D_\mu U = \mathcal{O}(q^1), \quad r_\mu, l_\mu = \mathcal{O}(q^1), \quad f^{R/L}_{\mu\nu} = \mathcal{O}(q^2), \quad \chi = \mathcal{O}(q^2),$$

where q denotes a small quantity such as pion momenta and meson masses.

Due to Lorentz invariance the mesonic Lagrangian only contains terms with even powers in the momenta or pion masses. As we are only interested in the coupling of the pions to an external electromagnetic field A_μ in the following we use

$$v_\mu = r_\mu = l_\mu = -e\frac{\tau_3}{2}A_\mu, \quad v_\mu^{(s)} = -\frac{e}{2}A_\mu. \tag{2.41}$$

The lowest-order Lagrangian reads [GL 84]

$$\mathcal{L}_2 = \frac{F^2}{4}\mathrm{Tr}[D_\mu U (D^\mu U)^\dagger] + \frac{F^2}{4}\mathrm{Tr}(\chi U^\dagger + U\chi^\dagger). \tag{2.42}$$

Note that the leading-order Lagrangian describes the interaction of any even number of pions, e.g. $\pi\pi \to \pi\pi$ or $\pi\pi \to \pi\pi\pi\pi$. We have two coupling constant at leading order, F which is related to the pion decay constant $F_\pi = F + \mathcal{O}(q^2)$ and B which is related to scalar quark condensate. The corresponding quantities are defined in the chiral limit. The pion mass is related to B according to

$$M_\pi^2 = 2\,B\left(\frac{m_u + m_d}{2}\right) = 2\,B\hat{m}.$$

Let us stress that the above construction of the effective mesonic Lagrangian can only generate terms with an even number of pions. The Lagrangian has an additional symmetry not present in QCD called intrinsic parity, more specifically the Lagrangian of Eq. (2.42) is invariant under transformations

$$\phi(x) \to -\phi(x).$$

However in the Lagrangian at fourth order a term occurs due to the chiral anomaly, which is responsible for the interaction of an odd number of mesons. The Lagrangian describing such processes was derived by Wess, Zumino and Witten [WZ 71, Wit 83]. In the calculation of VCS the only relevant vertex is $\pi^0\gamma^*\gamma^*$ and we only display the corresponding Lagrangian

$$\mathcal{L}^{\mathrm{WZW}} = -\frac{e^2}{32\pi^2 F_\pi}\epsilon^{\mu\nu\alpha\beta}F_{\mu\nu}F_{\alpha\beta}\pi^0, \tag{2.43}$$

where

$$F_{\mu\nu} = \partial_\mu A_\nu - \partial_\nu A_\mu. \tag{2.44}$$

Note that the WZW-Lagrangian does not contain any free parameters if one considers the number of colors to be fixed, $N_c = 3$.

2.4 Baryonic Lagrangian

So far we have only considered the interactions of pions among each other and with the electromagnetic field. When including nucleons we proceed in analogy to the

previous section, giving the basic building blocks and their behavior under chiral transformations first.

The external fields transform in the same way as in the previous section. The nucleons are collected in an isospinor

$$\Psi = \begin{pmatrix} p \\ n \end{pmatrix},$$

where p and n denote the proton and neutron four component Dirac field, respectively. The behavior of Ψ under chiral transformation is given in terms of the so-called compensator $K(V_L, V_R, U)$,

$$\Psi \mapsto K(V_L, V_R, U)\Psi, \tag{2.45}$$

$$\bar{\Psi} \mapsto \bar{\Psi} K^\dagger(V_L, V_R, U). \tag{2.46}$$

We denote the square root of U by u, $u^2(x) = U(x)$, and define the SU(2)-valued function $K(V_L, V_R, U)$ by

$$u(x) \mapsto u'(x) = \sqrt{V_R U V_L^\dagger} \equiv V_R u K^{-1}(V_L, V_R, U), \tag{2.47}$$

i.e.

$$K(V_L, V_R, U) = u'^{-1} V_R u = \sqrt{V_R U V_L^\dagger}^{-1} V_R \sqrt{U}.$$

Using the definition of the so-called chiral connection [Eck 95]

$$\Gamma_\mu = \frac{1}{2}\left[u^\dagger(\partial_\mu - i r_\mu)u + u(\partial_\mu - i l_\mu)u^\dagger\right], \tag{2.48}$$

the covariant derivative is given by

$$D_\mu \Psi = (\partial_\mu + \Gamma_\mu - i v_\mu^{(s)})\Psi. \tag{2.49}$$

It can be shown that the covariant derivative defined in this way transforms under chiral rotations in the same way as the isospinor nucleon field Ψ,

$$D_\mu \, \Psi \mapsto K(V_L, V_R, U) \, D_\mu \, \Psi. \tag{2.50}$$

At leading order there exists another Hermitian building block, the so-called vielbein [Eck 95],

$$u_\mu \equiv i\left[u^\dagger(\partial_\mu - i r_\mu)u - u(\partial_\mu - i l_\mu)u^\dagger\right], \tag{2.51}$$

which under parity transforms as an axial vector. For the construction of higher order terms it is convenient to define further building blocks[8]

$$\begin{aligned} \chi_\pm &= u^\dagger \chi u^\dagger \pm u \chi^\dagger u, \\ f_{\mu\nu}^\pm &= u f_{\mu\nu}^L u^\dagger \pm u^\dagger f_{\mu\nu}^R u, \\ v_{\mu\nu}^{(s)} &= \partial_\mu v_\nu^{(s)} - \partial_\nu v_\mu^{(s)} \end{aligned} \tag{2.52}$$

[8]Note that in Ref. [Fet+ 00] the vector current contains the isoscalar part.

which transform according to

$$X \mapsto K(V_L, V_R, U)\, X\, K^{-1}(V_L, V_r, U), \quad X = u_\mu,\, \chi_\pm,\, f^\pm_{\mu\nu}, \\ v^{(s)}_{\mu\nu} \mapsto v^{(s)}_{\mu\nu}. \tag{2.53}$$

Furthermore the covariant derivative acting on the building blocks transforms in the same way as the building blocks themselves. The lowest order Lagrangian reads [GSS 88]

$$\mathcal{L}^{(1)}_{\pi N} = \bar\Psi \left(i \not{D} - m + \frac{\mathrm{g}_A}{2} \gamma^\mu \gamma_5 u_\mu \right) \Psi, \tag{2.54}$$

where m is the nucleon mass in the chiral limit and g_A is the nucleon axial-vector coupling constant, also in the chiral limit. The Lagrangians up to fourth order have been constructed in [GSS 88, EM 96, Fet+ 00]. Here we only display the terms necessary for our calculations.

The next-to-leading-order pion-nucleon Lagrangian contains seven low-energy constants c_i[9]

$$\begin{aligned} \mathcal{L}^{(2)}_{\pi N} &= c_1 \mathrm{Tr}(\chi_+) \bar\Psi \Psi - \frac{c_2}{4m^2} \left[\bar\Psi \mathrm{Tr}\left(u_\mu u_\nu\right) D^\mu D^\nu \Psi + \mathrm{h.c.} \right] + \frac{c_3}{2} \bar\Psi \mathrm{Tr}\big(u_\mu\, u^\mu\big) \Psi \\ &\quad + \bar\Psi \left[i \frac{c_4}{4} \left[u_\mu, u_\nu\right] + \frac{c_6}{2} f^+_{\mu\nu} + \frac{c_7}{2} v^{(s)}_{\mu\nu} \right] \sigma^{\mu\nu} \Psi + \cdots , \end{aligned} \tag{2.55}$$

where h.c. refers to the Hermitian conjugate. The relevant parts of the Lagrangians of order three and four read [Fet+ 00]

$$\mathcal{L}^{(3)}_{\pi N} = \frac{d_6}{2m} \left[\bar\Psi\, i [D^\mu, \widetilde{F}^+_{\mu\nu}] D^\nu \Psi + \mathrm{h.c.} \right] + \frac{d_7}{2m} \left[\bar\Psi\, i [D^\mu, \mathrm{Tr}\left(F^+_{\mu\nu}\right)] D^\nu \Psi + \mathrm{h.c.} \right] + \ldots , \tag{2.56}$$

$$\begin{aligned} \mathcal{L}^{(3)}_{\pi N} = &- \frac{e_{54}}{2} \bar\Psi \left[D^\lambda, \left[D_\lambda, \mathrm{Tr}\left(F^+_{\mu\nu}\right) \right] \right] \sigma^{\mu\nu} \Psi - \frac{e_{74}}{2} \bar\Psi \left[D^\lambda, \left[D_\lambda, \widetilde{F}^+_{\mu\nu} \right] \right] \sigma^{\mu\nu} \Psi \\ &+ e_{89} \bar\Psi\, \mathrm{Tr}\left(F^+_{\mu\nu}\right) \mathrm{Tr}\left(F^{+\mu\nu}\right) \Psi - \frac{e_{90}}{4m^2} \left[\bar\Psi\, \mathrm{Tr}\left(F^+_{\lambda\mu}\right) \mathrm{Tr}\left(F^{+\lambda}{}_{\nu}\right) D^{\mu\nu} \Psi + \mathrm{h.c.} \right] \\ &+ e_{91} \bar\Psi\, \widetilde{F}^+_{\mu\nu} \mathrm{Tr}\left(F^{+\mu\nu}\right) \Psi - \frac{e_{92}}{4m^2} \left[\bar\Psi\, \widetilde{F}^+_{\lambda\mu} \mathrm{Tr}\left(F^{+\lambda}{}_{\nu}\right) D^{\mu\nu} \Psi + \mathrm{h.c.} \right] \\ &+ e_{93} \bar\Psi\, \mathrm{Tr}\left(\widetilde{F}^+_{\mu\nu} \widetilde{F}^{+\mu\nu} \right) \Psi - \frac{e_{94}}{4m^2} \left[\bar\Psi \mathrm{Tr}\left(\widetilde{F}^+_{\lambda\mu} \widetilde{F}^{+\lambda}{}_{\nu} \right) D^{\mu\nu} \Psi + \mathrm{h.c.} \right] \\ &- \frac{e_{105}}{2} \bar\Psi\, \mathrm{Tr}\left(F^+_{\mu\nu}\right) \mathrm{Tr}\left(\chi_+\right) \sigma^{\mu\nu} \Psi - \frac{e_{106}}{2} \bar\Psi\, \widetilde{F}^+_{\mu\nu} \mathrm{Tr}\left(\chi_+\right) \sigma^{\mu\nu} \Psi \\ &- \frac{e_{117}}{8m^2} \left[\bar\Psi\, \mathrm{Tr}\left(F^-_{\lambda\mu} F^{-\lambda}{}_{\nu} + F^+_{\lambda\mu} F^{+\lambda}{}_{\nu} \right) D^{\mu\nu} \Psi + \mathrm{h.c.} \right] \\ &+ \frac{e_{118}}{2} \bar\Psi\, \mathrm{Tr}\left(F^-_{\mu\nu} F^{-\mu\nu} + F^+_{\mu\nu} F^{+\mu\nu} \right) \Psi + \ldots . \end{aligned} \tag{2.57}$$

Note that $F^\pm_{\mu\nu}$ in the above equations corresponds to $f^\pm_{\mu\nu}$ if one includes the isoscalar vector current in the vector current v_μ. Moreover in the above equations the following definition is used

$$\widetilde{X} = X - \frac{1}{2} \mathrm{Tr}\left(X\right) \ . \tag{2.58}$$

[9] With the substitutions $f^+_{\mu\nu} \to F^+_{\mu\nu} - \frac{1}{2}\mathrm{Tr}(F^+_{\mu\nu})$ and $v^{(s)}_{\mu\nu} \to \frac{1}{4}\mathrm{Tr}(F^+_{\mu\nu})$ as well as $c_6 \to c_6/(4m)$ and $c_7 \to (c_6 + c_7)/(2m)$ one arrives at the next-to-leading order Lagrangian of [Fet+ 00].

The abbreviation $D^n_{\alpha\beta\ldots\omega} = \{D_\alpha, \{D_\beta, \{\ldots, D_\omega\}\}\}$ is used for the totally symmetrized product of n covariant derivatives. The corresponding Feynman rules are given in Appendix A.

2.4.1 Power counting in BχPT

The power counting in the baryonic sector is marked with problems as was first stated by Gasser, Sainio. and Svarc [GSS 88]. The generalization of the power counting from the mesonic sector is realized by assigning the following chiral orders to the individual components of a diagram:

1. The nucleon propagator counts as chiral order -1,
2. vertices from the Lagrangian $\mathcal{L}^{(n)}_{\pi N}$ count as chiral order n,
3. the mesonic power counting stays the same.

Eventually at some stage in a perturbative calculation loop corrections arise, which due to their divergence have to be treated carefully. The usual way in mesonic χPT is to use dimensional regularization and the so-called modified minimal subtraction scheme of χPT ($\widetilde{\text{MS}}$). When the same methods were applied to one-loop diagrams in BχPT one explicitly saw a breakdown of the power counting. The breakdown comprised of terms with smaller chiral dimension in the result than expected. As an example let us take a look at the self-energy of the nucleon. Let us first establish the chiral orders of the diagrams in Fig. 2.1 using the above power counting.

1. The left diagram in Fig.2.1 has chiral order (n is the space-time dimension)

$$D = n + 2 \cdot 1 - 1 - 2 = n - 1 \to 3.$$

2. The right diagram in Fig.2.1 has chiral order

$$D = n + 1 \cdot 2 - 2 = n = \to 4.$$

An explicit calculation of the diagrams in dimensional regularization in combination with the $\widetilde{\text{MS}}$-scheme shows that the left diagram in Fig. 2.1 actually contains terms violating power counting, whereas the right diagram fulfills power counting.

However one has to keep in mind that the power counting was obtained by rescaling the momenta and quark masses of a physical matrix element and looking at the behavior of individual diagrams contributing to this matrix element. Therefore

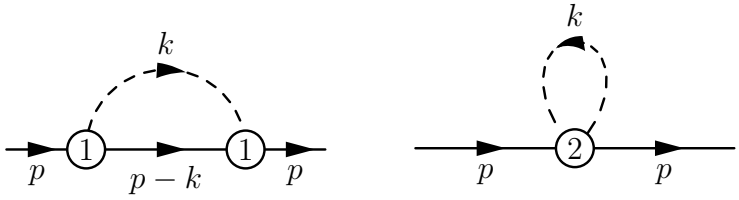

Figure 2.1: Self-energy diagrams.

power counting should be applied to renormalized diagrams only, thus the validity of a power counting scheme depends on the choice of the renormalization scheme. This was already realized in Ref. [GSS 88].

The first solution to this problem was given by the non-relativistic limit using techniques borrowed from heavy-quark effective theory. This approach is called heavy-baryon chiral perturbation theory (HBχPT) and essentially amounts to an expansion in inverse powers of the nucleon mass in the relativistic Lagrangian [JM 91, Ber+ 92]. The caveat in HBχPT is that manifest Lorentz invariance is lost. Moreover, in higher orders in the chiral expansion, the expressions due to $\frac{1}{m}$ corrections of the Lagrangian become increasingly complicated. Subsequently several manifestly Lorentz-invariant renormalization schemes have been developed that also result in a proper power counting [ET 98, BL 99, GJ 99, Goi+ 01, Fuc+ 03]. The most commonly used scheme is the so-called infrared regularization (IR) of Becher and Leutwyler [BL 99], which, in its reformulated version of Ref. [SGS 04] is also applied in this work.

2.4.2 Infrared regularization

Let us illustrate the main ideas of IR by looking at the left diagram of Fig. 2.1. In the calculation of the self-energy the following integral appears

$$I_{\pi N} = i \int \frac{d^D k}{(2\pi)^D} \frac{1}{[k^2 - M^2 + i0^+]\,[(k-p)^2 - m^2 + i0^+]}, \tag{2.59}$$

where D denotes the number of space-time dimensions and the masses m and M refer to the nucleon mass in the chiral limit and the lowest-order pion mass, respectively. Using the Feynman parametrization formula

$$\frac{1}{ab} = \int_0^1 \frac{dz}{[az + b(1-z)]^2}, \tag{2.60}$$

with $a = (k-p)^2 - m^2 + i0^+$ and $b = k^2 - M^2 + i0^+$, and performing the integration over loop momenta k we obtain

$$I_{\pi N} = -\frac{1}{(4\pi)^{D/2}}\,\Gamma(2 - D/2) \int_0^1 dz\ \left[A(z)\right]^{(D/2)-2}, \tag{2.61}$$

where

$$A(z) = -p^2(1-z)z + m^2 z + M^2(1-z) - i0^+.$$

In the approach of Becher and Leutwyler, the integral $I_{\pi N}$ in Eq. (2.61) is split into the so-called infrared singular part I and the regular part R,

$$I = -\frac{1}{(4\pi)^{D/2}}\,\Gamma(2 - D/2) \int_0^\infty dz\,\left[A(z)\right]^{(D/2)-2}, \tag{2.62}$$

$$R = \frac{1}{(4\pi)^{D/2}}\,\Gamma(2 - D/2) \int_1^\infty dz\,\left[A(z)\right]^{(D/2)-2}. \tag{2.63}$$

One can prove that the infrared singular part I satisfies power counting, thus all power counting violating terms are encoded in the regular part R. In contrast to the infrared singular part the regular part allows for an expansion in a Taylor series in the external momenta and the quark masses. Therefore using an appropriate renormalization procedure one can compensate these terms in the redefinition of the coupling constants and fields of the most general Lagrangian. Indeed the Green functions obtained from a one-loop diagram separated into an infrared singular and regular part separately satisfy the Ward identities of the theory. This ensures that regular parts can be incorporated in the coupling constants and fields of the most general Lagrangian. If one drops the regular part of the integral $I_{\pi N}$ the resulting expression satisfies power counting. Note that I and R contain additional divergences not present in $I_{\pi N}$ therefore these divergences have to cancel exactly.

We use the reformulated version of IR in this work. In Ref. [SGS 04] it has been shown that the regular part of any integral can be constructed without resorting to a splitting of the Feynman parameterized integral. Starting from a parameterized version of the integral, e.g. the Feynman parameter representation of Eq. (2.61), one constructs the regular part by performing a Taylor expansion of the integrand in *small* quantities with subsequent interchange of summation and integration. This coincides with the chiral expansion of the regular part R calculated in [BL 99]. The expansion of the regular part of $I_{\pi N}$ to third order reads

$$R = -\frac{1}{16\pi^2}\Big[1 - \frac{p^2-m^2}{2m^2} + \frac{3M^2}{2m^2} + \frac{\big(p^2-m^2\big)\big(p^4+m^4-2m^2\big(p^2+3M^2\big)\big)}{6m^2} + \dots\Big].$$

The main advantage of the reformulated version is that we can use the standard definition of the one-loop integrals, i.e. we do not have to calculate the infrared singular part explicitly. Therefore we can use standard libraries for the calculation of one-loop integrals such as the LoopTools library [Hah 01] and explicitly subtract the regular part in order to get the IR regularized integrals. The calculation of the chiral expansion of the regular part R is well suited for an implementation in a computer algebra system (CAS). We have implemented this procedure in Mathematica using the Schwinger parameter representation of the one loop integrals. At present the subtraction terms for integrals up to four denominators and tensor rank four is implemented. For calculational details see Appendix D.

Chapter 3

Virtual Compton scattering

Electromagnetic interactions of nucleons are a useful tool to get insight to the nucleon structure as well as the underlying dynamics governing the low-energy regime of QCD. Among the first scattering experiments using an electromagnetic probe was the elastic electron scattering off the proton. The results deviate from the electron scattering off a point-like spin-$\frac{1}{2}$ particle, indicating the composite structure of the nucleon. The corresponding response functions of the nucleon are called form factors, which allow for an interpretation as the spatial distribution of charge and magnetic moments inside the nucleon. The electromagnetic interaction we are interested in is Compton scattering on the proton. In this process we gain new information on the structure of the nucleon, which can be interpreted as the polarizability of a medium exposed to an external electromagnetic field. The polarizability of systems predominantly governed by electromagnetic interactions, e.g atoms, is approximately given by its volume. For nucleons the polarizabilities are four orders of magnitude smaller than its volume, thus indicating the prominent role of strong interactions. In analogy to the form factors, the spatial distribution of electric or magnetic polarizabilities can be measured by going from the real case to the virtual Compton scattering case.

Virtual Compton scattering (VCS) is accessible in the photon electro-production process $e\,p \to e'\,p'\,\gamma$. In the calculation of electro-production processes of mesons, e.g. pion electro-production, one usually employs the one-photon-exchange approximation. This approximation is justified, because one produces a strongly interacting particle and the cross sections are relatively large. As we are interested in the production of a photon, this approximation might be inaccurate. In fact, the radiative corrections give sizeable contributions to the cross section for photon electro-production. In Ref. [Van+ 00] the contributions from QED radiative corrections were found to give a 20 % effect on the cross sections in the MAMI kinematics. However, given the comparatively large mass of the nucleon the radiative corrections from the hadronic part of the process are expected to be strongly suppressed compared to the leptonic sector. Consequently, if one incorporates the effects of the QED radiative corrections in the experimental data analysis, the one-photon-approximation for the hadronic part is still valid.

In this chapter we lay out the basic formalism of the VCS process. This concerns in particular

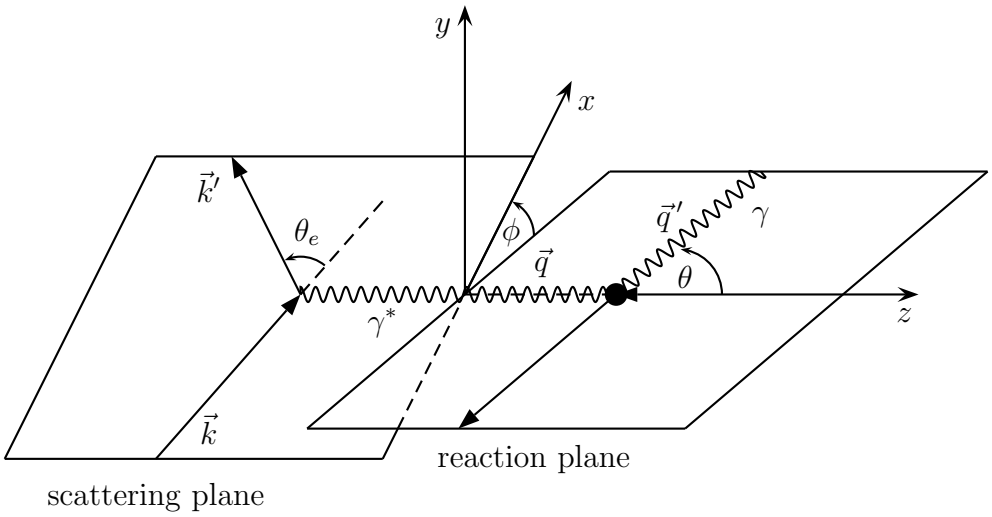

Figure 3.1: Kinematics of the reaction $e\,p \to e'\,p'\,\gamma$.

- the general kinematics for $e\,p \to e'\,p'\,\gamma$,
- the definition of the VCS process,
- and the definition of derived quantities, in particular polarizabilities.

First the separation of the genuine VCS process from competing processes in photon electro-production is discussed in detail. Next we establish model-independent constraints on the VCS process and give appropriate parameterizations of the hadronic part. Thereafter we introduce the concept of polarizabilities as a means to parameterize the new information on the structure of the nucleon exclusively accessible in the VCS process. Finally, the definitions of the physical observables calculated in this work are explicitly given.

3.1 Kinematics

In this section we define the kinematics and notations used in this work. The initial and final four momenta of the nucleon with mass m_N are denoted by p_i and p_f, respectively. The initial and final electron momenta are k and k', the electron mass is m_e and the final state photon momentum is q_2. The components of the momenta are specified as

$$\begin{aligned} p_i^\mu &= \big(E_i, \vec{p}\big), & p_f^\mu &= \big(E_f, \vec{p}\,'\big), \\ k^\mu &= \big(\omega_i, \vec{k}\big), & k'^\mu &= \big(\omega_f, \vec{k}'\big), \\ q_2^\mu &= \big(\omega', \vec{q}\,'\big). \end{aligned} \tag{3.1}$$

The spin of the initial (final) state nucleon is given by S_i (S_f), the initial (final) state electron spin is denoted s_i (s_f) and the polarization state of the final photon

is abbreviated with λ'. The four momentum of the virtual photon is given by $q_1^\mu = (k - k')^\mu = (\omega, \vec{q})$. In the following a bar denotes the absolute value of a three vector $\bar{x} = |\vec{x}|$ and $\hat{x}$ denotes the unit vector in the direction of $\vec{x}$. For the VCS process one has in general three independent kinematical variables. It is convenient to introduce the three Mandelstam variables

$$s = \big(p_i + q_1\big)^2, \quad t = \big(q_1 - q_2\big)^2, \quad u = \big(p_i - q_2\big)^2, \tag{3.2}$$

satisfying the relation $s + t + u = 2\,m_N^2 + q_1^2$. As we are interested in space-like virtuality we set $q_1^2 = -Q^2$.

The coordinate system in Fig. 3.1 is defined as in [GLT 95, GV 98]. The z direction is fixed by the propagation of the virtual photon and the polar angle θ describes the angle between the virtual and real photon. Thus the basis of our coordinate system is given by

$$\begin{aligned} \hat{e}_z &= \hat{q}, \\ \hat{e}_y &= \frac{\hat{q} \times \hat{q}'}{\sin\theta}, \\ \hat{e}_x &= \hat{e}_y \times \hat{e}_z. \end{aligned} \tag{3.3}$$

We work in the VCS center of mass frame, which is specified by

$$\vec{p} = -\vec{q}, \tag{3.4}$$

$$\vec{p}\,' = -\vec{q}\,'. \tag{3.5}$$

In the above coordinate system the three-momenta of the real and virtual photon have the following form

$$\vec{q} = \bar{q} \begin{pmatrix} 0 \\ 0 \\ 1 \end{pmatrix}, \tag{3.6}$$

$$\vec{q}\,' = \omega' \begin{pmatrix} \sin\theta \\ 0 \\ \cos\theta \end{pmatrix}. \tag{3.7}$$

The two polarization states of the real photon are described by the polarization vectors

$$\vec{\epsilon}\,'\big(\lambda' = \pm 1\big) = \frac{1}{\sqrt{2}} \begin{pmatrix} \mp\cos\theta \\ -i \\ \pm\sin\theta \end{pmatrix}. \tag{3.8}$$

The electron scattering plane and the reaction plane are rotated by the azimuthal angle ϕ. The three-momenta of the electrons in the reaction plane are given by

$$\vec{k} = \omega_i \begin{pmatrix} \sin\alpha\,\cos\phi \\ \sin\alpha\,\sin\phi \\ \cos\alpha \end{pmatrix}, \tag{3.9}$$

$$\vec{k}' = \omega_f \begin{pmatrix} \sin\alpha' \cos\phi \\ \sin\alpha' \sin\phi \\ \cos\alpha' \end{pmatrix}, \tag{3.10}$$

where the electron scattering angle is given by the difference of α' and α, i.e.

$$\theta_e = \alpha' - \alpha.$$

Finally, for later use, we define the polarization parameter of the virtual photon to be

$$\epsilon = \frac{(\omega_i + \omega_f)^2 - \vec{q}^2}{(\omega_i + \omega_f)^2 + \vec{q}^2}. \tag{3.11}$$

3.1.1 Differential cross section

Having set the kinematics we proceed with the differential cross section for the photon electro-production process $e\,p \to e'\,p'\,\gamma$,

$$\begin{aligned} d\sigma = \frac{m_N^2\, m_e^2}{2E_f \omega_f \omega'} \frac{1}{\sqrt{\left(p_i \cdot k\right)^2 - m_N^2 m_e^2}} \frac{1}{\left(2\pi\right)^5} \overline{|\mathcal{M}|}^2 \\ \times \delta^{(4)}\left(p_i + k - p_f - k' - q_2\right) d^3p'\, d^3k'\, d^3q', \end{aligned} \tag{3.12}$$

where the complete information on the dynamics of the process is encoded in the invariant matrix element $\mathcal{M}$. The bar indicates that the spin sum has been carried out, this concerns the spin sums over the final proton and electron spins as well as the real photon polarizations and the spin-averaging over the initial proton and electron spins. Usually experiments detect the final electron in coincidence with the final state proton[1], the photon is then reconstructed via a cut on the missing mass spectrum around $q_2^2 = 0$. Moreover experimental cross sections are analyzed in the laboratory frame. Performing suitable Lorentz transformations the differential cross section for the unpolarized process then reads

$$\frac{d\sigma_{\text{lab}}}{d\omega_{f,\text{lab}}\, d\Omega_{e',\text{lab}}\, d\Omega_{p',\text{lab}}} = \frac{1}{4} \frac{m_N^2\, m_e^2}{\left(2\pi\right)^5} \frac{\omega_{f,\text{lab}}}{\omega_{i,\text{lab}}} \frac{s - m_N^2}{s} \overline{|\mathcal{M}|}^2. \tag{3.13}$$

3.2 Definition of the VCS process

There are several contributions to the photon electro-production process, the VCS process being one of them. The final real photon may not be emitted from the proton but rather from the initial or final electron as depicted in the diagrams (b) and (c) of Fig. 3.2. This subprocess represents the Bethe-Heitler process and can be calculated using QED and the phenomenological form factors of the nucleon.

[1] The direct measurement of the photon polarization would require a secondary electromagnetic reaction, thus further decreasing the counting rates.

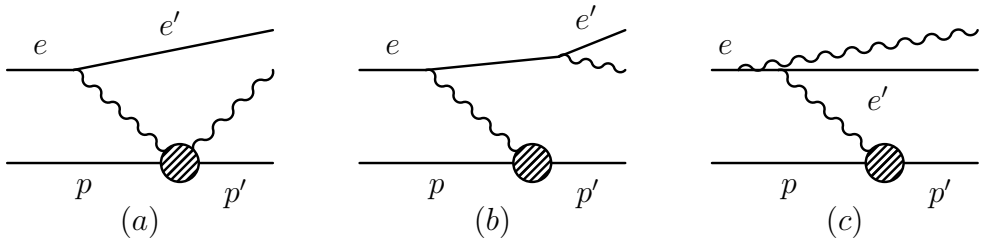

Figure 3.2: Feynman diagrams for the process $e\,p \to e'\,p'\,\gamma$. Diagram (a) is the genuine VCS process, (b) and (c) are the Bethe-Heitler diagrams.

The process we are interested in is depicted in diagram (a) of Fig. 3.2, which is the genuine VCS process. This process contains new information on the nucleon structure exclusively accessible in the VCS process. The invariant matrix elements can be decomposed into the contributions from VCS and the Bethe-Heitler part, $\mathcal{M} = \mathcal{M}^{\rm VCS} + \mathcal{M}^{\rm BH}$, which leads to interference terms in the spin-averaged squared matrix elements for the photon electro-production process

$$\begin{aligned}\overline{|\mathcal{M}|}^2 &= \frac{1}{4}\sum_j \Big(\mathcal{M}^{\rm VCS} + \mathcal{M}^{\rm BH}\Big)\Big(\mathcal{M}^{\rm VCS,*} + \mathcal{M}^{\rm BH,*}\Big), \quad j = \{s_i, s_f, S_i, S_f, \lambda'\} \\ &= \overline{|\mathcal{M}^{\rm VCS}|}^2 + \overline{|\mathcal{M}^{\rm BH}|}^2 + \overline{\mathcal{M}^{\rm VCS}\mathcal{M}^{\rm BH,*} + \mathcal{M}^{\rm VCS,*}\mathcal{M}^{\rm BH}}. \end{aligned} \tag{3.14}$$

Separating the hadronic and leptonic parts the Lorentz-invariant matrix element for the genuine VCS process $\gamma^* p \to \gamma p'$ reads[2]

$$\mathcal{M}^{\rm VCS} = \frac{e}{q_1^2}\,\chi_f^\dagger \varepsilon_\mu'^* H^{\mu\nu} \chi_i\; \bar{u}(k', s_f)\gamma_\nu\, u(k, s_i), \tag{3.15}$$

$$= -ie^2\,\chi_f \varepsilon_\mu'^* H^{\mu\nu}\, a_\nu\, \chi_i = \mathcal{M}^{\gamma^*\gamma}. \tag{3.16}$$

The polarization vector a_ν is related to the electron current according to

$$\begin{aligned} a^\nu &= \big(0, \vec{a}\big), \quad \vec{a} = \vec{\varepsilon}_T + \frac{q_1^2}{\omega^2}\,\vec{\varepsilon}\cdot\hat{q}\,\hat{q} = \vec{\varepsilon}_T + \frac{q_1^2}{\omega^2}\varepsilon_z\,\hat{q}, \\ \varepsilon_\mu &= \frac{e}{q_1^2}\,\bar{u}(k')\gamma_\mu u(k). \end{aligned} \tag{3.17}$$

Using current conservation the polarization vectors a^μ and ε^μ are related through the gauge transformation $\varepsilon^\mu \to a^\mu = \varepsilon_\mu + \zeta q_1^\mu$, with the particular choice $\zeta = -\vec{\varepsilon}\cdot\vec{q}/\omega^2$. Note that the polarization vector a_ν contains a longitudinal component. The Pauli space parametrization of the hadronic part is given by [Hem+ 97b],

$$\begin{aligned} \varepsilon_\mu'^* H^{\mu\nu} a_\nu = ie^2 \Big\{ &\vec{\varepsilon}'^* \cdot \vec{\varepsilon}_T\, A_1 + \vec{\varepsilon}'^* \cdot \hat{q}\,\vec{\varepsilon}_T \cdot \hat{q}\,'\, A_2 \\ &+ i\vec{\sigma}\cdot\big(\vec{\varepsilon}'^* \times \vec{\varepsilon}_T\big)\, A_3 + i\vec{\sigma}\cdot\big(\hat{q}\,' \times \hat{q}\big)\vec{\varepsilon}'^* \cdot \vec{\varepsilon}_T\, A_4 \\ &+ i\vec{\sigma}\cdot\big(\vec{\varepsilon}'^* \times \hat{q}\big)\vec{\varepsilon}_T \cdot \hat{q}\,'\, A_5 + i\vec{\sigma}\cdot\big(\vec{\varepsilon}'^* \times \hat{q}\,'\big)\vec{\varepsilon}_T \cdot \hat{q}'\, A_6 \end{aligned}$$

[2] In the following we suppress the spin index of the Dirac and Pauli spinors.

$$
\begin{aligned}
&- i\vec{\sigma}\cdot\left(\vec{\varepsilon}_T\times\hat{q}\,'\right)\vec{\varepsilon}\,'^{*}\cdot\hat{q}\,A_7 - i\vec{\sigma}\cdot\left(\vec{\varepsilon}_T\times\hat{q}\right)\vec{\varepsilon}\,'^{*}\cdot\hat{q}\,A_8 \\
&+ \frac{q_1^2}{\omega^2}\,\varepsilon_z\Big[\vec{\varepsilon}\,'^{*}\cdot\hat{q}\,A_9 + i\vec{\sigma}\cdot\left(\hat{q}\times\hat{q}\,'\right)\vec{\varepsilon}\,'^{*}\cdot\hat{q}\,A_{10} \\
&+ i\vec{\sigma}\cdot\left(\vec{\varepsilon}\,'^{*}\times\hat{q}\right)A_{11} + i\vec{\sigma}\cdot\left(\vec{\varepsilon}\,'^{*}\times\hat{q}\,'\right)A_{12}\Big]\Big\}. \qquad (3.18)
\end{aligned}
$$

χ_i and χ_f denote the two-component Pauli spinors of the incoming and outgoing nucleon, respectively, and σ_i are the Pauli matrices. The advantage of this parametrization over the one in Ref. [GLT 95] is that in the real Compton scattering limit simple relations between the A_i arise from time-reversal invariance.

The parametrization in Eq. (3.18) is a generalization of the parametrization for the real Compton scattering case in Ref. [BKM 95]. All amplitudes A_i are functions of three independent kinematical variables. Furthermore the amplitudes A_1 to A_8 are purely transverse, whereas A_9 to A_{12} are purely longitudinal. Therefore, in the real Compton scattering (RCS) limit ($q_1^2 = 0$) the amplitudes A_9 to A_{12} do not contribute and time-reversal invariance gives rise to the constraints

$$A_7 = A_5, \qquad (3.19)$$

$$A_8 = A_6, \qquad (3.20)$$

resulting in six independent structures for the RCS case.

Since we are interested in the calculation of the hadronic part we split the squared matrix element of VCS into a leptonic and a hadronic tensor

$$\overline{|\mathcal{M}^{\rm VCS}|}^2 = \frac{1}{4}\sum_j \mathcal{M}^{\rm VCS}\,\mathcal{M}^{\rm VCS,*}, \quad j = \{s_i, s_f, S_i, S_f, \lambda'\} \qquad (3.21)$$

$$= \frac{e^6}{4\,(q_1^2)^2} l_{\mu\nu}^{\rm VCS}\,W^{\mu\nu}, \qquad (3.22)$$

where the leptonic tensor $l_{\mu\nu}$

$$l_{\mu\nu}^{\rm VCS} = \sum_{s_i,s_f} \bar{u}(k')\,\gamma_\mu\,u(k)\;\bar{u}(k)\,\gamma_\nu\,u(k'), \qquad (3.23)$$

is well-known (see e.g. [DT 92]), while the hadronic tensor $W^{\mu\nu}$

$$W^{\mu\nu} = \frac{1}{e^4}\sum_{S_i,S_f,\lambda'} \chi_f^\dagger\,\varepsilon_\rho'^{*} H^{\rho\mu}\chi_i\,\chi_i^\dagger\,\varepsilon_\lambda' H^{\dagger,\lambda\nu}\,\chi_f, \qquad (3.24)$$

is specific for VCS.

The matrix element for the Bethe-Heitler process can be calculated using QED and electromagnetic nucleon form factors,

$$\mathcal{M}^{\rm BH} = i\frac{e^3}{t}\varepsilon'^{*,\mu} L_{\mu\nu}\,\bar{u}(p_f)\Gamma^\nu(p_f,p_i)u(p_i), \qquad (3.25)$$

where the leptonic part $L^{\mu\nu}$ reads

$$L^{\mu\nu} = \bar{u}(k')\Big(\gamma^\mu\frac{1}{\not{k}' + \not{q}_1 - m_e + i0^+}\gamma^\nu + \gamma^\nu\frac{1}{\not{k} - \not{q}_2 - m_e + i0^+}\gamma^\mu\Big)u(k), \qquad (3.26)$$

and the photon-nucleon vertex function $\Gamma^\nu(p_f, p_i)$ is given by

$$\Gamma^\nu(p_f, p_i) = F_1\big(q^2\big)\gamma^\nu + \frac{i\kappa}{2m_N} F_2\big(q^2\big)\sigma^{\nu\rho}q_\rho, \qquad \text{with } q = p_f - p_i. \tag{3.27}$$

F_1 and F_2 denote the Dirac and Pauli form factors respectively and κ is the nucleon magnetic moment[3]. For a calculation of the BH part see for example [GV 98].

3.2.1 Low-energy theorems

Using fundamental symmetries, such as Lorentz and gauge invariance as well as crossing symmetry, low energy theorems (LET) have been derived for Compton scattering. For RCS Thirring [Thi 50] showed that the scattering amplitude to leading order in the photon energy is solely described by the charge and the mass of the target, which corresponds to the well-known Thomson limit in classical electrodynamics. Subsequently Low [Low 54] and Gell-Mann and Goldberger [GMG 54] analyzed Compton scattering on spin-$\frac{1}{2}$ particles, and derived a relation between the term linear in the photon energy and the magnetic moments of the spin-$\frac{1}{2}$ particle. Generalizations of the LETs for the VCS case have been considered in Ref. [GLT 95, SKK 96]. In the derivation of LETs for VCS one decomposes the VCS amplitude into a nucleon pole part[4], or Born part $H_B^{\mu\nu}$, and the residual, or non-Born, amplitude $H_R^{\mu\nu}$,

$$H^{\mu\nu} = H_B^{\mu\nu} + H_R^{\mu\nu}. \tag{3.28}$$

The separation is such that $H_B^{\mu\nu}$ contains all nucleon pole terms in the s- and u-channel, whereas the residual part contains all terms regular in the limit $q_2^\mu \to 0$. The Born part is illustrated in Fig. 3.3, where the hatched blobs stand for the photon-nucleon vertex function in Eq. (3.27),

$$\begin{aligned} H_B^{\mu\nu} = -\frac{e^2}{4\pi}\bar{u}(p_f)\Big[&\Gamma^\nu(p_f, p_i + q_1)\frac{\not{p}_i + \not{q}_1 + m_N}{s - m_N^2}\Gamma^\mu(p_i + q_1, p_i) \\ &+ \Gamma^\mu(p_f, p_i - q_2)\frac{\not{p}_i - \not{q}_2 + m_N}{u - m_N^2}\Gamma^\nu(p_i - q_2, p_i)\Big]u(p_i). \end{aligned} \tag{3.29}$$

The LET for VCS essentially states that, to next-to-leading order in the photon energy, i.e. up to and including linear terms, the VCS amplitude is completely fixed by the Born part. Thus no information beyond the electromagnetic form factors and static properties of the nucleon enter in the VCS process. New information on the nucleon structure can only be extracted from the non-Born part of the VCS process. Of course the decomposition of Eq. (3.28) is not unique, however in [SKK 96] it has been shown that using the vertex function of Eq. (3.27) ensures that the Born and non-Born part are separately gauge invariant. As we are interested in contributions to VCS beyond the LET we concentrate on the calculation of the non-Born part in this work. Nevertheless in a theory obeying the above symmetries the LET has to be fulfilled.

[3] Note that any parametrization of the photon-nucleon vertex function which is on-shell equivalent, e.g. Sachs form factors, leads to the same result for the BH process.

[4] In the literature the nucleon pole part is often referred to as the Born part of the amplitude.

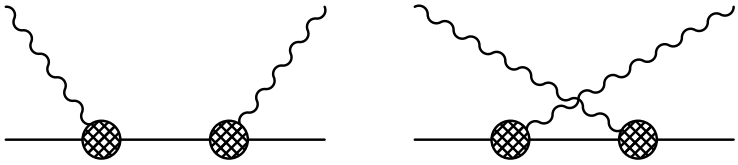

Figure 3.3: Contributions from intermediate nucleon pole diagrams.

In the following we focus on the residual part of the amplitude. For reasons of convenience we work in the four component Dirac space, where the invariant VCS amplitude reads

$$\mathcal{M}^{\gamma^*\gamma} = -ie^2\,\bar{u}(p_f)\varepsilon_\mu\,M_R^{\mu\nu}\,\varepsilon_\nu'^*\,u(p_i), \tag{3.30}$$

$$= \chi_f^\dagger \varepsilon_\mu'^* H_R^{\mu\nu} \varepsilon_\nu \chi_i. \tag{3.31}$$

It is always desirable to work with a set of amplitudes which only depend on the dynamics of the system with the kinematics being factored out. For VCS the construction of such a set of amplitudes, especially one which is free of kinematical singularities, is by no means a trivial task. The first construction of a pole free tensor basis was given by Tarrach [Tar 75]. For the VCS process we use the set of invariant amplitudes constructed in [Dre+ 98],

$$M_R^{\mu\nu} = \sum_{i=1}^{12} \rho_i^{\mu\nu}\, f_i(q_1^2, q_1\cdot q_2, q_1\cdot P), \tag{3.32}$$

where $P = p_f + p_i$ and the tensor basis $\rho_i^{\mu\nu}$ is defined in Eq. (B.2) in Appendix B. It is convenient to introduce the kinematical variable ν,

$$\nu = \frac{s-u}{4m_N}, \tag{3.33}$$

which changes sign under photon-crossing ($s \leftrightarrow u$). In the following we choose the amplitudes f_i to depend on the three independent kinematical variables t, Q^2 and ν. The relation to the four-momenta in Eq. (3.32) reads

$$\begin{aligned} q_1^2 &= -Q^2, \\ q_1\cdot q_2 &= -\frac{1}{2}\big(t+Q^2\big), \\ q_1\cdot P &= 2\,m_N\,\nu, \end{aligned} \tag{3.34}$$

where we have used the definitions in Eq. (3.2) and $q_2^2 = 0$ for the real photon. The particular choice of the $\rho_i^{\mu\nu}$ is such that for the real photon point $Q^2 = 0$ the corresponding amplitudes are either even or odd with respect to crossing,

$$\begin{aligned} f_i\,(0,\nu,t) &= +\,f_i\,(0,-\nu,t)\,,\ (i=1,2,6,11), \\ f_i\,(0,\nu,t) &= -\,f_i\,(0,-\nu,t)\,,\ (i=4,7,9,10). \end{aligned} \tag{3.35}$$

The remaining amplitudes f_3, f_5, f_8, f_{12} do not contribute, because the corresponding tensors vanish in this limit. Using nucleon crossing combined with charge conjugation, one arrives at constraints on the amplitudes for arbitrary virtuality Q^2,

$$\begin{aligned} f_i\left(Q^2,\nu,t\right) &= +f_i\left(Q^2,-\nu,t\right), \ (i=1,2,5,6,7,9,11,12), \\ f_i\left(Q^2,\nu,t\right) &= -f_i\left(Q^2,-\nu,t\right), \ (i=3,4,8,10). \end{aligned} \tag{3.36}$$

From Eqs. (3.35) and (3.36) it follows that f_7 and f_9 vanish at the real photon point. In the calculations of VCS using dispersion relations, it is convenient to work with 12 amplitudes F_i that are all even in ν. Keeping in mind that the non-Born amplitudes are regular functions in the limit $\nu \to 0$ one can define the F_i as

$$\begin{aligned} F_i(Q^2,\nu,t) &= f_i(Q^2,\nu,t), \quad (i=1,2,5,6,7,9,11,12), \\ F_i(Q^2,\nu,t) &= \frac{1}{\nu} f_i(Q^2,\nu,t), \quad (i=3,4,8,10). \end{aligned} \tag{3.37}$$

3.3 Generalized polarizabilities

So far we have established the general structure of the VCS tensor in Eq. (3.32) in terms of invariant amplitudes f_i. In the next step we look at the low-energy representation of the VCS process. As was shown in Ref. [GLT 95] the general VCS amplitude expanded to terms linear in the energy of the outgoing photon ω', can be described using so-called generalized polarizabilities. The term generalized polarizability originates from the analysis of real Compton scattering, where the contributions beyond the LET can be parameterized in terms of 6 independent structure functions, which, in a classical theory, correspond to induced magnetic and electric dipole moments [Rag 93, Rag 94]. Among these polarizabilities two are spin-independent and allow for an interpretation as the deformation of the nucleon charge distribution and magnetization under the influence of an incident photon. They are called electric (α) and magnetic (β) polarizabilities. We first elaborate on the structure functions of VCS and then address the limit to the RCS case.

In order to illuminate notations and the definition of the generalized polarizabilities (GP) we recall the construction of the multipoles [GLT 95]. We start by writing the partial wave decomposition of the regular part of the hadronic tensor

$$\begin{aligned} &H_R^{\mu\nu}(\vec{q}\,m,\vec{q}\,'\,m') = \\ &\mathcal{N} \sum_{L,M,L',M'} \sum_{\rho,\rho'=0}^{3} g_{\rho'\rho'}\, V^{\nu}(\rho'\,L'\,M',\hat{q}\,')H_R^{\rho'\,L'\,M',\rho\,L\,M}(\bar{q}\,m,\omega'\,m')g_{\rho\rho}\,V^{\mu\,*}(\rho\,L\,M,\hat{q}), \end{aligned} \tag{3.38}$$

where m (m') are the projection of the incoming (outgoing) nucleon spin on the z-axis, L (L') is the angular momentum of the initial (final) photon and the index ρ (ρ') indicates the type of multipole ($\rho = 0$ scalar, $\rho = 1$ magnetic, $\rho = 2$ electric, and $\rho = 3$ longitudinal). The basis vectors V^{μ} are functions of the spherical harmonics

Y_{LM}, satisfying the relations

$$\sum_{L,M}\sum_{\rho=0}^{3} g_{\rho\rho} V^{\mu}(\rho\, L\, M, \hat{k})\, V^{\nu\,*}(\rho\, L\, M, \hat{k}') = g^{\mu\nu}\delta(\hat{k}-\hat{k}'), \tag{3.39}$$

$$\int d\hat{k} V^{\mu\,*}(\rho\, L\, M, \hat{k})\, V_{\mu}(\rho'\, L'\, M', \hat{k} = g_{\rho\rho'}\delta_{LL'}\delta_{MM'}. \tag{3.40}$$

We choose the basis to be [GLT 95]

$$V^{\mu}(0LM,\hat{k}) = \big(Y_{LM}(\hat{k}), \vec{0}\,\big), \tag{3.41}$$

$$V^{\mu}(1LM,\hat{k}) = \big(0, \vec{\mathcal{M}}_{LM}(\hat{k})\big), \tag{3.42}$$

$$V^{\mu}(2LM,\hat{k}) = \big(0, \vec{\mathcal{E}}_{LM}(\hat{k})\big), \tag{3.43}$$

$$V^{\mu}(3LM,\hat{k}) = \big(0, \vec{\mathcal{L}}_{LM}(\hat{k})\big), \tag{3.44}$$

where the magnetic ($\vec{\mathcal{M}}$), electric ($\vec{\mathcal{E}}$) and longitudinal ($\vec{\mathcal{L}}$) vectors are defined by

$$\vec{\mathcal{M}}_{LM}(\hat{k}) = \vec{\mathcal{Y}}^{L}_{LM}(\hat{k}), \tag{3.45}$$

$$\vec{\mathcal{E}}_{LM}(\hat{k}) = \sqrt{\frac{L+1}{2L+1}}\,\vec{\mathcal{Y}}^{L-1}_{LM}(\hat{k}) + \sqrt{\frac{L}{2L+1}}\,\vec{\mathcal{Y}}^{L+1}_{LM}(\hat{k}), \tag{3.46}$$

$$\vec{\mathcal{L}}_{LM}(\hat{k}) = \sqrt{\frac{L}{2L+1}}\,\vec{\mathcal{Y}}^{L-1}_{LM}(\hat{k}) - \sqrt{\frac{L+1}{2L+1}}\,\vec{\mathcal{Y}}^{L+1}_{LM}(\hat{k}), \tag{3.47}$$

using the definition

$$\vec{\mathcal{Y}}^{l}_{LM}(\hat{k}) = \sum_{\lambda,\mu}\langle l\lambda, 1\mu|LM\rangle Y_{l\lambda}(\hat{k})\hat{e}(\mu), \qquad \mu = 0, \pm 1, \tag{3.48}$$

and $\hat{e}(\mu)$ denotes the helicity eigenstate of a photon with momentum k. For symmetry reasons the outgoing photon is at first not assumed to be real, i.e ρ' runs from 0 to 3. Using Eq. (3.40) one can write the multipoles as

$$H_R^{\rho'\,L'\,M',\rho\,L\,M}(\bar{q}\,m,\omega'\,m') = \frac{1}{\mathcal{N}}\int d\hat{q}\int d\hat{q}'\, V_{\mu}(\rho LM,\hat{q}) H_R^{\mu\nu}(\vec{q}m,\vec{q}'m') V_{\nu}^{*}(\rho' L' M',\hat{q}'). \tag{3.49}$$

Utilizing current conservation, i.e. $q_{\mu}H_R^{\mu\nu} = 0$, constraints arise between multipoles with $\rho, \rho' = 0, 3$

$$H_R^{\rho' L' M', 3LM}(\bar{q}m,\omega',m') = -\frac{\omega}{\bar{q}} H_R^{\rho' L' M', 0LM}(\bar{q}m,\omega',m'), \tag{3.50}$$

$$H_R^{3L'M',\rho LM}(\bar{q}m,\omega',m') = -H_R^{0L'M',\rho LM}(\bar{q}m,\omega',m'), \tag{3.51}$$

therefore one can eliminate $\rho', \rho = 3$ in favor of $\rho, \rho' = 0$[5]. Through an appropriate redefinition of the basis vectors

$$W^{\mu}(\rho LM,\hat{q}) = V^{\mu}(\rho LM,\hat{q}), \quad (\rho = 1, 2) \tag{3.52}$$

[5]This amounts to replacing the longitudinal multipoles with the corresponding charge or scalar multipoles.

$$W^\mu(0LM,\hat{q}) = V^\mu(0LM,\hat{q}) + \frac{\omega}{\bar{q}} V^\mu(3LM,\hat{q}), \tag{3.53}$$

the multipoles can be defined with ρ (ρ') running from 0 to 2. Using the Wigner-Eckart theorem the dependence of the multipoles on magnetic quantum numbers of the photons and nucleons can be expressed via Clebsch-Gordan coefficients and we define the reduced multipoles as

$$H_R^{(\rho' L',\rho L)S}(\bar{q},\omega) = \sum_{m,m',M,M'} (-1)^{\frac{1}{2}+m'+L+M} \langle \frac{1}{2} - m', \frac{m}{2} | Ss \rangle \langle L'M', L - M | Ss \rangle H_R^{\rho' L' M',\rho L M}(\bar{q}m,\omega' m'), \tag{3.54}$$

where the spins of the nucleons have been combined to the total spin S and any of the projections s can be taken. In the nomenclature of the reduced multipoles ρ (ρ') characterizes the incoming (outgoing) photon, $\rho = 0$ scalar or charge type, $\rho = 1$ magnetic type, $\rho = 2$ electric type, whereas L (L') denotes the angular momentum of the incoming (outgoing) photon. We furthermore distinguish multipoles with $S = 0$ (scalar multipoles) describing a transition without spin-flip of the nucleons, and $S = 1$ (vector multipoles) describing a spin-flip transition. The reduced multipoles are subject to selection rules

$$S = 0, 1, \qquad |L' - s| \leq L \leq L' + S, \qquad (-1)^{\rho'+L'} = (-1)^{\rho+L} \quad (\rho, \rho' = 0, 1, 2),$$

stemming from parity and angular momentum conservation.

We are interested in the low-energy behavior of the reduced multipoles, i.e. $(\bar{q},\omega') \to (0,0)$. If the outgoing photon is real the case of electric transitions ($\rho' = 2$) can be related to charge multipoles ($\rho' = 0$) using Siegert's theorem [Sie 37]. However, the incoming photon is virtual and the electric multipole cannot be replaced with the charge multipoles anymore. In [GLT 95] so-called mixed multipoles $\hat{H}_R^{\mu\nu}$ were introduced, which are no longer characterized by a well-defined multipole type but have the desired low-energy behavior. The definition of the GPs in terms of reduced and mixed multipoles read

$$P^{(\rho' L',\rho L)S}(\bar{q}) = \Big[\frac{1}{\omega'^{L'} \bar{q}^L} H_R(\rho' L', \rho L) S(\bar{q},\omega') \Big]_{\omega'=0}, \qquad (\rho, \rho' = 0, 1) \tag{3.55}$$

$$\hat{P}^{(\rho' L',L)S}(\bar{q}) = \Big[\frac{1}{\omega'^{L'} \bar{q}^{L+1}} \hat{H}_R(\rho' L', L) S(\bar{q},\omega') \Big]_{\omega'=0}, \qquad (\rho' = 0, 1). \tag{3.56}$$

The expansion of the reduced multipoles to leading order in ω', can be parameterized using the above GPs,

$$H_R^{(1L',\rho L)S}(\bar{q},\omega') = \omega'^{L'}\, \bar{q}^L P^{(1L',\rho L)S}(\bar{q}) + \mathcal{O}\big(\omega'^{L'+1}\big), \tag{3.57}$$

$$H_R^{(2L',\rho L)S}(\bar{q},\omega') = -\omega'^{L'}\, \bar{q}^L \sqrt{\frac{L'+1}{L'}} P^{(0L',\rho L)S}(\bar{q}) + \mathcal{O}\big(\omega'^{L'+1}\big), \tag{3.58}$$

$$H_R^{(1L',2L)S}(\bar{q},\omega') = -\omega'^{L'}\, \bar{q}^L \Big[\sqrt{\frac{L+1}{L}} \frac{\omega_0}{\bar{q}} P^{(1L',0L)S}(\bar{q}) + \sqrt{\frac{2L+1}{L}} \bar{q} \hat{P}^{(1L',L)S}(\bar{q}) \Big]$$

$$+\mathcal{O}\big(\omega'^{L'+1}\big), \tag{3.59}$$

$$H_R^{(2L',2L)S}(\bar{q},\omega') = \omega'^{L'}\,\bar{q}^L\sqrt{\frac{L'+1}{L'}}\Big[\sqrt{\frac{L+1}{L}}\frac{\omega_0}{\bar{q}}P^{(0L',0L)S}(\bar{q}) + \sqrt{\frac{2L+1}{L}}\bar{q}\hat{P}^{(0L',L)S}(\bar{q})\Big]$$
$$+\mathcal{O}\big(\omega'^{L'+1}\big), \tag{3.60}$$

where

$$\omega_0 = m_N - E_i.$$

Since the VCS amplitudes are expanded to terms linear in ω' the final state only allows for electric and magnetic dipole transitions ($L'=1$). Taking the selection rules into account, we are left with 10 independent multipoles and thus 10 GPs as well, where 3 are of scalar (spin-independent) and 7 of vector type (spin-dependent). An indication that not all of the GPs are independent was first seen in an explicit calculation in the linear sigma model [MD 96], where a relation between the scalar polarizabilities was found. In [Dre+ 97] this relation was derived in a model-independent way employing charge conjugation and nucleon crossing, and later in [Dre+ 98] the analysis was extended to the spin-dependent GPs leading to three additional relations. The relations read

$$0 = \sqrt{\frac{3}{2}}P^{(01,01)0}(\bar{q}^2) + \sqrt{\frac{3}{8}}P^{(11,11)0}(\bar{q}^2) + \frac{3\bar{q}^2}{2\omega_0}\hat{P}^{(01,1)0}(\bar{q}^2)\,, \tag{3.61}$$

$$0 = P^{(11,11)1}(\bar{q}^2) + \sqrt{\frac{3}{2}}\omega_0 P^{(11,02)1}(\bar{q}^2) + \sqrt{\frac{5}{2}}\bar{q}^2\hat{P}^{(11,2)1}(\bar{q}^2)\,, \tag{3.62}$$

$$0 = 2\omega_0 P^{(01,01)1}(\bar{q}^2) + 2\frac{\bar{q}^2}{\omega_0}P^{(11,11)1}(\bar{q}^2) - \sqrt{2}\bar{q}^2 P^{(01,12)1}(\bar{q}^2)$$
$$+\sqrt{6}\bar{q}^2\hat{P}^{(01,1)1}(\bar{q}^2)\,, \tag{3.63}$$

$$0 = 3\frac{\bar{q}^2}{\omega_0}P^{(01,01)1}(\bar{q}^2) - \sqrt{3}P^{(11,00)1}(\bar{q}^2) - \sqrt{\frac{3}{2}}\bar{q}^2 P^{(11,02)1}(\bar{q}^2)\,. \tag{3.64}$$

Thus, assuming charge conjugation and nucleon crossing symmetry, one can describe the residual part of the VCS tensor using 6 instead of 10 independent generalized polarizabilities. Two of the scalar polarizabilities are generalizations of the electric and magnetic polarizabilities of RCS,

$$\alpha(\bar{q}^2) = -\frac{e^2}{4\pi}\sqrt{\frac{3}{2}}P^{(01,01)0}(\bar{q}^2), \quad \beta(\bar{q}^2) = -\frac{e^2}{4\pi}\sqrt{\frac{3}{8}}P^{(11,11)0}(\bar{q}^2), \tag{3.65}$$

thus one conveniently eliminates $\hat{P}^{(01,1)0}$ using Eq. (3.61). For the spin-dependent GPs, however, it is not obvious which are preferable.

The leading-order terms in ω' of the amplitudes A_i defined in Eq. (3.18) read

$$A_1 = \omega'\sqrt{\frac{E_i}{m_N}}\Big[-\sqrt{\frac{3}{2}}\omega_0 P^{(01,01)0}(\bar{q}^2) - \frac{3}{2}\bar{q}^2\hat{P}^{(01,1)0}(\bar{q}^2) - \sqrt{\frac{3}{8}}\bar{q}\cos\theta P^{(11,11)0}(\bar{q}^2)\Big]$$
$$+\mathcal{O}(\omega'^2)\,,$$

$$
\begin{aligned}
A_2 &= \omega' \sqrt{\frac{E_i}{m_N}} \left[\sqrt{\frac{3}{8}} \bar{q} P^{(11,11)0}(\bar{q}^2) \right] + \mathcal{O}(\omega'^2) \,, \\
A_3 &= \omega' \sqrt{\frac{E_i}{m_N}} \frac{3}{4} \Bigg[-2\omega_0 P^{(01,01)1}(\bar{q}^2) + \sqrt{2}\bar{q}^2 \Big[P^{(01,12)1}(\bar{q}^2) - \sqrt{3} \hat{P}^{(01,1)1}(\bar{q}^2) \Big] \\
&\quad + \Big(-\bar{q} P^{(11,11)1}(\bar{q}^2) + \sqrt{\frac{3}{2}} \omega_0 \bar{q} P^{(11,02)1}(\bar{q}^2) + \sqrt{\frac{5}{2}} \bar{q}^3 \hat{P}^{(11,2)1}(\bar{q}^2) \Big) \cos\theta \Bigg] \\
&\quad + \mathcal{O}(\omega'^2) \,, \\
A_4 &= \omega' \sqrt{\frac{E_i}{m_N}} \frac{3}{4} \Bigg[-\bar{q} P^{(11,11)1}(\bar{q}^2) - \sqrt{\frac{3}{2}} \omega_0 \bar{q} P^{(11,02)1}(\bar{q}^2) - \sqrt{\frac{5}{2}} \bar{q}^3 \hat{P}^{(11,2)1}(\bar{q}^2) \Bigg] \\
&\quad + \mathcal{O}(\omega'^2) \,, \\
A_5 &= -A_4 \,, \\
A_6 &= \mathcal{O}(\omega'^2) \,, \\
A_7 &= \omega' \sqrt{\frac{E_i}{m_N}} \frac{3}{4} \left[\bar{q} P^{(11,11)1}(\bar{q}^2) - \sqrt{\frac{3}{2}} \omega_0 \bar{q} P^{(11,02)1}(\bar{q}^2) - \sqrt{\frac{5}{2}} \bar{q}^3 \hat{P}^{(11,2)1}(\bar{q}^2) \right] + \mathcal{O}(\omega'^2) \,, \\
A_8 &= \omega' \sqrt{\frac{E_i}{m_N}} \left[-\frac{3}{\sqrt{2}} \bar{q}^2 P^{(01,12)1}(\bar{q}^2) \right] + \mathcal{O}(\omega'^2) \,, \\
A_9 &= \omega' \sqrt{\frac{E_i}{m_N}} \left[-\omega_0 \sqrt{\frac{3}{2}} P^{(01,01)0}(\bar{q}^2) \right] + \mathcal{O}(\omega'^2) \,, \\
A_{10} &= \omega' \sqrt{\frac{E_i}{m_N}} \left[-\frac{3\sqrt{3}}{2\sqrt{2}} \omega_0 \bar{q} P^{(11,02)1}(\bar{q}^2) \right] + \mathcal{O}(\omega'^2) \,, \\
A_{11} &= \omega' \sqrt{\frac{E_i}{m_N}} \left[-\frac{3}{2} \omega_0 P^{(01,01)1}(\bar{q}^2) + \frac{3\sqrt{3}}{2\sqrt{2}} \omega_0 \bar{q} \cos\theta P^{(11,02)1}(\bar{q}^2) \right] + \mathcal{O}(\omega'^2) \,, \\
A_{12} &= \omega' \sqrt{\frac{E_i}{m_N}} \left[\frac{\sqrt{3}\omega_0}{2\bar{q}} \Big[P^{(11,00)1}(\bar{q}^2) - \sqrt{2}\bar{q}^2 P^{(11,02)1}(\bar{q}^2) \Big] \right] + \mathcal{O}(\omega'^2) \,.
\end{aligned}
$$

Since we extract the f_i of Eq. (3.32) in our calculation, we need to establish the connection between the GPs and the f_i. Evaluating Eq. (3.32) in the center of mass frame one can get another low-energy expansion of the A_i [Dre+ 98]. Subsequently using the relations arising from charge conjugation and nucleon crossing symmetry the GPs can be expressed as functions of the f_i, and the explicit expressions read

$$
\begin{aligned}
P^{(01,01)0}(\bar{q}^2) &= \sqrt{\frac{2}{3}} \sqrt{\frac{E_i + m_N}{2E_i}} \Big[f_1(\bar{q}^2) - 2m_N \frac{\bar{q}^2}{\omega_0} f_2(\bar{q}^2) \Big] = -\frac{4\pi}{e^2} \sqrt{\frac{2}{3}} \alpha(\bar{q}^2), \\
P^{(11,11)0}(\bar{q}^2) &= -\sqrt{\frac{8}{3}} \sqrt{\frac{E_i + m_N}{2E_i}} f_1(\bar{q}^2) = -\frac{4\pi}{e^2} \sqrt{\frac{8}{3}} \beta(\bar{q}^2), \\
\hat{P}^{(01,1)0}(\bar{q}^2) &= \frac{4}{3} m_N \sqrt{\frac{E_i + m_N}{2E_i}} f_2(\bar{q}^2), \\
P^{(01,12)1}(\bar{q}^2) &= \frac{\sqrt{2}}{3} \sqrt{\frac{E_i + m_N}{2E_i}} \frac{m_N \omega_0}{\bar{q}^2} \Big[8m_N f_6(\bar{q}^2) + f_7(\bar{q}^2) + 4m_N f_9(\bar{q}^2)
\end{aligned}
$$

$$
\begin{aligned}
&\quad + 4f_{11}(\bar{q}^2) - \omega_0 f_{12}(\bar{q}^2)\Big]\,,\\
P^{(11,02)1}(\bar{q}^2) &= \frac{2\sqrt{2}}{3\sqrt{3}}\sqrt{\frac{E_i+m_N}{2E_i}}\Big[\frac{\omega_0^2}{2\bar{q}^2}f_5(\bar{q}^2) + \frac{1}{2}f_7(\bar{q}^2) + 2f_{11}(\bar{q}^2) + \frac{m_N\omega_0^2}{\bar{q}^2}f_{12}(\bar{q}^2)\Big]\,,\\
P^{(01,01)1}(\bar{q}^2) &= \frac{1}{3}\sqrt{\frac{E_i+m_N}{2E_i}}\omega_0\Big[f_5(\bar{q}^2) + f_7(\bar{q}^2) + 4f_{11}(\bar{q}^2) + 4m_N f_{12}(\bar{q}^2)\Big]\,,\\
P^{(11,00)1}(\bar{q}^2) &= \frac{2}{3\sqrt{3}}\sqrt{\frac{E_i+m_N}{2E_i}}\Big[\big(\omega_0^2 - 3m_N\omega_0\big)f_5(\bar{q}^2) + \bar{q}^2 f_7(\bar{q}^2)\\
&\quad + 4\bar{q}^2 f_{11}(\bar{q}^2) + \big(3m_N\bar{q}^2 - 6m_N^2\omega_0 + 2m_N\omega_0^2\big)f_{12}(\bar{q}^2)\Big]\,,\\
P^{(11,11)1}(\bar{q}^2) &= -\frac{2}{3}\sqrt{\frac{E_i+m_N}{2E_i}}\frac{m_N\omega_0^2}{\bar{q}^2}\Big[f_5(\bar{q}^2) + \omega_0 f_{12}(\bar{q}^2)\Big]\,,\\
\hat{P}^{(11,2)1}(\bar{q}^2) &= -\frac{2\sqrt{2}}{3\sqrt{5}}\frac{\omega_0}{\bar{q}^2}\Big[\big(\frac{\omega_0^2}{2\bar{q}^2} - \frac{m_N\omega_0}{\bar{q}^2}\big)f_5(\bar{q}^2) + \frac{1}{2}f_7(\bar{q}^2) + 2f_{11}(\bar{q}^2)\Big]\,,\\
\hat{P}^{(01,1)1}(\bar{q}^2) &= \frac{1}{3\sqrt{6}}\sqrt{\frac{E_i+m_N}{2E_i}}\frac{\omega_0}{\bar{q}^2}\Big[\big(4m_N - 2\omega_0\big)f_5(\bar{q}^2) + 16m_N^2 f_6(\bar{q}^2) +\\
&\quad 2\big(m_N - \omega_0\big)f_7(\bar{q}^2) + 8m_N^2 f_9(\bar{q}^2) + 8\big(m_N - \omega_0\big)f_{11}(\bar{q}^2)\\
&\quad - 6m_N\omega_0 f_{12}(\bar{q}^2)\Big]\,.
\end{aligned}
\tag{3.66}
$$

In the above equations, due to the expansion in ω', the invariant amplitudes are functions of the three-momentum of the incoming photon, i.e. $f_i(\bar{q}^2) \equiv f_i|_{\omega'=0} = f_i(2m_N\omega_0, 0, 0)$. In terms of the kinematical invariants introduced in Eq. (3.34) this corresponds to $\nu \to 0$ and $t \to -Q^2$.

3.3.1 Observables

In general the GPs are only accessible in polarization experiments, with the exception of $\alpha(\bar{q}^2)$. For unpolarized experiments the extraction of four linear combinations of GPs was suggested in [GLT 95], which, using the abbreviation $Q_0^2 = -2m_N\omega_0$, are given by

$$
P_{LL}(\bar{q}) = -2\sqrt{6}m_N G_E(Q_0^2)P^{(01,01)0}(\bar{q}^2)\,, \tag{3.67}
$$

$$
P_{TT}(\bar{q}) = \frac{3}{2}G_M(Q_0^2)\Big[2\omega_0 P^{(01,01)1}(\bar{q}^2) + \sqrt{2}\bar{q}^2\Big(P^{(01,12)1}(\bar{q}^2) + \sqrt{3}\hat{P}^{(01,1)1}(\bar{q}^2)\Big)\Big]\,, \tag{3.68}
$$

$$
\begin{aligned}
P_{LT}(\bar{q}) &= \sqrt{\frac{3}{2}}\frac{m_N\bar{q}}{\sqrt{Q_0^2}}G_E(Q_0^2)P^{(11,11)0}(\bar{q}^2)\\
&\quad + \frac{\sqrt{3}\sqrt{Q_0^2}}{2\bar{q}}G_M(Q_0^2)\Big(P^{(11,00)1}(\bar{q}^2) + \frac{\bar{q}^2}{\sqrt{2}}P^{(11,02)1}(\bar{q}^2)\Big)\,,
\end{aligned}
\tag{3.69}
$$

$$
P'_{LT}(\bar{q}) = \sqrt{\frac{3}{2}}\frac{m_N}{\sqrt{Q_0^2}}G_E(Q_0^2)\Big(2\omega_0 P^{(01,01)0}(\bar{q}^2) + \sqrt{6}\bar{q}^2\hat{P}^{(01,1)0}(\bar{q}^2)\Big)
$$

$$- \frac{3}{2}\sqrt{Q_0^2} G_M(Q_0^2) P^{(01,01)1}(\bar{q}^2)\,, \tag{3.70}$$

with $G_E(Q_0^2)$ and $G_M(Q_0^2)$ denoting the electric and magnetic Sachs form factors respectively. In [Dre+ 98] it was shown that P'_{LT} and P_{LT} satisfy the relation

$$P_{LT}(\bar{q}) + \frac{\bar{q}}{\omega_0} P'_{LT}(\bar{q}) = 0\,. \tag{3.71}$$

The conclusion is that for an unpolarized experiments 3 structure functions are extractable, which are parameterized by 5 generalized polarizabilities.

The RCS limit corresponds to $Q^2 \to 0$. The relations between the f_i and the polarizabilities of RCS by Ragusa [Rag 94] read

$$\alpha(0) = \frac{e^2}{4\pi}\big(-f_{1,0} - 4m_N^2 f_{2,0}\big), \tag{3.72}$$

$$\beta(0) = \frac{e^2}{4\pi} f_{1,0}, \tag{3.73}$$

$$\gamma_1 = \frac{e^2}{4\pi}\big(-8m_N^2 f_{4,1} - 4m_N f_{10,1} - 4f_{11,0}\big), \tag{3.74}$$

$$\gamma_2 = \frac{e^2}{4\pi} 4m_N f_{10,1}, \tag{3.75}$$

$$\gamma_3 = \frac{e^2}{4\pi}\big(4m_N f_{6,0} + 2f_{11,0}\big), \tag{3.76}$$

$$\gamma_4 = -\frac{e^2}{4\pi}\big(4m_N f_{10,1} + 2f_{11,0}\big). \tag{3.77}$$

The subscript denotes differentiation with respect to ν, i.e.

$$f_{i,a} = \frac{\partial^a}{\partial \nu^a} f_i(Q^2, \nu)|_{\nu=0}, \tag{3.78}$$

or equivalently using Eq. (3.37)

$$f_{i,0} = \bar{F}_i(Q^2) \qquad (i = 1, 2, 5, 6, 7, 9, 11, 12), \tag{3.79}$$

$$f_{i,1} = \bar{F}_i(Q^2) \qquad (i = 3, 4, 8, 10), \tag{3.80}$$

where

$$\bar{F}_i(Q^2) = F_i(Q^2, \nu = 0, t = -Q^2). \tag{3.81}$$

In [Bab+ 98] linear combinations of the spin-dependent polarizabilities have been defined, which allow for a straightforward physical interpretation in terms of the interaction of the nucleon with an external electromagnetic field. For the spin-dependent transitions four parameters are needed, which describe the electric and magnetic dipole transitions (γ_{E1E1} and γ_{M1M1}) and dipole-quadrupole transitions (γ_{M1E2} and γ_{E1M2}) respectively. The relations between the polarizabilities of [Rag 94] and [Bab+ 98] read

$$\gamma_{E1E1} = -\gamma_1 - \gamma_3, \tag{3.82}$$

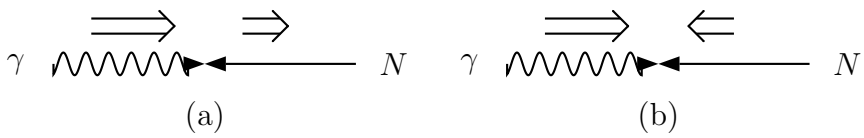

(a) (b)

Figure 3.4: Illustration of the helicity cross section. Double arrows denote the the spin projection. The helicity 3/2 (a) and helicity 1/2 (b) transitions are depicted.

$$\gamma_{M1M1} = \gamma_4, \tag{3.83}$$
$$\gamma_{E2M1} = \gamma_2 + \gamma_4, \tag{3.84}$$
$$\gamma_{M2E1} = \gamma_3. \tag{3.85}$$

Moreover in the forward (backward) kinematics, the RCS amplitudes only depend on the sum (difference) of α and β and the forward spin polarizability γ_0 (backward spin polarizability γ_π). The forward and backward spin polarizability are defined as

$$\gamma_0 = \gamma_1 - \gamma_2 + 2\gamma_4 = -\gamma_{E1E1} - \gamma_{M1M1} - \gamma_{M1E2} - \gamma_{E1M2}, \tag{3.86}$$
$$\gamma_\pi = \gamma_1 + \gamma_2 + 2\gamma_4 = -\gamma_{E1E1} + \gamma_{M1M1} + \gamma_{M1E2} - \gamma_{E1M2}. \tag{3.87}$$

The RCS amplitude for forward scattering ($\theta = 0, \hat{q} = \hat{q}\,'$) is particularly interesting, because it allows for the investigation of sum rules. As mentioned above the RCS amplitude depends on two structure functions

$$T(\nu, \theta = 0) = \vec{\varepsilon}^{\,\prime *} \cdot \vec{\varepsilon}\, f(\nu) + i\vec{\sigma} \cdot \left(\vec{\varepsilon}^{\,\prime *} \times \vec{\varepsilon}\right) g(\nu). \tag{3.88}$$

The expansion of the structure functions f and g reads

$$f(\nu) = -\frac{e^2}{4\pi}\frac{e_N^2}{m_N} + \left(\alpha + \beta\right)\nu^2 + \mathcal{O}(\nu^4), \tag{3.89}$$
$$g(\nu) = -\frac{e^2}{4\pi}\frac{\kappa_N^2}{2m_N^2}\,\nu + \gamma_0\nu^3 + \mathcal{O}(\nu^5). \tag{3.90}$$

The first term on the right hand side of Eq. (3.89) is the well-known Thomson limit, whereas the sum of the electric and magnetic polarizability is related to the total photo absorption cross section via the Baldin sum rule [Bal 60]

$$\alpha + \beta = \frac{1}{2\pi^2}\int\limits_{\nu_0}^{\infty} d\nu'\, \frac{\sigma_{\gamma N \to X}(\nu')}{\nu'^2}. \tag{3.91}$$

For the structure function $g(\nu)$ the first term involves the anomalous magnetic moment of the nucleon and can be related to the weighted integral over the difference of the helicity cross sections (see Fig. 3.4) according to the Gerasimov-Drell-Hearn sum rule [Ger 66, DH 66]

$$-\frac{e^2}{4\pi}\frac{\kappa_N^2}{2m_N^2} = \int\limits_{\nu_0}^{\infty} d\nu'\, \frac{\sigma_{3/2}(\nu') - \sigma_{1/2}(\nu')}{\nu'}. \tag{3.92}$$

The forward spin polarizability γ_0 fulfills the corresponding sum rule [GMG 54, GMGT 54]

$$\gamma_0 = -\frac{1}{4\pi^2} \int\limits_{\nu_0}^{\infty} d\nu' \, \frac{\sigma_{3/2}(\nu') - \sigma_{1/2}(\nu')}{\nu'^3}. \tag{3.93}$$

Finally in [L'v+ 01] the generalized scalar polarizabilities were introduced. They are defined in a fully covariant framework as opposed to the multipole decomposition of [GLT 95]. In order to fully recover the induced electric polarization it is mandatory to include, in addition to the longitudinal polarizability α_L, the transverse electric polarizability α_T. This in turn affects the *local* response of the nucleon to an external electromagnetic field, i.e. the polarizability has to be treated as tensor rather than a scalar quantity. More specifically, if the nucleon is exposed to a static and uniform electric field $\vec{E}$, the polarizability can be written as

$$\mathcal{P}_i(\vec{r}) = 4\pi\alpha_{ij}(\vec{r})\, E_j. \tag{3.94}$$

The generalized scalar polarizabilities in terms of our invariant amplitudes are defined as

$$\alpha_L(Q^2) = -\frac{e^2}{4\pi}\sqrt{1-\frac{Q^2}{4m_N^2}}\left[\bar{F}_1 + (4m_N^2 - Q^2)\bar{F}_2 - Q^2(2\bar{F}_6 + \bar{F}_9 - \bar{F}_{12})\right], \tag{3.95}$$

$$\begin{aligned}\alpha_T(q_1^2) = \alpha_L(Q^2) + \frac{e^2}{4\pi}Q^2\sqrt{1-\frac{Q^2}{4m_N^2}}\Bigg[&\frac{4m_N^2 - Q^2}{2m_N}\bar{F}_3 - 2\bar{F}_6 - \bar{F}_9 \\ &+ \frac{1}{m_N}\bar{F}_{10} + \bar{F}_{12}\Bigg].\end{aligned} \tag{3.96}$$

In particular, if the longitudinal and transverse polarizability are equal, the polarization of the nucleon points in the direction of the external electric field. In this case the longitudinal polarizability suffices to fully describe the induced polarization.

Chapter 4

Technical details

In this chapter we present technical details of our calculation. This concerns in particular the computer aided calculation of Feynman diagrams. More specifically we give an account of the existing programs used in this work and further elaborate on self-written programs as well as the adjustments of the existing programs necessary for calculations in BχPT. It is worth noting that using the reformulated version of the infrared regularization scheme allows us to use most of the programs developed in the high-energy physics community, especially concerning the numerical evaluation of the one-loop integrals, e.g. LoopTools [Hah 01]. This is a major advantage of the relativistic calculation over heavy-baryon chiral perturbation theory.

With the growing complexity of perturbative calculations, foremost in high-energy physics, a lot of improvements and new developments in the automatization of several common tasks have emerged in recent years. There is a large variety of programs specialized on certain aspects of Feynman diagram evaluations, e.g. FeynArts, FormCalc, FeynCalc, LoopTools [Hah 01, HPV 99, MBD 91] or the FF library [OV 90]. Some projects aim at providing a complete environment for the calculation of Feynman diagrams, e.g. GiNaC/Xloops [BFK 00, BD 02] or Diana/aITALC [TF 00, LR 06]. For the algebraic part most programs use modern computer algebra systems (CAS), such as Mathematica, Maple or FORM [Ver 00]. The numerical part of the calculation is usually carried out using either C or FORTRAN. Deciding which programs are best suited depends on the problem at hand as well as personal taste. A full account of the strengths and weaknesses of the various programs is beyond the scope of this work. Therefore we merely state our preferences concerning the calculations in this work. As we are most familiar with Mathematica and FORM, we choose programs based on these CAS over other systems. Whenever the loss in performance is not too large, we chose convenience over efficiency. Moreover, in an attempt to keep the calculations as transparent as possible, we prefer algorithms which emulate calculations performed by hand over computer optimized algorithms. Even though we did not intend to provide a general purpose system for calculations in BχPT, most of the programs have been kept as general as possible. Since we use existing C-code for the calculation of physical observables from our invariant amplitudes, we choose C for numerical evaluation of the amplitudes. The C-code for the numerical calculation of Compton scattering

observables (CSO) was developed by Barbara Pasquini [Pas 05].

We split the calculation into three distinct parts. The first part is concerned with the generation of the diagrams contributing to the given process. In the second part algebraic simplifications are performed, e.g. Dirac or isospin algebra. Finally the numerical evaluation is carried out, e.g. calculation of cross sections. In the following we give an account of the implementations of these three steps. We will mostly concentrate on the problems arising in the calculation of one-loop diagrams.

4.1 Diagram generation

The generation of diagrams is based on the Lagrangian, providing the complete dynamics of the theory. One starts out by deriving all possible Feynman rules, which may contribute to a given process. Because the number of possible interaction terms quickly grows with the chiral order, already this step is rather cumbersome in BχPT. The Lagrangian of Ref. [Fet+ 00] contains 7 terms at order $\mathcal{O}(q^2)$, 23 terms at order $\mathcal{O}(q^3)$ and 118 terms at order $\mathcal{O}(q^4)$. Furthermore, given the nonlinear representation of the pions, each order contains all interactions with *any* number of pions. Therefore, in order to obtain the Feynman rules, one has to expand the Lagrangian of each order to the sought-after number of pions. Only a limited number of all possible terms at each order is actually necessary to derive all Feynman rules needed in this work. The necessary Feynman rules are given in Appendix A. We have checked the manually derived Feynman rules with expressions obtained using the *Phi* package by Frederik Orellana. *Phi* is an extension to the FeynCalc package, supporting the expansion of Lagrangians in terms of pion fields.

Using these rules one has to draw all possible diagrams contributing to the given process. The complexity of this task grows with an increasing number of particles in the initial and final state and, for BχPT, with the chiral order one is interested in. The one-loop calculation of the nucleon self-energy to order $\mathcal{O}(q^4)$ requires the calculation of two diagrams, whereas for VCS we need to calculate 100 one-loop diagrams. Given the relatively large number of diagrams the use of a computer based diagram generator is highly desirable. Of course the available diagram generators were not developed for χPT calculations, but rather for calculations within the Standard Model where up to several thousands of diagrams contribute to a given process. In fact our demands on the diagram generator differ from the Standard Model. Since we are working with an effective field theory (EFT) we need *non-renormalizable* vertices, i.e. vertices with more than 4 adjacent lines. Moreover, we need vertices with the same number of adjacent lines but different chiral order. The list of available general purpose diagram generators matching our needs is rather short. There are two packages we are aware of, the Fortran program QGRAF [Nog 93] and the Mathematica package FeynArts [Hah 01]. They substantially differ in design and functionality. Both require model files, defining the theory, as input from the user. QGRAF is certainly more efficient in producing symbolical expressions for a large number of diagrams, thus for large scale calculations QGRAF seems to be a better choice. However since we are more familiar with Mathematica and the possibility

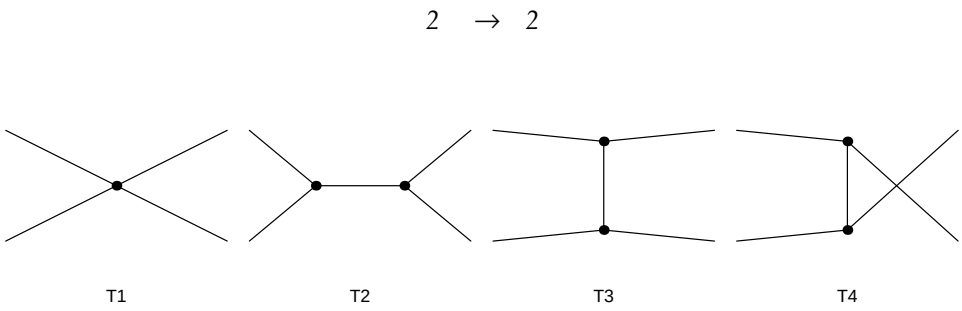

Figure 4.1: Topologies for a $2 \to 2$ scattering process at tree order.

of interactive usage as well as graphical output we choose FeynArts over QGRAF. FeynArts allows for *non-renormalizable* vertices, but there is no built-in support for topologically identical vertices of different chiral order. Consequently we developed Mathematica code implementing the desired feature. In the following we give a short introduction to FeynArts and give details of our modifications.

Specifying the number of external particles, the loop order and the type of vertices, i.e. the number of adjacent lines, FeynArts generates the possible topologies. The graphical output for a scattering process is shown in Fig. 4.1. It is possible to discard subsets of topologies, e.g. topologies contributing to wave function corrections. In the next step the lines are attributed with particle fields from a user defined model as depicted in Fig. 4.2. The model has to be provided in two separate files, one for the generic structure of particles, propagators and vertices, and one defining the types of particles and couplings specific for the model. The generic model contains only general information on the structure of the particles. More specifically, one defines the Lorentz and isospin structure of the propagators and vertices, e.g. one can define a generic vector field having isospin and Lorentz indices. The model file in turn specifies the actual particle content and particle attributes, as well as the possible vertices among the defined particles, e.g. a charged massive vector particle

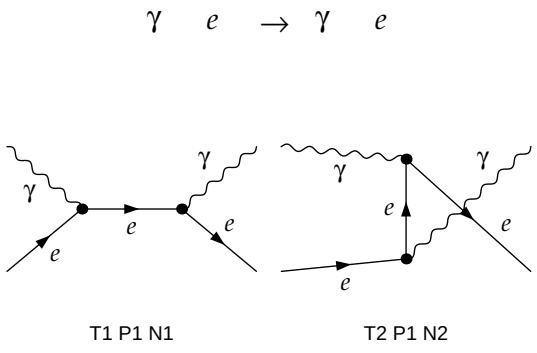

Figure 4.2: Insertion of fields in the topologies of Fig. 4.1 using the predefined QED model of FeynArts. Note that after insertions of fields only two topologies from Fig. 4.1 are left over.

interacting with a nucleon. For more details of the basic techniques and usage of FeynArts we refer to [Hah 01, KBD 90].

Even though FeynArts does not support vertices of the same topological type but different chiral orders from the outset, it has a built-in system for the generation of counter term diagrams. We exploit this feature to set up a modified version of FeynArts suitable for our calculations in BχPT. In fact, the only modification to the FeynArts source code concerns the graphical representation of the counter term diagrams in Mathematica and postscript files. All other modifications are separate extensions of FeynArts with self-written Mathematica code or appropriately adapted model files.

Without resorting to details of the inner working of FeynArts we briefly outline our approach. Instead of counter term vertices we define the various vertices of BχPT, where the chiral order corresponds to the counter term order. We generate the diagrams of the process in the standard way, which, in its Mathematica representation, is a list of the vertices and propagators making up each diagram. We first analyze the propagators for each diagram and assign a preliminary chiral order to each diagram. The user has to provide the maximum chiral order and the loop number. Based on these numbers and the preliminary chiral order of the diagram, a list of possible counter term (CT) vertices[1] resulting in diagrams with a chiral order smaller or equal to the maximum chiral order is generated. Finally, for each element in the list of possible CT vertices a separate diagram is generated. The graphical output is shown in Fig. 4.3. More importantly we also get symbolic expressions for all diagrams to a given process, in particular FeynArts also generates the correct symmetry factors. We have checked that the symbolic expressions generated by FeynArts agree with manually defined expressions based on the graphics output only, however, in our calculation we use the latter expressions, as the distribution of the momenta turns out to be more convenient. All diagrams relevant for our calculation are displayed in Appendix F.

4.2 Calculation of invariant amplitudes

As FeynArts generates the diagrams in Mathematica form it is most convenient to use Mathematica based packages, e.g. FeynCalc [MBD 91] or FormCalc [HPV 99], for the algebraic simplifications. In the early stages of this work we used the FeynCalc package in combination with self-written extensions, most of which were also used for the calculation of pion electro-production performed at the same time in our group [Leh 07]. Unfortunately Mathematica has severe limitations concerning the complexity of algebraic expressions it can handle. This limitation shows up only for the more complicated diagrams, in particular the box diagrams are subject to problems in the size of intermediate expressions. To overcome this limitation we implemented a procedure, in which formally higher-order terms are discarded, thus considerably reducing the size of the problem. More specifically, one discards

[1] Note that we use the counter term vertices in FeynArts as placeholders for the vertices of the BχPT lagrangian of corresponding chiral order. We do not generate counter term diagrams.

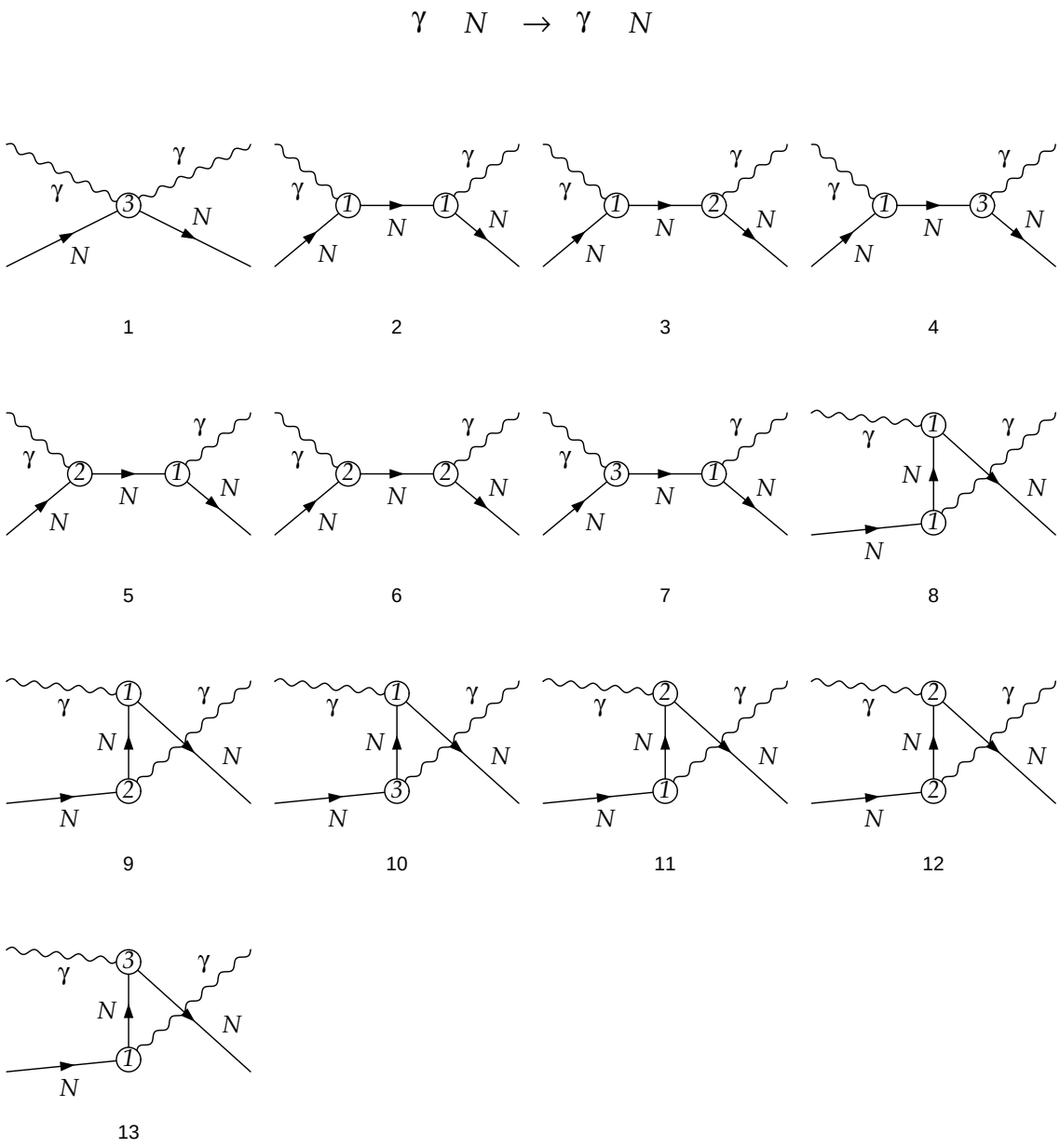

Figure 4.3: Graphical output of the modified FeynArts version for the topologies in Fig. 4.1 to chiral order $\mathcal{O}(q^3)$.

higher-rank tensor integrals by virtue of rescaling the loop momenta and retaining only contributions to a specific chiral order. Even with this simplification the calculation of some diagrams is still very slow, it takes typically one hour for the most complicated diagrams. Let us stress that from a conceptual point of view this procedure is completely consistent, as we only drop terms which are beyond the accuracy of our calculation. Moreover, if the perturbative series converges reasonably well, the size of the dropped terms should be small. However the above procedure has the drawback that constraints on the amplitudes stemming from symmetries, e.g.

crossing symmetry, are not exact anymore, i.e. the constraints or relations among the amplitudes are only valid up to terms of higher order. The FormCalc package addresses some of the issues related to calculational limitations of Mathematica. In fact FormCalc is aimed at combining the advantages of Mathematica concerning user friendliness and large amount of predefined functions with the computational speed of FORM. However FormCalc is not best suited for our purposes, as the primary goal of FormCalc is to calculate squared matrix elements within the Standard Model. Nevertheless we adopted FormCalc's philosophy and wrote a Mathematica program serving as an interface between Mathematica and FORM, letting FORM handle the cumbersome algebraic simplifications. This approach enabled us to calculate the full amplitudes without discarding any terms, thus the amplitudes exactly fulfill all restrictions coming from symmetry relations.

Mathematica interface

FORM is a computer algebra system tailor-made for quantum field theoretical calculations involving very large expressions. For most of the tasks needed in our calculation, FORM is significantly faster than Mathematica. This is mostly due to the rather restrictive and limited set of possible manipulations and built-in functions. On the other hand Mathematica is, because of its interactive use and the large amount of predefined functions, much more user-friendly than FORM. We combine the advantages of both systems in a hybrid approach using Mathematica and FORM, where the communication between both is realized via text files. The flow of the calculation is controlled by Mathematica.

Mathematica has several built-in functions for the generation and manipulation of text files. Moreover one can start external programs from within Mathematica. We use both properties to set up an interface between FORM and Mathematica. Note that some parts of this interface are not specific to the calculations in this work and thus can be used in a more general context. The first obstacle in setting up such an interface is the difference in semantics between FORM and Mathematica. In FORM all variables have to be declared in a preamble first, followed by a *local* expression representing the actual input, thereafter commands are put defining the actions of the FORM program. We developed a Mathematica package which, starting from an expression in Mathematica syntax, generates the preamble and the local expression in FORM syntax. For common functions, such as the metric tensor and Dirac and Pauli matrices, we have to specify the notations. It is convenient to use the notations defined in the FeynCalc package. This ensures compatibility with older programs based on this package. The FORM instructions for a calculational task are encapsulated in FORM procedures, which will be described below. For a given task the corresponding FORM procedure is appended to the preamble and local expression, and subsequently written to a file with the suffix *frm*. Next we invoke the FORM binary with the Mathematica-generated file as input. The FORM program performs all calculations defined in the FORM procedures and finally generates a file which in turn is read back into Mathematica. All of the above, especially the execution of the FORM binary, is running from within Mathematica,

using only built-in functions[2].

The FORM program

In the following we describe the calculational steps implemented in various self-written FORM procedures. Since the programming paradigm in FORM is very different from Mathematica, the Mathematica versions of the procedures serve as useful checks on the FORM result.

In a first step we separate the isospin algebra elements from the Dirac algebra elements. The resulting expression can be generically written as

$$\mathcal{D} \sim \underbrace{\bar{u}(p_f)\gamma_{i_1}\gamma_{i_2}\ldots\gamma_{i_r}\gamma_{\alpha_1}\ldots\gamma_{\alpha_n}u(p_i)\,p_1^{\alpha_1}\ldots p_n^{\alpha_n}}_{\text{spinor chain}}\cdot\underbrace{\tau_{a_1}\tau_{a_2}\ldots\tau_{a_N}}_{\text{isospin}}, \tag{4.1}$$

where τ_i and γ_α are the Pauli and Dirac matrices respectively. We start the calculation by performing the isospin algebra. To that end we repeatedly apply the relation

$$\tau^a\tau^b = \delta^{ab} + i\varepsilon^{abc}\tau^c, \tag{4.2}$$

until at most one Pauli matrix is left over.

In the next step the spinor chain is simplified. First all pairs of momenta in the spinor chain are eliminated[3], e.g.

$$\bar{u}(p_f)\not{p}\gamma_\mu\gamma_\nu\not{p}u(p_i). \tag{4.3}$$

Using the relation

$$\{\gamma_\mu,\gamma_\nu\} = 2\,g_{\mu\nu}, \tag{4.4}$$

we commute the utmost right momentum to the left until we can use the identity $\not{p}\cdot\not{p} = p^2$. In the next step we use (4.4) to shift p_f (p_i) to the left (right) until the Dirac equation

$$\bar{u}(p_f)\not{p}_f = \bar{u}(p_f)m_N, \tag{4.5}$$

$$\not{p}_i\,u(p_i) = m_N\,u(p_i), \tag{4.6}$$

is applicable. Subsequently we order the spinor chain, starting with the uncontracted indices μ and ν followed by the loop momentum $\not{k}$, and the photon momenta $\not{q}_1$ and $\not{q}_2$. In principle the ordering has to be supplied by the user with the above ordering being the default. The procedure for the isospin algebra is only called in the beginning, whereas the procedure for the Dirac algebra is applied to several intermediate expressions.

[2]Note that FormCalc uses a C-program to rewrite the syntax.

[3]Note that our expressions never contain a pair of identical indices, thus no explicit dependence on the dimension D occurs. Nevertheless we implemented all procedures acting on Dirac matrices in D dimensions.

The next procedures implement the identification and simplification of one-loop integrals. It gathers all denominators containing the user-defined loop momentum k into one single function

$$\frac{1}{k^2-m_1^2}\frac{1}{(k+p_1)^2-m_2^2}\ldots = I\big(\{k,m_1\},\{k+p_1,m_2\},\ldots\big). \tag{4.7}$$

Thereafter all terms proportional to powers of k^2 are reduced, using the identity

$$\begin{aligned}
\mathcal{D} \sim & \int \frac{d^Dk}{(2\pi)^D}\,A(k,p_i)\cdot k^2 I\big(\{k,m_1\},\{k+p_1,m_2\},\ldots\big)\\
&= \int \frac{d^Dk}{(2\pi)^D}\,A(k,p_i)\cdot \frac{k^2}{[k^2-m_1^2][(k+p_1)^2-m_2^2]+\ldots},\\
&= \int \frac{d^Dk}{(2\pi)^D}\,A(k,p_i)\cdot \frac{(k^2-m_1^2)+m_1^2}{[k^2-m_1^2][(k+p_1)^2-m_2^2]+\ldots},\\
&= \int \frac{d^Dk}{(2\pi)^D}\,A(k,p_i)\cdot \Big\{\frac{1}{[(k+p_1)^2-m_2^2]+\ldots}+\frac{m_1^2}{[k^2-m_1^2][(k+p_1)^2-m_2^2]+\ldots}\Big\},\\
&= \int \frac{d^Dk}{(2\pi)^D}\,A(k-p_1,p_i)\cdot I\big(\{k,m_2\},\ldots\big)\\
&\quad + \int \frac{d^Dk}{(2\pi)^D}\,A(k,p_i)\cdot m_1^2\, I\big(\{k,m_1\},\{k+p_1,m_2\},\ldots\big),
\end{aligned}$$

where in the last line the substitution $k \to k-p_1$ has been made in the first term[4]. At this stage the use of the infrared regularization scheme already manifests itself. All loop integrals containing only nucleon masses are discarded, as their contributions can be compensated by appropriate redefinitions of the various low-energy constants. Let us take a look at the above reduction of an integral containing only one denominator with a pion mass, e.g. a self-energy type diagram

$$I_1 = \int \frac{d^Dk}{(2\pi)^D}\frac{k^2}{[k^2-M_\pi^2][(k+p_1)^2-m_N^2]}, \tag{4.8}$$

$$= \int \frac{d^Dk}{(2\pi)^D}\frac{1}{[(k+p_1)^2-m_N^2]} + \int \frac{d^Dk}{(2\pi)^D}\frac{M_\pi^2}{[k^2-M_\pi^2][(k+p_1)^2-m_N^2]}, \tag{4.9}$$

$$= \cancel{\int \frac{d^Dk}{(2\pi)^D}\frac{1}{[k^2-m_N^2]}} + \int \frac{d^Dk}{(2\pi)^D}\frac{M_\pi^2}{[k^2-M_\pi^2][(k+p_1)^2-m_N^2]}, \tag{4.10}$$

$$= \int \frac{d^Dk}{(2\pi)^D}\frac{M_\pi^2}{[k^2-M_\pi^2][(k+p_1)^2-m_N^2]}. \tag{4.11}$$

One has to keep in mind that in the reduction of integrals, one drops all contributions coming from integrals containing only nucleon masses. For terms proportional to $k\cdot p_i$ and $\not{k}$ we split the scalar product[5], i.e.

$$k\cdot p_i = p_i^{\beta_1}\,k_{\beta_1}, \quad \not{k} = \gamma^{\alpha_1}k_{\alpha_1}.$$

[4]Note that the expressions contain an integral over k which is translational invariant.

[5]Note that after the Dirac algebra is performed at most $\not{k}$ can occur within spinor chains.

We are left with products of the denominators containing k, abbreviated with $I(\dots)$, and uncontracted loop momenta. We collect the indices of the loop momenta and the $I(\dots)$ in the functions $\tilde{I}$, e.g.

$$\begin{aligned}\mathcal{D} \sim\ & i \int \frac{d^D k}{(2\pi)^D}\, k\cdot p_1\, k\cdot p_2\, k_\mu\, k_\nu \frac{1}{[k^2-m_1^2][(k+p_1)^2-m_2^2]\dots} \\ &= p_1^{\beta_1}\, p_2^{\beta_2} \cdot \tilde{I}\big(\{k,m_1\},\{k+p_1,m_2\},\dots;\{\beta_1,\beta_2,\mu,\nu\}\big).\end{aligned}$$

After applying this procedure all terms containing the loop momentum k are cast into the functions $\tilde{I}$. Thus at this step the diagrams can be written as

$$\mathcal{D} = (i_1 + i_2\tau^3)\cdot \mathcal{F}(q_1,q_2,p_i,p_f)^{\alpha_1\dots\alpha_n} \cdot \tilde{I}(\{k,m_1\},\dots;\{\alpha_1,\dots,\alpha_n\}), \tag{4.12}$$

where i_1 and i_2 are real numbers, and the function $\mathcal{F}$ is independent of k. The decomposition of the tensorial integrals $\tilde{I}$ is done using the LoopTools notation. LoopTools supplies the coefficients of the Passarino-Veltman (PV) decomposition[6] of the one-loop tensorial integrals [PV 79]. The basic definitions for the LoopTools functions are given in Appendix C.1.2. One basically replaces the tensor integrals with the most general parametrization using metric tensors and combinations of the external four-momenta running in the loop, e.g.

$$\tilde{I}\big(\{k,m_1\},\{k+p_1,m_2\};\{\alpha,\beta\}\big) = -\frac{1}{16\pi^2}\Big[g^{\alpha\beta} B_{00}\big(p_1^2,m_1^2,m_2^2\big) + p_1^\alpha p_1^\beta B_{11}\big(p_1^2,m_1^2,m_2^2\big)\Big]. \tag{4.13}$$

The tensor coefficients can be either calculated numerically via the LoopTools library or analytically reduced to scalar integrals. In [DD 06] a compact recursion formula for the PV decomposed tensor coefficients was given, which is best suited for an implementation in a Mathematica program. The explicit reduction to scalar integrals for the above example reads

$$\begin{aligned} B_{00}(p_1^2,m_1^2,m_2^2) = \frac{1}{6}\Big(& 2B_0\left(p_1^2,m_1^2,m_2^2\right) m_1^2 + m_1^2 + m_2^2 - \frac{p_1^2}{3} + A_0\left(m_2^2\right) \\ & - \frac{(m_1^2-m_2^2+p_1^2)}{2p_1^2}\big[-A_0\left(m_1^2\right) + A_0\left(m_2^2\right) \\ & + B_0\left(p_1^2,m_1^2,m_2^2\right)\left(m_1^2-m_2^2+p_1^2\right)\big]\Big), \end{aligned} \tag{4.14}$$

$$\begin{aligned} B_{11}(p_1^2,m_1^2,m_2^2) = \frac{1}{18p_1^4}\Big(& \left(p_1^2 - 3\left(m_1^2+m_2^2\right)\right) p_1^2 - 6A_0\left(m_1^2\right)\left(m_1^2-m_2^2+p_1^2\right) \\ & + 6B_0\left(p_1^2,m_1^2,m_2^2\right)\Big(\left(p_1^2\right)^2 + \left(m_1^2-2m_2^2\right)p_1^2 + \left(m_1^2-m_2^2\right)^2\Big) \\ & + 6A_0\left(m_2^2\right)\left(m_1^2-m_2^2+2p_1^2\right)\Big). \end{aligned} \tag{4.15}$$

The explicit expressions for the tensor coefficients quickly grow in size for higher-rank tensors. Therefore, and for reasons we will discuss later, it is convenient to keep

[6] Note that the PV decomposition is not carried out explicitly.

the tensor coefficients in the LoopTools notation. At this stage we have arrived at expressions for the diagrams, where the complete dependence on the loop momenta is encoded in scalar tensor coefficients. Moreover the expressions have only two uncontracted indices, namely μ and ν.

The next procedure concerns the chiral order of individual terms, in order to determine the subtraction terms needed for the reformulated version of IR. To that end all scalar products of p_i, p_f, q_1 and q_2 are replaced using the three Mandelstam invariants ν, t, Q^2 and the nucleon mass. The Mandelstam variables have been defined in Eq. (3.2) and the relations to the scalar products read

$$p_i \cdot p_i = p_i^2 = m_N^2, \qquad p_f \cdot p_f = p_f^2 = m_N^2, \tag{4.16}$$

$$q_1 \cdot q_1 = q_1^2 = -Q^2, \qquad q_2 \cdot q_2 = q_2^2 = 0, \tag{4.17}$$

$$p_i \cdot p_f = -\frac{1}{2}\,t + m_N^2, \qquad q_1 \cdot q_2 = -\frac{1}{2}\big(t + Q^2\big), \tag{4.18}$$

$$q_1 \cdot p_i = \frac{1}{2}\big(s + Q^2 - m_N^2\big), \qquad q_1 \cdot p_f = -\frac{1}{2}\big(u + Q^2 - m_N^2\big), \tag{4.19}$$

$$q_2 \cdot p_i = -\frac{1}{2}\big(u - m_N^2\big), \qquad q_2 \cdot p_f = \frac{1}{2}\big(s - m_N^2\big) \tag{4.20}$$

$$\nu = \frac{s-u}{4m_N}, \qquad s + t + u = 2m_N^2 - Q^2. \tag{4.21}$$

We rescale the Mandelstam variables according to their respective chiral orders

$$\nu \mapsto \aleph\,\nu, \quad t \mapsto \aleph^2\,t, \quad Q^2 \mapsto \aleph^2 Q^2,$$

where $\aleph$ denotes a small quantity. Furthermore we rescale the momenta of the incoming and outgoing photons, $q_1^\mu \mapsto \aleph\, q_1^\mu$ and $q_2^\mu \mapsto \aleph\, q_2^\mu$, as well as the pion mass $M_\pi^2 \mapsto \aleph^2 M_\pi^2$ and the propagators

$$\frac{1}{p_j^2 - M_\pi^2} \mapsto \frac{1}{\aleph^2}\frac{1}{p_j^2 - M_\pi^2}, \quad \frac{1}{p_j^2 - m_N^2} \mapsto \frac{1}{\aleph}\frac{1}{p_j^2 - m_N^2}, \tag{4.22}$$

where p_j is some linear combination of the external momenta, independent of the loop momentum k. In this way each term multiplying a tensor coefficient is assigned a chiral order N, according to which we determine the subtraction terms for the individual tensor coefficients[7]. Let us illustrate this procedure by a typical example. Suppose a diagram has been reduced to the following form

$$\begin{aligned} D^{\mu\nu} = {} & \frac{e^2\,\tau^3}{64\pi^2 F_\pi^2}\,\frac{Q^2}{(p_i - q_1)^2 - m_N^2}\,\bar u(p_f)\gamma^\mu\,u(p_i)\,q_2^\nu \cdot B_{11}(Q^2, M_\pi^2, m_N^2) \\ & + \frac{e^2}{32\pi^2 F_\pi^2}\,\frac{1}{(p_i - q_1)^2 - m_N^2}\,\bar u(p_f)\gamma^\nu\,u(p_i)\,q_1^\mu \cdot B_{00}(Q^2, M_\pi^2, m_N^2). \end{aligned} \tag{4.23}$$

Rescaling this expression according to the above prescription we get

$$D^{\mu\nu} = \frac{e^2\,\tau^3}{64\pi^2 F_\pi^2}\,\frac{\big(Q^2 \cdot \aleph^2\big)}{\big((p_i - q_1)^2 - m_N^2\big) \cdot \aleph}\,\bar u(p_f)\gamma^\mu\,u(p_i)\,\big(\aleph \cdot q_2^\nu\big) \cdot B_{11}(Q^2, M_\pi^2, m_N^2)$$

[7]Note that only the coefficients of the one-loop integrals are rescaled, since we are interested in the determination of the chiral order of the subtraction terms for these integrals.

$$
\begin{aligned}
&+\frac{e^2}{32\pi^2 F_\pi^2}\,\frac{1}{\left((p_i-q_1)^2-m_N^2\right)\cdot\aleph}\,\bar u(p_f)\gamma^\nu\,u(p_i)\left(\aleph\cdot q_1^\mu\right)\cdot B_{00}(Q^2,M_\pi^2,m_N^2),\\
&=\frac{e^2\,\tau^3}{64\pi^2 F_\pi^2}\,\frac{Q^2}{(p_i-q_1)^2-m_N^2}\,\bar u(p_f)\gamma^\mu\,u(p_i)\,q_2^\nu\cdot\aleph^{(2-1+1)}\cdot B_{11}(Q^2,M_\pi^2,m_N^2)\\
&\quad+\frac{e^2}{32\pi^2 F_\pi^2}\,\frac{1}{(p_i-q_1)^2-m_N^2}\,\bar u(p_f)\gamma^\nu\,u(p_i)\,q_1^\mu\cdot\aleph^{(-1+1)}\cdot B_{00}(Q^2,M_\pi^2,m_N^2).
\end{aligned}
\tag{4.24}
$$

We see that in Eq. (4.24) the factors multiplying the tensor coefficients have chiral order 2 and 0 for the first and second terms respectively. Since we are interested in a calculation of VCS to fourth order in BχPT using the reformulated IR, all contributions analytic in the pion mass and small momenta with chiral order lower or equal to four have to be subtracted. Let us stress that in the calculation of matrix elements the polarization vectors of the incoming and outgoing photon, which we treat as small quantities, have to be taken into account. Thus the expression in Eq. (4.24) will eventually be multiplied with the polarization vectors, increasing the chiral order of all terms by 2. Therefore if we neglect the polarization vectors we need to subtract all analytic contributions up to and including terms of chiral order 2. Consequently, if the chiral order of the prefactor of a tensor coefficient is denoted by N, we need to calculate the subtraction terms of the tensor coefficient to order $2-N$. For our example we get

$$
\begin{aligned}
D_1^{\mu\nu}&=\frac{e^2\,\tau^3}{64\pi^2 F_\pi^2}\,\frac{Q^2}{(p_i-q_1)^2-m_N^2}\,\bar u(p_f)\gamma^\mu\,u(p_i)\,q_2^\nu\cdot\aleph^{(2)}\cdot B_{11}(Q^2,M_\pi^2,m_N^2)\\
&\quad+\frac{e^2}{32\pi^2 F_\pi^2}\,\frac{1}{(p_i-q_1)^2-m_N^2}\,\bar u(p_f)\gamma^\nu\,u(p_i)\,q_1^\mu\cdot\aleph^{(0)}\cdot B_{00}(Q^2,M_\pi^2,m_N^2),\\
&=\frac{e^2\,\tau^3}{64\pi^2 F_\pi^2}\,\frac{Q^2}{(p_i-q_1)^2-m_N^2}\,\bar u(p_f)\gamma^\mu\,u(p_i)\,q_2^\nu\cdot B_{11}^{(0)}(Q^2,M_\pi^2,m_N^2)\\
&\quad+\frac{e^2}{32\pi^2 F_\pi^2}\,\frac{1}{(p_i-q_1)^2-m_N^2}\,\bar u(p_f)\gamma^\nu\,u(p_i)\,q_1^\mu\cdot B_{00}^{(2)}(Q^2,M_\pi^2,m_N^2),
\end{aligned}
\tag{4.25}
$$

where the superscript in the tensor coefficients denotes the order to which the subtraction terms are needed. The calculation of the subtraction terms has been implemented in a Mathematica program.

In the last step we identify the tensor structures $\widetilde{K}_i^{\mu\nu}$ given in Eq. (B.5) in the Appendix and store the results in Mathematica format.

The calculation of the 100 one-loop diagrams in FORM takes approximately 10 minutes on a Pentium 4 (4 GHz) with 2 GB RAM. All results are stored in one file, which is roughly 33 MB large. This concludes the FORM part of the calculation.

Mathematica programs

All further manipulations are carried out in Mathematica. To that end the expressions for all one-loop diagrams are read from the FORM generated file. As we want to calculate the invariant amplitudes f_i, we need to extract the coefficients of $\rho_i^{\mu\nu}$,

defined in Eq. (B.2), from the results of the diagrams. However, given the complexity of the $\rho_i^{\mu\nu}$, a direct extraction from the FORM expressions is unfeasible. We instead use the $\widetilde{K}_i^{\mu\nu}$, identified by the FORM program, to reconstruct the f_i. To that end we simply express the $\rho_i^{\mu\nu}$ in terms of the $\widetilde{K}_i^{\mu\nu}$, and by comparing coefficients we arrive at relations between the coefficients of the $\widetilde{K}$ and ρ structures. The details of the extraction are given in Appendix B.

As pointed out in Section 3.2.1, we need to separate the amplitudes in Born and non-Born parts. The Born part is calculated by performing an expansion of the amplitudes in s (u) around $s = m_N^2$ ($u = m_N^2$) keeping only terms up to and including $1/(s - m_N^2)$ ($1/(u - m_N^2)$). By subtracting the Born part from the full result one arrives at the non-Born part. The expressions for the full result and the non-Born part are very lengthy, we therefore refrain from explicitly giving the results in this work.

In principle, for the purpose of numerical evaluation of the invariant amplitudes, we could stop here, since the LoopTools package offers the possibility for a numerical calculation of the one-loop integrals in Mathematica. However since we have existing C code for the calculation of all observables from the invariant amplitudes, we have collected the results in a C program. The C program has been generated using Mathematica. It consists of source files for each of the 12 invariant amplitudes f_i, containing the contributions from all loop diagrams in the form of an array of complex numbers. The index of the array corresponds to a specific diagram, i.e. one can take a look at the contributions of individual diagrams to the respective invariant amplitude. Especially one can investigate classes of diagrams, for example only contributions from diagrams at chiral order $\mathcal{O}(q^3)$. Let us stress that the one-loop integrals in the final expression are supposed to be the IR regulated integrals. Therefore in the Mathematica program, which writes out the C code, the integrals are replaced by subtracted integrals. The subtracted integrals have been calculated using Mathematica. Details concerning the calculation of the subtraction terms are given in Appendix D.

4.3 Derivatives of one-loop-functions

For the calculation of the generalized polarizabilities, defined in Eq. (3.66), we need the invariant amplitudes[8] $\bar{F}_i(Q^2)$. In the extraction of the F_i for the full VCS process one inevitably introduces a factor of $1/\nu$, even though the $\rho_i^{\mu\nu}$ were constructed such that the non-Born part is free of kinematical singularities. Since we construct the non-Born part by subtracting the Born part from the full amplitudes, the singularity for ν remains as an artefact. This is because our results for the non-Born part are complicated functions of tensorial integrals for which the cancelation of the singularity is not easily seen. Therefore we have to take special care of the limit $\nu \to 0$ in our calculation. In order to get an explicit cancelation of the kinematical singularity we have to reduce the tensorial integrals to scalar ones and subsequently perform an expansion in ν around 0. In this expansion derivatives of scalar one-loop

[8] From now on we use the F_i defined in Eq. (3.37) instead of the f_i.

functions arise. In the following we briefly describe our procedure of obtaining the correct limit for $\nu \to 0$.

First of all we have to reduce all tensorial integrals to scalar ones. To that end we implemented the reduction of the tensorial integrals according to the Passarino-Veltman (PV) scheme using the recursive formula given in [DD 06]. The Mathematica program is capable of reducing integrals in the PV scheme up to rank 7, even though the highest tensor rank in our calculation is four. Let us illustrate this reduction by two examples

$$\begin{aligned} B_1(-\frac{1}{2}x, M_\pi^2, m_N^2) = -\frac{1}{2x}\Big[&2\big(A_0(M_\pi^2) - A_0(m_N^2)\big) \\ &+ (t + Q^2 + 4m_N\nu - 2M_\pi^2)B_0(-\frac{1}{2}x, M_\pi^2, m_N^2)\Big], \end{aligned} \tag{4.26}$$

where

$$\begin{aligned} x &= (t + Q^2 + 4m_N\nu - 2m_N^2), \\ C_{0012}(-Q^2, t, 0, M_\pi^2, M_\pi^2, M_\pi^2) &= \frac{1}{288\big(t+Q^2\big)^2}\Big[(t+Q^2)(48M_\pi^2 + t + 7Q^2) \\ &\quad + 72(t+Q^2)M_\pi^4\, C_0(-Q^2, t, 0, M_\pi^2, M_\pi^2, M_\pi^2) \\ &\quad + 6(t^2 + 2t(M_\pi^2 + Q^2) - 8Q^2M_\pi^2)B_0(t, M_\pi^2, M_\pi^2) \\ &\quad + 6Q^2(10M_\pi^2 + Q^2)B_0(-Q^2, M_\pi^2, M_\pi^2) \\ &\quad - 12(t+Q^2)A_0(M_\pi^2)\Big]. \end{aligned} \tag{4.27}$$

The last example illustrates a problem concerning the PV reduction. In the limit $t \to -Q^2$ the right hand side of Eq. (4.27) is singular, which indicates the breakdown of this reduction scheme for special kinematics. The failure of the PV scheme can be traced back to the vanishing of the so-called Gram determinant. We will elaborate on how to handle this problem in detail in the next section. In fact through the reduction of tensorial integrals we get additional negative powers of ν, further aggravating the situation.

After reduction of all tensor integrals to scalar ones we perform an expansion in ν around 0. The coefficient of ν^0 contains scalar integrals as well as derivatives of scalar integrals. In the calculation of the derivatives we adopted the techniques presented in [DS 98], where the derivatives of the 2- and 3- point integrals have been calculated. The crucial observation is that any derivative of a scalar n-point one-loop integral can be expressed as a function of the integral itself and mass derivatives of (n-1)-point integrals. The details of the derivation are given in Appendix C.2, where the derivatives of 4-point functions are also calculated. We have implemented the formulas in a Mathematica program, which is used recursively for higher-order derivatives. In our calculation the maximum number of derivatives for the 2-point function (B's) was 6, for the 3-point functions (C's) 7 and for the 4-point functions (D's) we needed up to 5 derivatives. Let us stress that we have explicitly (analytically) checked that all amplitudes F_i are regular in the limit $t \to -Q^2$ and $\nu \to 0$,

i.e. all terms proportional to negative powers of ν vanish exactly. It is worth noting that the final result comprises of scalar 1-, 2- and 3-point functions only. This is due to the fact that the Gram determinants of all 4-point functions are proportional to ν, thus in the limit $\nu \to 0$ these functions reduce to simpler ones.

4.4 Exceptional kinematics

We have seen that, for some cases, the calculation of tensorial integrals is involved. Especially in the calculation of the Born part tensor integrals arise for which the PV reduction scheme fails. Let us stress that the singularities one encounters are due to the reduction scheme, and not properties of the tensor coefficients. The PV scheme is plagued by the occurrence of inverse Gram determinants. These determinants depend only on the external momenta running in the loop, thus it is possible to have a kinematical situation in which the determinant exactly vanishes, leading to a singular behavior for the tensor coefficients. In the following we refer to the kinematics for which the Gram determinant vanishes as exceptional kinematics. For most calculations the problem of vanishing Gram determinants usually shows up only at a few points in phase space, e.g. the extreme forward limit in $2 \to 2$ processes, and in most cases these contributions may be neglected. However in our calculation the problem persists for a large region in phase space.

Several strategies have been developed to cope with the problem of reducing tensorial integrals for exceptional kinematics. One can distinguish between approaches based on a fully numerical calculation of tensor coefficients, e.g, [Fer+ 03], and analytical calculations employing different reduction schemes for exceptional kinematics [Dav 91, DD 06, DS 98]. Also admixtures of both approaches are being used. Since we are interested in analytical expressions we follow the analytical approach of Ref. [DD 06].

Let us briefly describe the approach by Denner and Dittmaier. For the case of a non-vanishing Gram determinant the conventional Passarino-Veltman reduction is used. If the Gram determinants are very small the case for 1- and 2-point integrals is handled differently from the case for 3- and 4-point functions. The 1- and 2-point functions allow for an explicit numerically stable calculation. The 3- and 4-point integrals on the other hand are reduced to 2- and 3-point functions respectively. In [DD 06] several reduction schemes are proposed, depending on the explicit form of the kinematics. Using the standard scalar integrals A_0, B_0, C_0 and D_0, the tensor coefficients are iteratively deduced up to terms systematically suppressed by small Gram determinants or by other kinematical determinants in specific kinematical configurations. We have implemented the explicit formula for the iterative calculation of tensor coefficients given in Ref. [DD 06]. For our calculation it turns out that only the so-called Gram expansion and the expansion in Gram and modified Cayley determinants is necessary. Let us stress that we have implemented these procedures in Mathematica as well as in C. Moreover we would like to emphasize that, as a first step, only the reduction for exactly vanishing Gram determinants has been implemented.

The C program is written as an extension to the LoopTools package. A function tests for each integral, i.e. tensor coefficient and scalar integrals, if the corresponding Gram determinant Δ is smaller than some user defined threshold parameter. If Δ is larger than the threshold parameter the function invokes the LoopTools package and returns the corresponding result using the standard PV scheme. For the case of very small Δ, separate routines are called, in which the algorithms of [DD 06] have been implemented. Note that within these routines the LoopTools package is still used for the calculation of the scalar integrals. Which routine is called depends on an estimate of certain kinematical determinants, roughly determining the accuracy of each routine. Thereafter the most promising routine calculates all tensor coefficients corresponding to the kinematical configuration up to tensor rank 4. The results are saved using the STL map container, serving as a lookup table. In this way all tensor coefficients belonging to a specific kinematical configuration have to be calculated only once and upon reuse can be read off the lookup table. This procedure enormously speeds up the calculation, as the number of tensor coefficients is quite large in our expressions. However there is still a small performance decrease with respect to the calculation using LoopTools only, nevertheless all numerical calculations take at the order of minutes. Even though the reduction for exceptional kinematics was only implemented up to terms suppressed by one power of the Gram determinant (or modified Cayley determinant), we found sufficient numerical stability for our purposes. To that end we have varied the threshold parameter over the range of $10^{-4} - 10^{-6}$, where no significant changes to our results were observed, i.e. a few percent for the integrals and even less for the observables.

Since the programming paradigm of Mathematica and C are completely different, the Mathematica implementation serves as a useful check of the C program. To that end we checked that the numerical limits of the tensor coefficients for certain kinematical configurations using LoopTools agree with the results using the Mathematica program[9]. More importantly the Mathematica implementation is used in the calculation of the generalized polarizabilities, where derivatives of the tensor coefficients are needed. Note that the majority of one-loop integrals allow for a reduction in the conventional PV scheme. We encounter vanishing Gram determinants foremost in the Born part of the amplitudes and for the kinematical limit $t \to -Q^2$ and $\nu \to 0$. However we have also encountered numerical problems for the calculation in the kinematics of the MAMI experiment. These instabilities were handled based purely on the C program.

Let us illustrate the reduction for exceptional kinematics with the help of two examples. First let us take a look at the limit $t \to -Q^2$ for the tensor coefficient in Eq. (4.27), which is a common example for the calculation of generalized polarizabilities. The reduction in the limit of vanishing Gram determinant reads

$$C_{0012}(-Q^2, -Q^2, 0, M_\pi^2, M_\pi^2, M_\pi^2) = \frac{1}{M_\pi^2\big(4M_\pi^2 + Q^2\big)}\Big[-A_0(M_\pi^2) + M_\pi^2\big(-1 + B_0\big(-Q^2, M_\pi^2, M_\pi^2\big)\big)\Big]. \qquad (4.28)$$

[9]Let us stress that checking all cases is practically impossible, so we restricted ourselves to integrals at kinematical configurations of interest in our calculation.

Another example emerging in the non-Born part reads

$$C_0(m_N^2, 0, m_N^2, M_\pi^2, M_\pi^2, m_N^2) = \frac{B_0(m_N^2, M_\pi^2, m_N^2) - B_0(m_N^2, M_\pi^2, M_\pi^2)}{m_N^2 - M_\pi^2}. \tag{4.29}$$

From these two examples one can already see that, for vanishing Gram determinant, the reduction gives simpler results. Let us stress that the implementation of the reduction of tensor coefficients is crucial for obtaining analytic results for the generalized polarizabilities.

Chapter 5

Results

In this chapter we present the results for virtual Compton scattering (VCS) to fourth order in manifestly Lorentz-invariant baryon chiral perturbation theory. We compare our results to the experiments and discuss some aspects of the convergence of the series. At fourth order new unknown low-energy constants (LECs) enter in the calculation. Restricting ourselves to the VCS case on the proton only two new coupling constants appear. Below we present procedure for fitting the two unknown LECs using experiments on real Compton scattering off the proton.

5.1 Fitting procedure

For the masses and coupling constant at leading order we use the following values [Yao+ 06]

$$m_N = 0.9383\,\mathrm{GeV}, \qquad M_\pi = 0.1346\,\mathrm{GeV}, \tag{5.1}$$

$$g_A = 1.267, \qquad F_\pi = 0.0924\,\mathrm{GeV}. \tag{5.2}$$

Note that we use the neutral pion mass and the proton mass. All LECs from the second- and third-order Lagrangians are known from fits to the nucleon form factors or πn scattering. The invariant amplitudes F_1 and F_2 receive additional contributions from 4 linear combinations of LECs at the fourth order

$$e_x^\pm = (2e_{90} + e_{94} + e_{117}) \pm e_{92}\,, \tag{5.3}$$

$$e_y^\pm = (2e_{89} + e_{93} + e_{118}) \pm e_{91}\,. \tag{5.4}$$

Restricting ourselves to VCS on the proton we are left with e_x^+ and e_y^+. These are specific to VCS and thus cannot be extracted from a fit to other observables. However they contribute not only to VCS but also to RCS. More specifically the unknown LECs are related to the static electric and magnetic polarizabilities α and β. In order to find the best fit, we used three different methods to obtain the values of e_x^+ and e_y^+. Let us start by summarizing the values for the known LECs.

5.1.1 Known low energy constants

An account of the available values for the coupling constants at second order, using results for πN scattering [BM 00, FMS 98], was given in [Mei 06]. For c_1 and c_3 we use the central values stated in [Mei 06], c_2 and c_4 are taken from [SGS 05], i.e.

$$c_1 = -0.9\,\mathrm{GeV}^{-1}, \tag{5.5}$$
$$c_2 = 2.66\,\mathrm{GeV}^{-1}, \tag{5.6}$$
$$c_3 = -4.7\,\mathrm{GeV}^{-1}, \tag{5.7}$$
$$c_4 = 2.45\,\mathrm{GeV}^{-1}. \tag{5.8}$$

In [Mei 06] it is argued that the fairly large values for $c_{2,3}$ (c_4) are mostly generated by $\Delta(1232)$ (ρ) exchange. The coupling constants c_6 and c_7 contribute to the magnetic moments of the nucleon. Since the order four contributions to the magnetic moments essentially amount to a quark mass renormalization, we choose to use the linear combinations

$$\tilde{c}_6 = c_6 - 4\,M_\pi^2\,e_{106}, \tag{5.9}$$
$$\tilde{c}_7 = c_7 - 16\,M_\pi^2\,e_{105}. \tag{5.10}$$

Because the one-loop amplitudes for VCS start at order 3, the modifications from using these linear combinations for the loop part start at order five. Thus the difference is beyond the accuracy of our calculation and it is justified to use $\tilde{c}_6$ and $\tilde{c}_7$ in the loop part as well. The LECs are fixed using the anomalous magnetic moments of the nucleon $\kappa_{p/n}$[1]. The relations read

$$\tilde{c}_6 = \frac{\kappa_v}{4m_N}, \quad \tilde{c}_7 = \frac{\kappa_s}{2m_N}, \tag{5.11}$$

where the isoscalar and isovector anomalous magnetic moment are defined as

$$\kappa_p = \frac{1}{2}\big(\kappa_s + \kappa_v\big) = 1.793, \quad \kappa_n = \frac{1}{2}\big(\kappa_s - \kappa_v\big) = -1.913. \tag{5.12}$$

Using the experimental values for the magnetic moments, the two LECs read

$$\tilde{c}_6 = 0.987\,\mathrm{GeV}^{-1}, \tag{5.13}$$
$$\tilde{c}_7 = -0.064\,\mathrm{GeV}^{-1}. \tag{5.14}$$

At third order two LECs contribute, namely d_6 and d_7. They are accompanied by the fourth order LECs e_{54} and e_{74}. These LECs may be fitted to the electromagnetic radii of the nucleons. Here we use the values from [SGS 05]

$$d_6 = 0.98\,\mathrm{GeV}^{-2}, \qquad d_7 = 0.24\,\mathrm{GeV}^{-2}, \tag{5.15}$$
$$e_{54} = -0.26\,\mathrm{GeV}^{-3}, \qquad e_{74} = -0.9\,\mathrm{GeV}^{-3}. \tag{5.16}$$

[1] Note that this amounts to fixing the magnetic moments to the tree order calculation only. Since in our calculation the anomalous magnetic moments contribute only in the one-loop part the one-loop corrections for the anomalous magnetic moments may be discarded.

Fit	e_x^+	e_y^+	χ^2	α	β
I	-4.52	1.50	(371.95/101)=3.68	12.17	1.65
II	-4.61 ± 0.30	0.85 ± 0.12	(136.6/69)=2.37	15.83	1.77
III	-4.85 ± 0.30	1.17 ± 0.09	(308.4/101)=3.05	14.75	-0.07

Table 5.1: Summary of the values for the LECs e_x^+ and e_y^+ as obtained from three different fits. e_x^+ and e_y^+ are given in GeV^{-3}, α and β are given in units of $10^{-4}\,\mathrm{fm}^3$.

5.1.2 Unknown low energy constants

In the following we describe three different approaches to fitting the unknown LECs e_x^+ and e_y^+. All fits use data from RCS only.

Fit I

In the first fit we simply fix the LECs to the experimental values of α and β from [Leo+ 01][2],

$$\alpha = 12.17 \times 10^{-4}\,\mathrm{fm}^3, \qquad \beta = 1.65 \times 10^{-4}\,\mathrm{fm}^3. \tag{5.17}$$

This leads us to the following values for the fourth order LECs

$$e_x^+ = -4.52\,\mathrm{GeV}^{-3}, \qquad e_y^+ = 1.50\,\mathrm{GeV}^{-3}. \tag{5.18}$$

The photon Energy dependence of the experimental data is completely neglected in this fit.

Fit II

Next we use the fitting procedure proposed in Ref. [Bea+ 03], utilizing the fact that the expansion used in our calculations works best in a certain domain. Here the LECs are fitted to the experimental data on differential cross sections of RCS on the proton well below pion threshold, i.e. E_γ, $\sqrt{|t|} \leq 0.18$ GeV. To that end we use the data from [Mac+ 95, Fed+ 91, Zie+ 92, Leo+ 01], which amounts to a total of 69 data points. We use the program package MINUIT from the CERNlib to fix the LECs. The fitted values are

$$e_x^+ = \big(-4.61 \pm 0.30\big)\,\mathrm{GeV}^{-3}, \qquad e_y^+ = \big(0.85 \pm 0.12\big)\,\mathrm{GeV}^{-3}. \tag{5.19}$$

Fit III

In the last fit we drop the upper limit from the second fit, and fix the LECs using the complete data set from [Mac+ 95, Fed+ 91, Zie+ 92, Leo+ 01] for RCS, which

[2]Note that the Baldin sum rule was used to constrain the fit in [Leo+ 01].

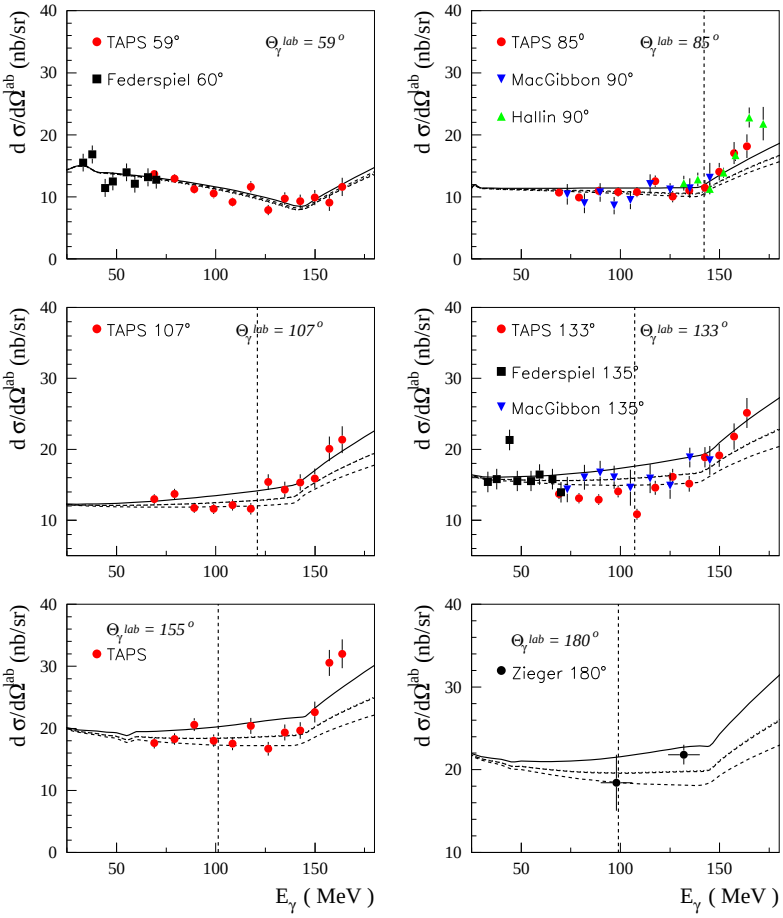

Figure 5.1: Differential cross sections for RCS off the proton as function of the lab photon energy E_γ and at different scattering angles. The full, dashed and dotted lines correspond to fit I, II and III respectively. The vertical lines correspond to the upper limit E_γ, $\sqrt{|t|} \leq 0.18$ GeV. Data points are taken from [Mac+ 95, Fed+ 91, Zie+ 92, Leo+ 01].

amounts to 101 data points. Performing again a least χ^2 fit we obtain the following values

$$e_x^+ = \left(-4.85 \pm 0.30\right) \text{GeV}^{-3}, \qquad e_y^+ = \left(1.17 \pm 0.09\right) \text{GeV}^{-3}. \tag{5.20}$$

Additionally we have fitted the experimental data using the constraint on the sum of α and β coming from the Baldin sum rule, i.e. $\alpha + \beta = 13.82 \times 10^{-4}\,\text{fm}^3$, and utilizing a modified definition of χ^2 accounting for normalization errors of different data sets [Bar+ 01]. However, the so obtained values are compatible with the above fits, therefore in the following we use the above values for the unknown LECs at fourth order.

The fitted values for e_x^+ and e_y^+ are summarized in Table 5.1. We conclude that a fairly good description of the differential cross sections for RCS on the proton can

be obtained with rather natural coupling constants at fourth order. If we use the nucleon mass as the natural scale of the problem the dimensionless couplings read

$$\tilde{e}_x^+ \approx -1.55, \qquad \tilde{e}_y^+ \approx 1.07\,, \tag{5.21}$$

where

$$e_{x,y}^+ = \left(\frac{\tilde{e}_{x,y}^+}{m_N}\right)^3. \tag{5.22}$$

The results for the differential cross sections are shown in Fig.5.1.

5.2 Real Compton scattering

The results for RCS are obtained by performing the limit $Q^2 \to 0$ in the amplitudes calculated for VCS. Therefore the comparison to previous calculations in HBχPT and covariant BχPT serves as a strong check on our results. Let us stress that the IR formulation of Becher and Leutwyler [BL 99] is constructed such that in the limit of $m_N \to \infty$ the HBχPT results are reproduced. This holds true in the reformulated version of IR we are using.

The quantities of interest in RCS are the polarizabilities of the nucleon. In the following we use the definitions of Babusci et al. [Bab+ 98]. Let us first collect the results of HBχPT to fourth order for the spin-dependent polarizabilities [VKMB 00, GHM 00].

$$\gamma_{E1E1} = \frac{\alpha_e\, g_A^2}{96\pi^2 F_\pi^2 M_\pi^2}\Big[-5 + \frac{11\pi M_\pi}{4m_N}\big(2+\tau^3\big)\Big], \tag{5.23}$$

$$\gamma_{M1M1} = \frac{\alpha_e\, g_A^2}{96\pi^2 F_\pi^2 M_\pi^2}\Big[-1 + \frac{\pi M_\pi}{4m_N}\big(15 + 4\kappa_v + 4\big(1+\kappa_s\big)\tau^3\big)\Big], \tag{5.24}$$

$$\gamma_{E1M2} = \frac{\alpha_e\, g_A^2}{96\pi^2 F_\pi^2 M_\pi^2}\Big[1 - \frac{\pi M_\pi}{4m_N}\big(6+\tau^3\big)\Big], \tag{5.25}$$

$$\gamma_{M1E2} = \frac{\alpha_e\, g_A^2}{96\pi^2 F_\pi^2 M_\pi^2}\Big[1 - \frac{\pi M_\pi}{4m_N}\big(1 + 2\kappa_v - 2\big(1+\kappa_s\big)\tau^3\big)\Big], \tag{5.26}$$

$$\gamma_0 = \frac{\alpha_e\, g_A^2}{24 F_\pi^2 M_\pi^2}\Big[1 - \frac{\pi\, M_\pi}{8m_N}\big(15 + 3\kappa_v + \big(6+\kappa_s\big)\tau^3\big)\Big]. \tag{5.27}$$

The scalar polarizabilities have been calculated in [Ber+ 93] and are given by

$$\begin{aligned}\alpha = {} & \frac{\alpha_e}{96\pi^2 F_\pi^2 M_\pi}\Big[5\pi g_A^2 - 2M_\pi\big(\tilde{c} + 2c_2\,\ln\mu\big) \\ & + \frac{g_A^2\, M_\pi}{m_N}\big(27 + 8\tau^3 + 12\big(2+\tau^3\big)\ln\mu\big)\Big] + \delta\bar{\alpha}, \\ \beta = {} & \frac{\alpha_e}{96\pi^2 F_\pi^2 M_\pi}\Big[\frac{1}{2}\Big(\pi\, g_A^2 - 4\big(2c_2 - \tilde{c} + 2c_2 \ln\,\mu\big)\Big)\end{aligned} \tag{5.28}$$

$$+\frac{g_A^2\,M_\pi}{m_N}\Big(13+6\big(1+\kappa_s\big)\tau^3+12\big(2+\big(1+\kappa_s\big)\tau^3\big)\ln\mu\Big)\Big]+\delta\bar{\beta}, \tag{5.29}$$

where

$$\tilde{c}=4c_1+c_2-2c_3,\quad \mu=\frac{M_\pi}{m_N},\quad \alpha_e=\frac{e^2}{4\pi}, \tag{5.30}$$

$\delta\bar{\alpha}$ and $\delta\bar{\beta}$ parameterize the contributions coming from the fourth-order Lagrangian.

Expanding our results, displayed in Appendix E, in m_N^{-1} we exactly reproduce the above expressions. This serves as a powerful check on the consistency of our calculation. The forward spin-polarizability γ_0 is also accessible in a calculation of doubly virtual Compton scattering (VVCS) in the forward limit. This has been carried out in covariant BχPT using the infrared renormalization scheme in Ref. [BHM 03]. Results are explicitly given for the chiral expansion of γ_0 for the proton and neutron, which we have to compare to

$$\begin{aligned}\gamma_0=\frac{e^2\,g_A^2}{96\pi^3F_\pi^2\,M_\pi^2}\Bigg[&1-\frac{\pi\,\mu}{8}\big(3\big(5+\kappa_v\big)+\big(6+\kappa_s\big)\tau^3\big)\\&-\frac{\mu^2}{4}\big(50+3\kappa_s+15\kappa_v+3\big(10+5\kappa_s+\kappa_v\big)\tau^3\\&+\big(60+6\kappa_s+22\kappa_v\big)+2\big(22+11\kappa_s+3\kappa_v\big)\ln\mu\big)\\&+\frac{15\pi\,\mu^3}{64}\big(65+21\kappa_s+32\kappa_v+\big(60+42\kappa_s+17\kappa_v\big)\tau^3\big)\Bigg].\end{aligned} \tag{5.31}$$

Our result perfectly agrees with Ref. [BHM 03]. Since we use a different strategy for the calculation of γ_0 and additionally employ the reformulated IR scheme, the above check is very non-trivial.

We have summarized the numerical values of the polarizabilities for RCS in Tab. 5.2. No unknown LECs enter in the leading order results, whereas at next-to-leading order the two LECs of Eqs. (5.3) and (5.4) contribute to α and β. More precisely the combination $e_x^+ + 2\,e_y^+$ enters in α while β only receives contribution proportional to e_y^+. Let us stress that the fitted LECs at fourth order are of rather natural size, thus the inclusion of heavier degrees of freedom, e.g. Δ (1232 MeV), is not mandatory to describe the experimental data reasonably well. The values in our covariant calculation substantially differ from the ones obtained in HBχPT[3]. In HBχPT the expansion is performed in the ratio M_π/m_N, therefore we expect the corrections of next-to-leading order to be suppressed by a factor of around 1/7. Clearly this is not the case and the relatively large corrections are mostly due to large prefactors spoiling the convergence of the series. One of the problems is the fairly large value for the isovector anomalous magnetic moment $\kappa_v \approx 3.07$. In this context it is worth noting that the good description of α and β at leading order in HBχPT is a mere coincidence. Our results also indicate large corrections at next-to-leading order,

[3]Note that our results correspond to the resummation of an infinite number of specific terms in HBχPT.

	This work		HBχPT		DR	
	$\mathcal{O}(q^3)$	$\mathcal{O}(q^4)$	$\mathcal{O}(q^3)$	$\mathcal{O}(q^4)$	HDPV	BGLMN
α	6.93	12.17*	13.6	–	11.0	11.9
β	−1.93	1.65*	1.4	–	1.0	1.9
γ_{E1E1}	−3.22	−2.54	−5.7	−1.4	−4.3	−3.4
γ_{M1M1}	−0.23	−3.09	−1.1	3.3	2.9	2.7
γ_{E1M2}	0.65	0.76	1.1	0.2	−0.01	0.3
γ_{M1E2}	0.81	0.21	1.1	1.8	2.1	1.9
γ_0	1.99	4.67	4.6	−3.9	−0.7	−1.5
γ_π	3.16	−1.11	4.6	6.3	9.3	7.8

Table 5.2: Theoretical predicitons for the scalar and vector polarizabilities. The HBχPT predictions are from [Hem+ 98, VKMB 00] and the fixed-t dispersion relation analysis are from [Hol+ 00] and [Bab+ 98]. The values marked with an asterisk have been fitted. The scalar polarizabilities are in units of $10^{-4}\,\mathrm{fm}^3$ and the vector polarizabilities are given in units of $10^{-4}\,\mathrm{fm}^4$.

however the absolute values of the corrections are smaller than in HBχPT, with the exception of the backward spin-polarizability γ_π. The comparison to the dispersive analysis shows disagreement for all polarizabilities, not only for the absolute values but in some cases also for the sign. This disparity indicates that there are large contributions from effective degrees of freedom in the dispersive analysis, which are not explicitly present in our calculation. The model input for the dispersive analysis is the pion electro-production amplitudes from MAID 2007 [DKT 07], which incorporates the most prominent nucleon excitations and resonances in the range of 1-2 GeV. Since we are only working with nucleons and pions all contributions from resonances and excited states are buried in the LECs of our theory.

A conclusion on the convergence of covariant BχPT based on the numbers in Tab. 5.2 would be premature, since at next-to-leading order new LECs contribute, i.e. e_x^+, e_y^+, $c_6\,(\kappa_v)$ and $c_7\,(\kappa_s)$. The magnitude of the next-to-leading order corrections depends on the LECs, which cannot be fixed impeccably. Therefore it is not inconceivable that for certain values of LECs the series converges. One can still observe that the absolute size of the corrections is smaller in the covariant calculation.

5.3 Virtual Compton scattering

In this section we present the main results for VCS off the proton to fourth order in BχPT, using the coupling constants from the previous section.

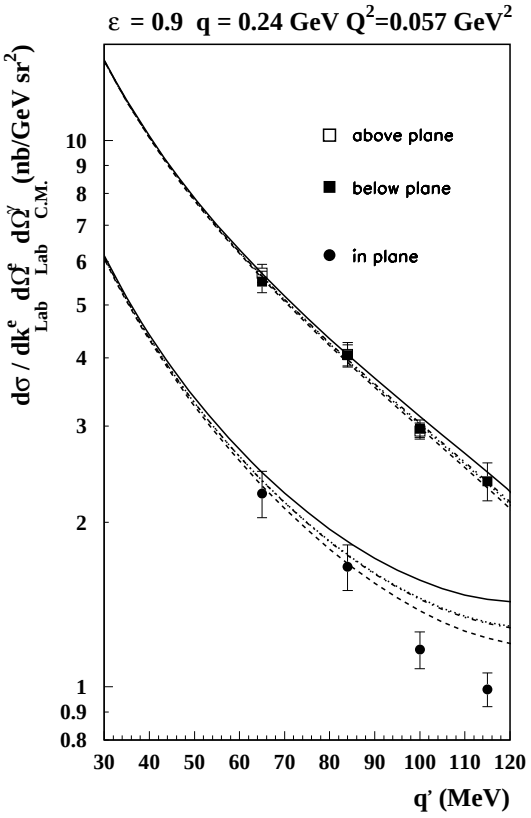

Figure 5.2: Differential cross sections for the photo electro-production off the proton as a function of the outgoing photon energy in the MIT-Bates kinematics. Description of the curves is the same as in Fig. 5.1. Data points are from [Bou+ 06].

5.3.1 Differential cross sections

Let us first take a look at the differential cross sections for different kinematics. This allows us to estimate the range of applicability of our calculation. Note that in the following we use our results for the VCS process and resort to phenomenological form factors of the proton when calculating cross sections.

In Fig. 5.2 we show the results for the reaction $ep \to e'p'\gamma$ from the MIT-Bates experiment [Bou+ 06]. We see that our calculation nicely describes the out-of-plane measurements over the whole range of the outgoing photon energy. For in-plane kinematics the agreement between theory and experiment is limited to moderate values of the outgoing photon energy, i.e. $q' \leq 80\,\mathrm{MeV}$. The differential cross sections are largely dominated by the Bethe-Heitler and Born parts, however we expect the effect of the VCS process to be enhanced for the out-of-plane kinematics at higher values of q'. It is interesting to note that for in-plane kinematics the contributions from the VCS process are expected to be very small. As can be seen in Fig. 5.2 this is not the case, indicating the limitations of our approach for the

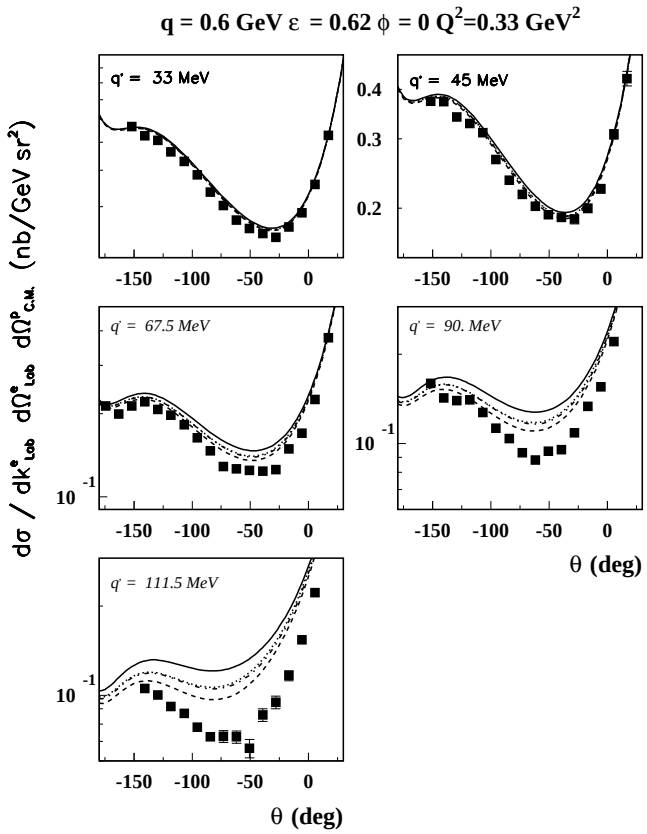

Figure 5.3: Differential cross section for the reaction $ep \to e'p'\gamma$ as a function of the photon scattering angle θ in the MAMI kinematics specified in the plot. Again the full, dashed and dotted lines correspond to fit I, II and III respectively. Data points are from [Roc+ 00].

description of VCS[4].

The experiments at the MAMI facility in Mainz are performed at a relatively large photon virtuality of $Q^2 = 0.33$ GeV^2. Since we perform an expansion in momenta over a characteristic scale Λ, e.g. $\Lambda = 4\pi F_\pi$ or $\Lambda = m_N$, at this value of Q^2 the applicability of BχPT is questionable at best. In Fig. 5.3 the differential cross section for photon electro-production in the MAMI kinematics [Roc+ 00] is shown. We reproduce the experiment only up to photon energies of about 45 MeV. For larger q' and scattering angles around $-50°$, the theoretical predictions largely overestimate the measured cross sections.

From the plots for the differential cross sections we can already see that the description using BχPT will fail for larger values of q' in the MAMI setup, whereas in the MIT-Bates kinematics we can expect reasonable description of experiments up to a photon lab energy of about 80 MeV.

[4]One should keep in mind that we use the fitted values from the RCS differential cross sections.

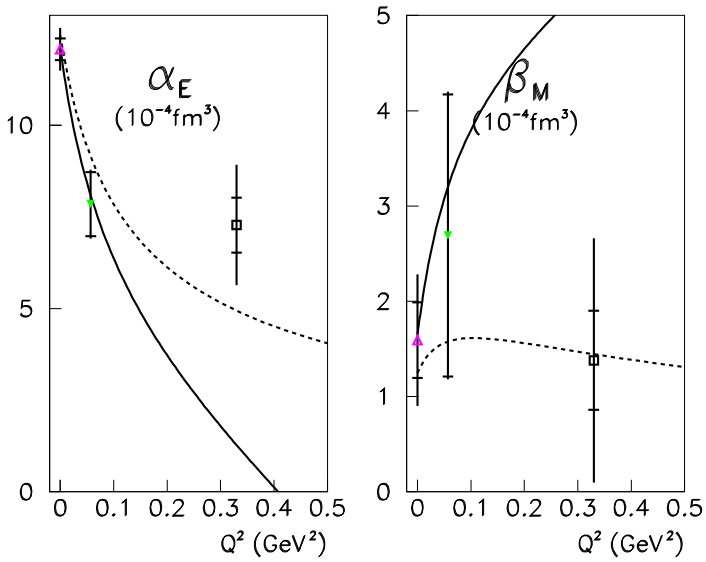

Figure 5.4: The electric $\alpha_{E1}(Q^2)$ (left panel) and magnetic $\beta_{M1}(Q^2)$ (right panel) generalized polarizabilities. The full lines represents our result using the LECs obtained in fit I, the dashed lines are results from HBχPT at order $\mathcal{O}(q^3)$ [Hem+ 97a].

5.3.2 Generalized polarizabilities

We now give our results for the generalized polarizabilities defined in section 3.3. First we give results for the Q^2 dependence of the generalized scalar polarizabilities $\alpha(Q^2)$ and $\beta(Q^2)$.

Our results are shown in Fig. 5.4, together with predictions from HBχPT at third order [Hem+ 97a]. In this plot we use the values for LECs as obtained by the fit to the experimental values of the static electric and magnetic polarizabilities, i.e. fit I. Thus the results match exactly the experimental points at $Q^2 = 0$, however the Q^2 dependence can be viewed as a prediction. Clearly our results deviate from the ones obtained in HBχPT. It should be noted that the leading order HBχPT results receive large contributions at fourth order, thus the good agreement with experiment seems to be accidental. In our opinion the MAMI point at $Q^2 = 0.33$ GeV^2 is most probably beyond the range of applicability of BχPT. We will comment on the convergence of both series below. For now let us state that the Q^2 dependence of the scalar polarizabilities is in accordance with the MIT-Bates point.

Next we show the results for the spin-dependent polarizabilities. The results in Fig. 5.5 show a comparison between a dispersive analysis, the HBχPT calcula-

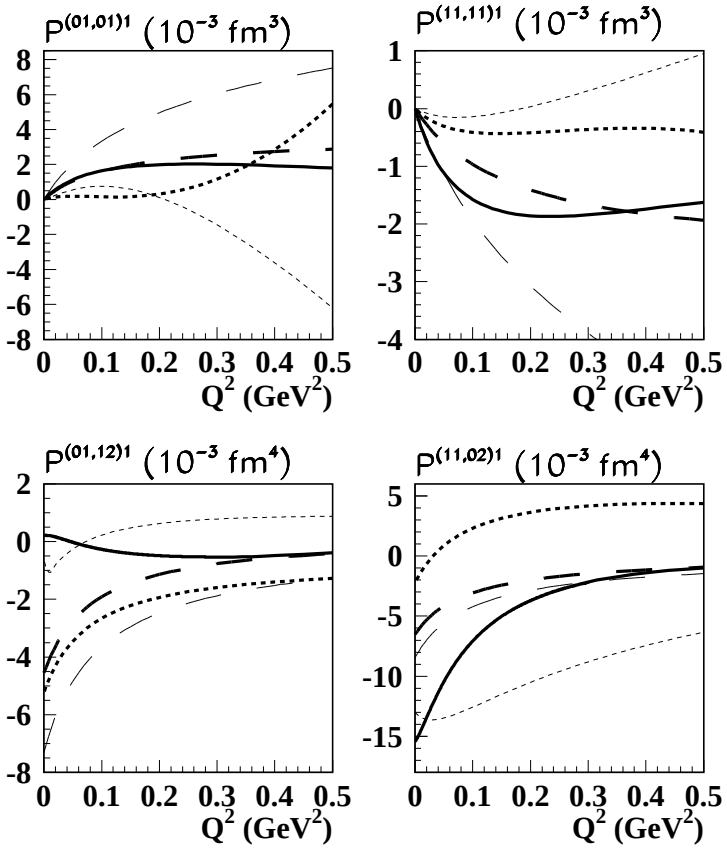

Figure 5.5: Results for the spin-dependent generalized polarizabilities. Full line is the dispersive result using MAID 2007 as input [DPV 03]. Thick long-dashed and thick dashed lines are our results at order $\mathcal{O}(q^3)$ (leading order) and $\mathcal{O}(q^4)$ (next-to-leading order) respectively. Thin long-dashed and thin dashed lines are the results of HBχPT at $\mathcal{O}(q^3)$ (leading order) and $\mathcal{O}(q^4)$ (next-to-leading order) respectively [KV 02, KPV 04].

tion to fourth order and our results. One can see that the results in our covariant calculation largely differ form the HBχPT and dispersion theoretical results. The difference between the leading and next-to-leading order results is less pronounced in our calculation compared to heavy baryon. We also see that the fourth order contributions show a different trend for the GPs in the lower panel of Fig. 5.5, i.e. $P^{(01,12)1}$ and $P^{(11,02)1}$. If one assumes the dispersive analysis to be a good approximation for the real world, one can conclude that neither HBχPT nor our calculation successfully describe the Q^2 dependence of the GPs. However the measurement of the Q^2 dependence of the GPs requires double polarization experiments and so far there are no published data for a direct measurement of the GPs. Thus the picture remains inconclusive as to which of the curves give the best description.

Contrary to the spin-dependent GPs the structure functions accessible in an

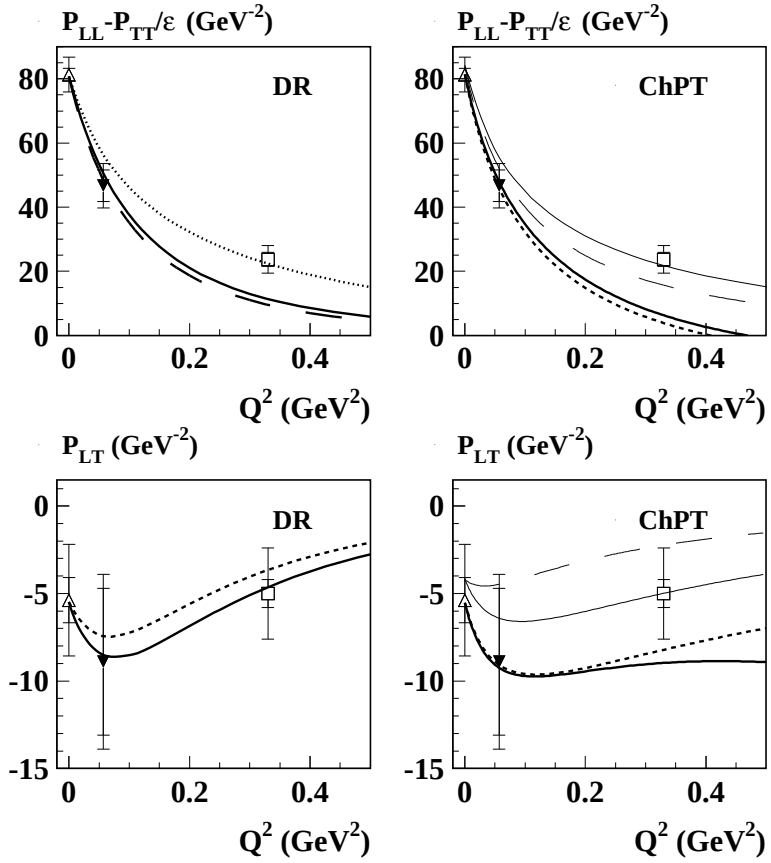

Figure 5.6: Comparison between the unpolarized structure functions calculated by dispersion relation (DR) [Pas+ 01] (left column), HBχPT at $\mathcal{O}(q^3)$ (thin lines in right column) [Hem+ 97b, Hem+ 00] and our results at order $\mathcal{O}(q^4)$ (thick lines in right column). Upper row: Result for $P_{LL}-P_{TT}/\varepsilon$ with $\varepsilon = 0.62$ (solid lines) and $\varepsilon = 0.9$ (dashed-dotted lines) compared to the results for α_{E1} only and $\varepsilon = 0.62$ (dashed lines). The DR results for $\varepsilon = 0.62$ and $\varepsilon = 0.9$ are obtained with $\Lambda_\alpha = 1.79\,\mathrm{GeV}$ and $\Lambda_\alpha = 0.7\,\mathrm{GeV}$, respectively. Lower row: Results for P_{LT} (solid line) compared to the results for β_{M1} only (dashed line). The data are from [Leo+ 01, Bou+ 06, Roc+ 00].

unpolarized experiment have been measured. In Fig. 5.6 we show a comparison between the results obtained from a dispersive analysis [Pas+ 01], HBχPT to $\mathcal{O}(q^3)$ [Hem+ 97b, Hem+ 00] and our results. The structure functions are linear combinations of the GPs defined in Eqs. (3.68 - 3.70). In order to make the effects of the spin-dependent polarizabilities explicit, we plot the spin-independent (dashed lines) part together with the full result (solid lines). In the dispersive approach the Q^2 dependence of the electric (α_{E1}) and magnetic (β_{M1}) dipole polarizabilities have been parameterized using a dipole ansatz, i.e.

$$\alpha_{E1}(Q^2) = \frac{\alpha_{E1}(0)}{\left(1 + Q^2/\Lambda_\alpha^2\right)^2}. \tag{5.32}$$

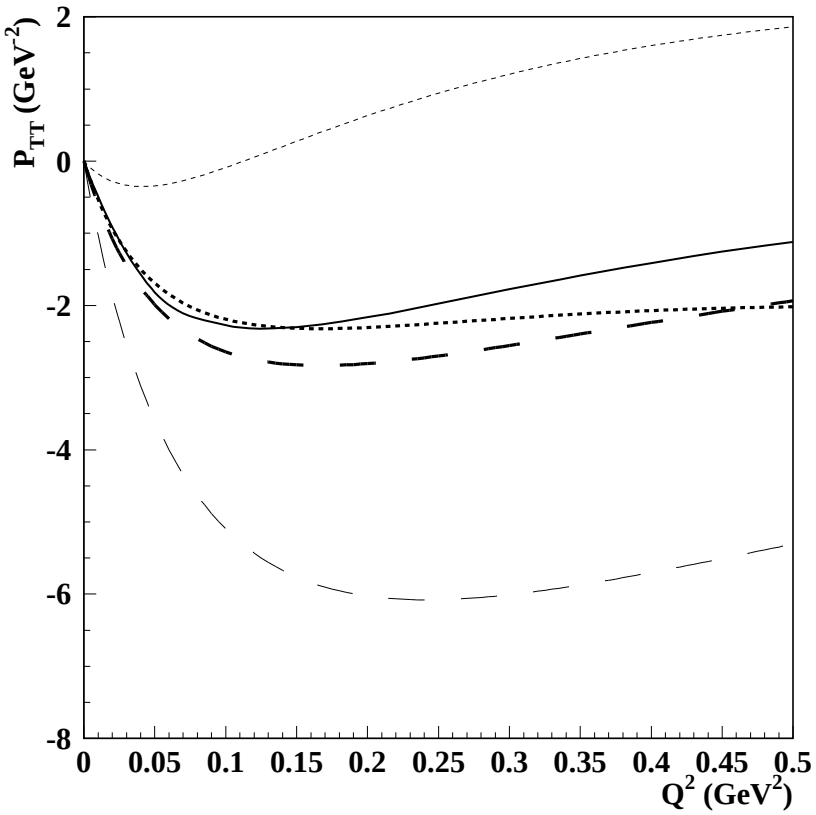

Figure 5.7: P_{TT} as a function of Q^2 as obtained by DR (solid line) [Pas+ 00], HBχPT at leading (thin dashed line), next-to-leading order (thin short-dashed line) [Hem+ 97b, KV 02] and our calculation at leading order (thick dashed line) and next-to-leading order (thick short-dashed line).

The effect of the spin-dependent GPs increases with larger values of Q^2 in all models, however the effect is very pronounced in the HBχPT calculations. In accordance with the results obtained in DR, our calculation is less sensitive to contributions from the spin-dependent GPs. As expected we again fail to describe the experimental point for MAMI kinematics. In Fig. 5.7 the situation is shown for P_{TT}, which only depends on the spin-dependent GPs. At fourth order in BχPT this quantity is purely fixed by g_A and the anomalous magnetic moments κ_N, thus our calculations are pure predictions of the theory. One observes that P_{TT} receives large contributions at next-to-leading order in HBχPT, and largely deviates from the DR result. Our result on the other hand supports the DR analysis for $Q^2 \leq 0.1\,\mathrm{GeV}^2$. Moreover the convergence of P_{TT} is improved in our covariant calculation. The large next-to-leading order effects cast serious doubt on the convergence of the HBχPT calculation for the spin-dependent polarizabilities. Since P_{LL} is proportional to $\alpha(Q^2)$ and P_{LT} receives contributions from $\beta(Q^2)$, a good understanding of the spin-dependent GPs

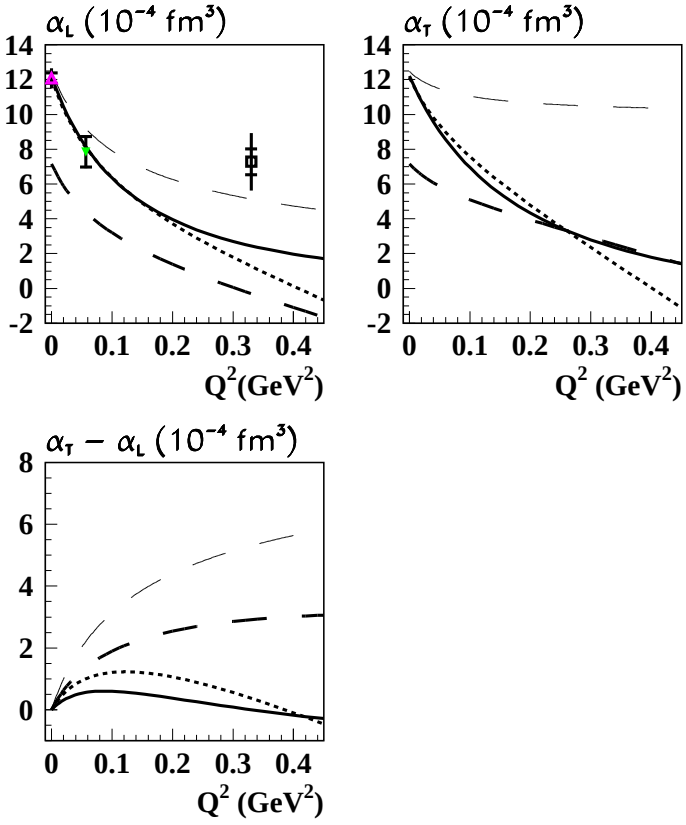

Figure 5.8: Predictions for the generalized dipole polarizabilities of the proton. The solid line represents the DR results with MAID 2007 as input and $\Lambda_\alpha = 0.6$ for the dipole parametrization of $\alpha_L(Q^2)$. The thick long-dashed and thick dashed lines are our results of covariant BχPT. The thin long-dashed line is the leading order result of HBχPT [Hem+ 97b, Hem+ 97a, Hem+ 00].

is mandatory in order to extract the scalar polarizabilities from an unpolarized experiment. Our results agree with the DR analysis for P_{TT}, therefore supporting the extraction of $\alpha(Q^2)$ from the unpolarized experiments.

Finally we present the results for the generalized electric dipole polarizabilities introduced in [L'v+ 01]. In order to completely recover the polarization of the nucleon induced by an external electromagnetic field one needs 2 scalar electric dipole polarizabilities. These generalized dipole polarizabilities are denoted by α_L and α_T, which are equal at the real photon point. A difference between α_L and α_T results in an orientation-dependent polarization of the nucleon, and therefore a complicated spatial distribution of dipole density. In Fig. 5.8 we show the results for α_L and α_T together with the difference of both. Our results are shown for fit I. In contrast to the leading order HBχPT results the covariant calculation is in fairly good agreement with the DR analysis up to $Q^2 = 0.1\,\mathrm{GeV}^2$. The difference of the longitudinal and transverse electric dipole polarizabilities is smaller in the covariant calculation and with increasing order tends to the DR result. Our calculation thus

supports the DR perception that the nucleon is predominantly polarized parallel to the orientation of the incident electric field.

Chapter 6

Summary and conclusions

In this thesis we have performed a calculation of virtual Compton scattering (VCS) off the nucleon to fourth order in manifestly Lorentz-invariant BχPT using the reformulated version of the infrared regularization scheme [SGS 04]. This represents the first complete fourth-order calculation of the generalized polarizabilities in relativistic BχPT. We have calculated the contributions to VCS beyond the low-energy theorems, which are parameterized using six generalized polarizabilities [GLT 95]. To that end the calculation of 100 one-loop diagrams is necessary. We lessened the calculational burden by implementing various routines for the computer-aided calculation of the most demanding tasks. The first part of this thesis is concerned with the implementation and modification of computer programs helpful for the calculations in BχPT in general. As a second part we have successfully applied these programs in the calculation of VCS.

The first obstacle is the diagram generation, for which we have used the Mathematica (MMA) package FeynArts [HPV 99]. We have set up extensions to FeynArts, accounting for vertices of the same type, i.e. with the same number of particles attached to a vertex, but different chiral order. Additionally we changed parts of the FeynArts source code adapting the graphical representation of diagrams to our needs. Because of the severe limitations in speed or size of intermediate expressions we decided to use FORM [Ver 00] for the cumbersome task of the algebraic simplifications. We have followed a hybrid approach merging the advantages of MMA and FORM, similar to FormCalc [HPV 99]. To that end we have implemented a MMA interface delegating parts of the calculation to FORM. We have implemented FORM procedures performing isospin and Dirac algebra simplifications, identification of one-loop integrals and decomposition of tensor integrals in the LoopTools notation. The Dirac algebra procedures are capable of eliminating multiple occurrences of momenta and indices, and the ordering of momenta and indices either lexicographically or user-defined. All procedures work in D dimensions by default. The FORM procedure for the identification of one-loop integrals performs elementary reductions of even powers of the loop momentum in the numerator. Subsequently the tensor structure, i.e. uncontracted loop-momenta, is identified and cast into one single function, which in turn is decomposed according to the notations introduced in the LoopTools package. The calculation of all

100 one-loop diagrams takes about 10 minutes on an ordinary personal computer. These results comprise of the genuine VCS process as well as the parts fixed by the low-energy theorems (LET). In order to separate the genuine VCS contributions we further analyzed the amplitudes by subtracting all nucleon pole contributions. This causes severe problems in the numerical evaluation of the tensor coefficients using LoopTools. LoopTools employs the Passarino-Veltman reduction scheme for the calculation of tensor coefficients. This reduction scheme is plagued by the occurrence of so-called Gram determinants. Unfortunately these determinants vanish for most of the nucleon pole diagrams, thus demanding special treatment. This problem also persists for a large region in phase space for the MAMI kinematics. We have therefore implemented different reduction schemes introduced in the work of Denner and Dittmaier [DD 06], coping with the problem of exceptional kinematics. More specifically we have implemented the reductions corresponding to an expansion in Gram determinants and in modified Cayley and Gram determinants to leading order. Since we use existing C code the implementation was necessarily done in C, nevertheless we have a working implementation of the reduction schemes in MMA as well. The C implementation is designed as an extension to LoopTools, i.e. for safe kinematics the standard LoopTools library is called. For exceptional kinematics the C program calculates all tensor coefficients up to rank 4 and saves them together with the kinematical setup in a lookup table. In this way all numerical instabilities in our calculation are tamed. The implementation of the reduction schemes turned out to be crucial for the calculation of the generalized polarizabilities (GP) as well. Since the GPs are defined in terms of the invariant amplitudes at very specific kinematics, the problem of exceptional kinematics is enhanced. Moreover one inevitably introduces kinematical singularities in the extraction of the invariant amplitudes. These singularities should vanish for the genuine VCS process, however we obtained the genuine VCS contribution by subtracting the nucleon pole parts from the full results. Thus the regularity of our amplitudes is not easily seen. We have therefore performed a Laurent series expansion in the critical variable ν. Unfortunately this gives rise to derivatives of the one-loop integrals. To that end we have first reduced all tensor one-loop integrals to scalar ones with the above mentioned implementations. Finally we have implemented the calculation of derivatives of one-loop integrals in a MMA program. This program is based on the results of Devaraj and Stuart [DS 98] for the 2- and 3-point functions, which was extended to the 4-point function in this work.

All of these developments were necessary to arrive at analytic expressions for all GPs to fourth order in relativistic chiral perturbation theory. This also enabled us to perform very non-trivial checks on our calcualtions, in comparing our results with previously obtained results from heavy-baryon χPT and partial results in relativistic BχPT.

In the expressions for VCS off the nucleon four new low-energy constants (LEC) appear at fourth order, two for the proton and neutron respectively. The new constants only contribute to the scalar polarizabilities α and β. We have performed three different fits using the available data on real Compton scattering (RCS) only. The data is described reasonably well with rather natural values for the coupling

constants. Next we have collected our results for the polarizabilities of RCS. To that end we have taken the real-photon limit in our amplitudes and separated the contributions from third and fourth order. We see large differences to the heavy-baryon results for all polarizabilities. Since the spin-dependent polarizabilities do not get contributions from tree graphs they are pure predictions of our theory. All LECs contributing here are fixed from fits to either the anomalous magnetic moments or πn scattering. The convergence of the series seems not to be reached at fourth order, although the absolute corrections to the polarizabilities are smaller than in HBχPT. We also see that our results are in conflict with predictions from the dispersive analysis. This might indicate that contributions from nucleon resonances to the polarizabilities, which are not explicitly incorporated in our calculations, are very important.

Using the fitted values from RCS we have calculated the differential cross sections for the MIT-Bates and the MAMI experiments. We have seen that while the description for the MIT-Bates cross section is reasonable for moderate values of the outgoing photon lab energy, the cross section for the MAMI kinematics are largely overestimated already at very small values of the outgoing photon momentum. This can be attributed to the fairly large virtuality of $Q^2 = 0.33\,\mathrm{GeV}^2$ at which the MAMI experiment operates. We conclude that our calculations seem to be not applicable for the MAMI kinematics.

As a next quantity we have compared the results for the structure functions accessible in an unpolarized experiment. We have compared our results with a dispersion theoretical analysis and the results from HBχPT. The first striking observation is that our results are in much better agreement with the DR analysis than the HBχPT results, especially concerning the insensitivity of $P_{LL} - P_{TT}/\epsilon$ to the spin-dependent GPs. Additionally we see a much better-behaved convergence in the structure function P_{TT}. Thus we support the DR perception that the scalar polarizabilities of the nucleon are extractable from unpolarized measurements. However the GPs themselves substantially differ from the DR analysis. For an extraction of all GPs double polarization experiments are needed. Therefore the picture remains inconclusive as to which model describes the GPs best.

Finally we have shown results for the generalized dipole polarizabilities of the nucleon as introduced in [L'v+ 01]. In accordance with DR we see only small differences between α_L and α_T.

We have seen that for some quantities the convergence of the series is not too good. It would be very interesting to see if the inclusion of the Δ and vector mesons as explicit degrees of freedom considerably improves the convergence. Additionally, the inclusion of the Δ and vector mesons should enlarge the range of applicability of BχPT, which seems to be necessary for the VCS experiments performed at MAMI and JLAB. We have also calculated the invariant amplitudes for VVCS, however the calculation of observables was not completed. Therefore these amplitudes should prove useful as the basis for future calculations of observables in VVCS. The programs developed in the course of this work have already been used for other calculations in our group. We hope they will be helpful for future calculations not only in BχPT. However, some effort is required to improve the user-friendliness of

the programs and, of course, to further develop the routines. One example would be to implement the reduction schemes of Denner and Dittmaier beyond leading order, or improve the FORM programs for the algebraic simplifications. Exploratory calculations including the Δ clearly indicate that some improvements need to be made for the FORM program.

Appendix A

Feynman rules

Here we list the Feynman rules needed for the calculations of VCS as derived from the Lagrangians of [GSS 88, Fet+ 00]. All photon momenta are assumed to be incoming.

A.1 Propagators

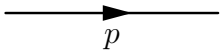

$$\frac{i}{\not{p} - m_N}$$

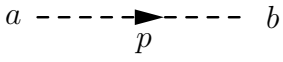

$$\frac{i\,\delta_{ab}}{p^2 - M_\pi^2}$$

A.2 Vertices

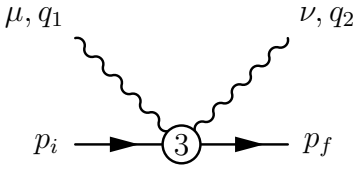

$$\frac{i\,e^2}{2m_N}(d_6 + 2\,d_7)\left(q_1^\mu q_1^\nu + q_2^\mu q_2^\nu - g^{\mu\nu}(q_1^2 + q_2^2)\right)(\mathbb{1} + \tau^3)$$

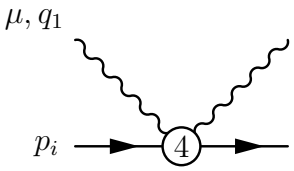

$$\frac{2\,i\,e^2}{m_N^2}\Big\{ e_y\, 4m_N^2\,(q_1^\nu q_2^\mu - g^{\mu\nu} q_1\cdot q_2) + e_x\Big[- g^{\mu\nu}\,(p_f\cdot q_1 p_f\cdot q_2 + p_i\cdot q_1 p_i\cdot q_2) + q_1^\nu\left(p_f^\mu p_f\cdot q_2 + p_i^\mu p_i\cdot q_2\right) - p_f^\nu\left(p_f^\mu q_1\cdot q_2 - q_2^\mu p_f\cdot q_1\right) - p_i^\nu\,(p_i^\mu q_1\cdot q_2 - q_2^\mu p_i\cdot q_1)\Big]\Big\}$$

The coupling constants e_x and e_y are linear combinations of the coupling constants of the fourth order Lagrangian and are given by

$$e_x = (2e_{90} + e_{94} + e_{117})\,\mathbb{1} + e_{92}\,\tau^3,$$
$$e_y = (2e_{89} + e_{93} + e_{118})\,\mathbb{1} + e_{91}\,\tau^3.$$

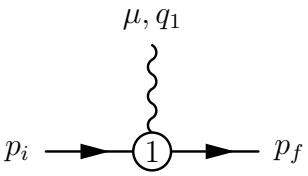

$$-\frac{1}{2} ie\left(\mathbb{1} + \tau^3\right)\gamma^\mu$$

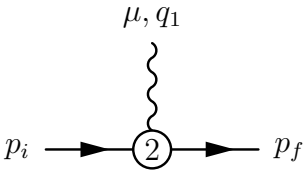

$$\frac{1}{2} e\sigma^{\mu\alpha} q_1^\alpha \left(c_7\,\mathbb{1} + 2c_6\,\tau^3\right)$$

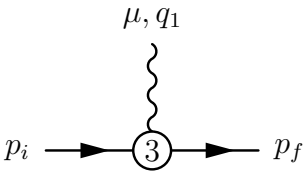

$$\frac{-i\,e}{2m_N}\left(2d_7\mathbb{1} + d_6\,\tau^3\right)\left(q_1^\mu\,(p_f + p_i)\cdot q_1 - \left(p_f^\mu + p_i^\mu\right) q_1^2\right)$$

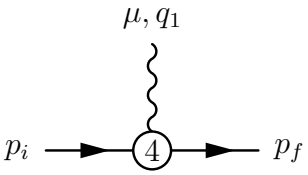

$$e\sigma^{\mu\alpha} q_1^\alpha \left(q_1^2\left(2e_{54}\,\mathbb{1} + e_{74}\,\tau^3\right) - 4M_\pi^2\left(2e_{105}\,\mathbb{1} + e_{106}\,\tau^3\right)\right)$$

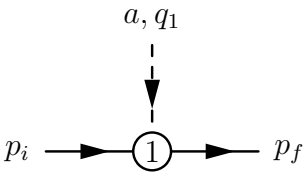

$$\frac{g_A}{2F_\pi}\tau^a\,\gamma^5 \not{q}_1$$

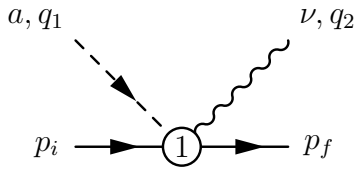

$$-\frac{i\,e\,g_A}{2F_\pi}\,\varepsilon^{3ab}\,\tau^b\,\gamma^5\gamma^\nu$$

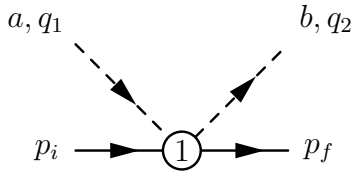

$$\frac{1}{4F_\pi^2}\,\varepsilon^{abc}\,\tau^c\,\left(\not{q}_1+\not{q}_2\right)$$

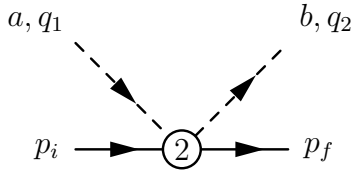

$$\begin{aligned}&\frac{i}{m_N^2F_\pi^2}\delta_{ab}\left[-4c_1M_\pi^2m_N^2+2c_3m_N^2q_1\cdot q_2\right.\\&\left.+c_2\left(p_f\cdot q_1p_f\cdot q_2+p_i\cdot q_1p_i\cdot q_2\right)\right]\\&-\frac{i}{F_\pi^2}c_4\varepsilon^{abc}\tau^c\sigma^{\alpha\beta}q_1^\alpha q_2^\beta\end{aligned}$$

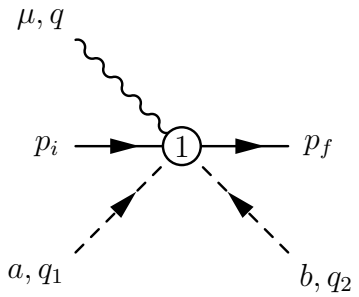

$$\frac{i\,e}{4F_\pi^2}\left(2\delta_{ab}\,\tau^3-\delta_{a3}\,\tau^b-\delta_{b3}\,\tau^a\right)\gamma^\mu$$

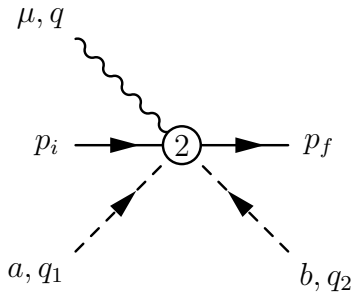

$$\begin{aligned}&\frac{e}{2m_N^2F_\pi^2}\Bigg\{4c_3m_N^2\varepsilon^{3ab}\left(q_1^\mu-q_2^\mu\right)\\&+ic_2\left(\mathbb{1}+\tau^3\right)\Big[\delta_{ab}\left[q_1^\mu q_2\cdot(p_f+p_i)+q_2^\mu q_1\cdot(p_f+p_i)\right]\\&+2i\varepsilon^{3ab}\left[\left(p_f^\mu\left(q_1-q_2\right)\cdot p_f+p_i^\mu\left(q_1-q_2\right)\cdot p_i\right)\right]\Big]\\&-2c_4m_N^2\sigma^{\mu\alpha}\Big[q_1^\alpha\left(\delta_{ab}\,\tau^3-\delta_{3a}\,\tau^b\right)+q_2^\alpha\left(\delta_{ab}\tau^3-\delta_{3b}\tau^a\right)\Big]\\&-c_6m_N^2\sigma^{\mu\alpha}q^\alpha\left(2\delta_{ab}\,\tau^3-\delta_{3a}\,\tau^b-\delta_{3b}\,\tau^a\right)\Bigg\}\end{aligned}$$

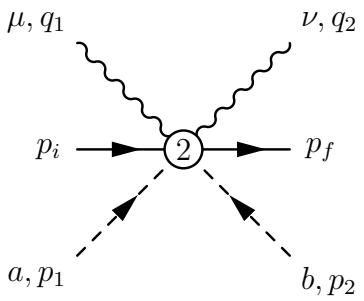

$$\frac{e^2}{2F_\pi^2 m_N^2}\Big\{ 8ic_3\, m_N^2\ (\delta_{ab}-\delta_{3a}\delta_{3b})\, g^{\mu\nu}$$
$$+ c_2\Big[2\, g^{\mu\nu}\varepsilon^{3ab}\left(\mathbb{1}+\tau^3\right)(p_2-p_1)\cdot(p_i+p_f) - 4i\delta_{3a}\delta_{3b}\left(p_f^\mu p_f^\nu + p_i^\mu p_i^\nu\right)$$
$$+ \varepsilon^{3ab}\left(\mathbb{1}+\tau^3\right)\left((p_2^\mu - p_1^\mu)\left(p_i^\nu + p_f^\nu\right) + (p_2^\nu - p_1^\nu)\left(p_i^\mu + p_f^\mu\right)\right)$$
$$+ 2i\delta_{ab}\left(\left(2p_f^\mu p_f^\nu + 2p_i^\mu p_i^\nu\right)\mathbb{1} - \left(p_1^\mu p_2^\nu + p_1^\nu p_2^\mu\right)\left(\mathbb{1}+\tau^3\right)\right)\Big]\Big\}$$

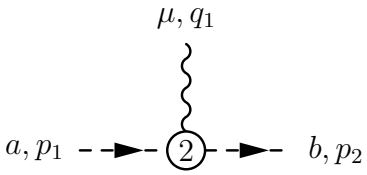

$$e\,\varepsilon^{abc}\,(p_1^\mu + p_2^\mu)$$

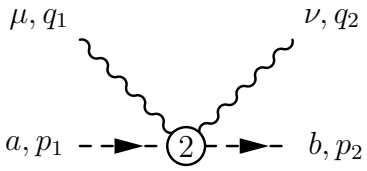

$$2ie^2\ (\delta_{ab}-\delta_{3a}\delta_{3b})\ g^{\mu\nu}$$

Appendix B

Basis of the Compton tensor

The most general form of the Compton tensor $M^{\mu\nu}$ for the VVCS process $\gamma^* + N \to \gamma^* + N$ has been given by Tarrach [Tar 75].
All tensor structures $K_i^{\mu\nu}$ are built up from the Lorentz structures q_1^μ, q_2^μ, P^μ, Q^μ, γ^μ, $\gamma^\mu\gamma^\nu$ and $g^{\mu\nu}$, where q_1 (q_2) is the momentum of the incoming (outgoing) photon and p_i (p_f) is the momentum of the incoming (outgoing) nucleon.

$$
\begin{array}{lll}
K_1^{\mu\nu} = g^{\mu\nu}, & K_{13}^{\mu\nu} = q_2^\mu q_1^\nu \not{Q}, & K_{25}^{\mu\nu} = q_2^\mu \gamma^\nu + q_1^\nu \gamma^\mu, \\
K_2^{\mu\nu} = q_1^\mu q_2^\nu, & K_{14}^{\mu\nu} = (q_1^\mu q_1^\nu + q_2^\mu q_2^\nu)\, \not{Q}, & K_{26}^{\mu\nu} = q_2^\mu \gamma^\nu - q_1^\nu \gamma^\mu \\
K_3^{\mu\nu} = q_2^\mu q_1^\nu, & K_{15}^{\mu\nu} = (q_1^\mu q_1^\nu - q_2^\mu q_2^\nu)\, \not{Q}, & K_{27}^{\mu\nu} = \left[(P^\mu \gamma^\nu + P^\nu \gamma^\mu), \not{Q} \right], \\
K_4^{\mu\nu} = q_1^\mu q_1^\nu + q_2^\mu q_2^\nu, & K_{16}^{\mu\nu} = P^\mu P^\nu \not{Q}, & K_{28}^{\mu\nu} = \left[(P^\mu \gamma^\nu - P^\nu \gamma^\mu), \not{Q} \right], \\
K_5^{\mu\nu} = q_1^\mu q_1^\nu - q_2^\mu q_2^\nu, & K_{17}^{\mu\nu} = (P^\mu q_1^\nu + P^\nu q_2^\mu)\, \not{Q}, & K_{29}^{\mu\nu} = \left[(q_1^\mu \gamma^\nu + q_2^\nu \gamma^\mu), \not{Q} \right], \\
K_6^{\mu\nu} = P^\mu P^\nu, & K_{18}^{\mu\nu} = (P^\mu q_1^\nu - P^\nu q_2^\mu)\, \not{Q}, & K_{30}^{\mu\nu} = \left[(q_1^\mu \gamma^\nu - q_2^\nu \gamma^\mu), \not{Q} \right], \\
K_7^{\mu\nu} = P^\mu q_1^\nu + P^\nu q_2^\mu, & K_{19}^{\mu\nu} = (P^\mu q_2^\nu + P^\nu q_1^\mu)\, \not{Q}, & K_{31}^{\mu\nu} = \left[(q_2^\mu \gamma^\nu + q_1^\nu \gamma^\mu), \not{Q} \right], \\
K_8^{\mu\nu} = P^\mu q_1^\nu - P^\nu q_2^\mu, & K_{20}^{\mu\nu} = (P^\mu q_2^\nu - P^\nu q_1^\mu)\, \not{Q}, & K_{32}^{\mu\nu} = \left[(q_2^\mu \gamma^\nu - q_1^\nu \gamma^\mu), \not{Q} \right], \\
K_9^{\mu\nu} = P^\mu q_2^\nu + P^\nu q_1^\mu, & K_{21}^{\mu\nu} = P^\mu \gamma^\nu + P^\nu \gamma^\mu, & K_{33}^{\mu\nu} = \left[\gamma^\mu, \gamma^\nu \right], \\
K_{10}^{\mu\nu} = P^\mu q_2^\nu - P^\nu q_1^\mu, & K_{22}^{\mu\nu} = P^\mu \gamma^\nu - P^\nu \gamma^\mu, & K_{34}^{\mu\nu} = \left\{ \left[\gamma^\mu, \gamma^\nu \right], \not{Q} \right\}, \\
K_{11}^{\mu\nu} = g^{\mu\nu} \not{Q}, & K_{23}^{\mu\nu} = q_1^\mu \gamma^\nu + q_2^\nu \gamma^\mu, & \\
K_{12}^{\mu\nu} = q_1^\mu q_2^\nu \not{Q}, & K_{24}^{\mu\nu} = q_1^\mu \gamma^\nu - q_2^\nu \gamma^\mu, & \qquad \text{(B.1)}
\end{array}
$$

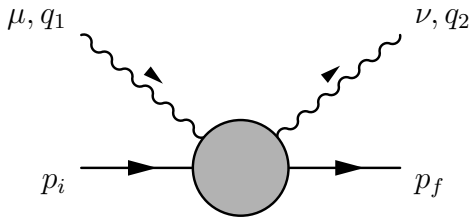

Figure B.1: VVCS process $\gamma^* + N \to \gamma^* + N$.

where

$$P = p_i + p_f,$$
$$Q = q_1 + q_2,$$

and $[\cdot,\cdot]$, $\{\cdot,\cdot\}$ denote the commutator and anti-commutator, respectively.
In fact the number of independent tensors can be reduced by two nontrivial relations among several of the $K_i^{\mu\nu}$, thus leaving us with 32 independent tensors. The number of independent tensors for Compton scattering can also be deduced from counting the helicities of the involved particles.

For virtual Compton scattering we will work with a gauge-invariant tensor basis $\rho_i^{\mu\nu}$ which incorporates current conservation at both photon vertices. The construction of such a basis, and the avoidance of kinematical singularities has been outlined by Bardeen and Tung [BT 68] and explained in more detail in [Dre+ 97, FS 98]. Here we only list the 12 independent tensors relevant for VCS introduced in [Dre+ 98],

$$\begin{aligned}
\rho_1^{\mu\nu} &= -q_1\cdot q_2\, g^{\mu\nu} + q_2^\mu q_1^\nu,\\
\rho_2^{\mu\nu} &= -\left(q_1\cdot P\right)^2 g^{\mu\nu} - q_1\cdot q_2\, P^\mu P^\nu + q_1\cdot P\left(P^\mu q_1^\nu + P^\nu q_2^\mu\right),\\
\rho_3^{\mu\nu} &= q_1\cdot P\, q_1^2\, g^{\mu\nu} - q_1\cdot P q_1^\mu q_1^\nu - q_1^2 P^\nu q_2^\mu + q_1\cdot q_2\, P^\nu q_1^\mu,\\
\rho_4^{\mu\nu} &= P^\mu P^\nu \not{Q} - q_1\cdot P\left(P^\mu\gamma^\nu + P^\nu\gamma^\mu\right) + i\, q_1\cdot P\gamma^5\varepsilon^{\mu\nu\alpha\beta}Q_\alpha\gamma_\beta,\\
\rho_5^{\mu\nu} &= \frac{1}{4}\, P^\nu q_1^\mu \not{Q} + \frac{q_1^2}{4}\left(P^\mu\gamma^\nu - P^\nu\gamma^\mu\right) - \frac{q_1\cdot P}{2}\, q_1^\mu\gamma^\nu + \frac{i}{4}\, q_1^2\varepsilon^{\mu\nu\alpha\beta}Q_\alpha\gamma_\beta,\\
\rho_6^{\mu\nu} &= -2\, q_1\cdot q_2 P^\mu P^\nu + q_1\cdot P\left(P^\mu q_1^\nu + P^\nu q_2^\mu\right) + 2\, m_N\, q_1\cdot q_2\left(P^\mu\gamma^\nu + P^\nu\gamma^\mu\right)\\
&\quad - 2\, m_N\, q_1\cdot P\left(q_2^\mu\gamma^\nu + q_1^\nu\gamma^\mu\right) + i\, q_1\cdot P\left(q_2^\mu\sigma^{\nu\alpha}Q_\alpha - q_1^\nu\sigma^{\mu\alpha}Q_\alpha\right)\\
&\quad + 2\, i\, q_1\cdot q_2 q_1\cdot P\sigma^{\mu\nu} + 2\, i\, m_N\, q_1\cdot q_2\gamma^5\varepsilon^{\mu\nu\alpha\beta}Q_\alpha\gamma_\beta,\\
\rho_7^{\mu\nu} &= \frac{1}{4}\left(P^\mu q_1^\nu - P^\nu q_2^\mu\right)\not{Q} - \frac{q_1\cdot q_2}{2}\left(P^\mu\gamma^\nu - P^\nu\gamma^\mu\right) + \frac{q_1\cdot P}{2}\left(q_2^\mu\gamma^\nu - q_1^\nu\gamma^\mu\right),\\
\rho_8^{\mu\nu} &= \frac{q_1\cdot P}{2} q_1^\mu q_1^\nu - \frac{q_1^2}{4}\left(P^\mu q_1^\nu - P^\nu q_2^\mu\right) - \frac{q_1\cdot q_2}{2}\, P^\nu q_1^\mu - \frac{m_N}{2}\, q_1^\mu q_1^\nu\not{Q}\\
&\quad + m_N\, q_1\cdot q_2 q_1^\mu\gamma^\nu - \frac{m_N}{2}\, q_1^2\left(q_2^\mu\gamma^\nu - q_1^\nu\gamma^\mu\right) + \frac{i}{4}\, q_1^2\left(q_2^\mu\sigma^{\nu\alpha}Q_\alpha - q_1^\nu\sigma^{\mu\alpha}Q_\alpha\right)\\
&\quad + \frac{i}{2}\, q_1\cdot q_2 q_1^2\sigma^{\mu\nu},\\
\rho_9^{\mu\nu} &= \frac{q_1\cdot P}{2}\left(P^\mu q_1^\nu - P^\nu q_2^\mu\right) - m_N\, q_1\cdot q_2\left(P^\mu\gamma^\nu - P^\nu\gamma^\mu\right) + m_N\, q_1\cdot P\left(q_2^\mu\gamma^\nu - q_1^\nu\gamma^\mu\right)\\
&\quad + \frac{i}{2}\, q_1\cdot q_2\left(P^\mu\sigma^{\nu\alpha}Q_\alpha + P^\nu\sigma^{\mu\alpha}Q_\alpha\right) - \frac{i}{2}\, q_1\cdot P\left(q_2^\mu\sigma^{\nu\alpha}Q_\alpha + q_1^\nu\sigma^{\mu\alpha}Q_\alpha\right),\\
\rho_{10}^{\mu\nu} &= -2\, q_1\cdot P g^{\mu\nu} + P^\mu q_1^\nu + P^\nu q_2^\mu + 2\, m_N\, g^{\mu\nu}\not{Q} - 2\, m_N\left(q_2^\mu\gamma^\nu + q_1^\nu\gamma^\mu\right)\\
&\quad - i\, q_2^\mu\sigma^{\nu\alpha}Q_\alpha + i\, q_1^\nu\sigma^{\mu\alpha}Q_\alpha - 2\, i\, q_1\cdot q_2\sigma^{\mu\nu},\\
\rho_{11}^{\mu\nu} &= \left(P^\mu q_1^\nu + P^\nu q_2^\mu\right)\not{Q} - 2\, q_1\cdot P\left(q_2^\mu\gamma^\nu + q_1^\nu\gamma^\mu\right) + 2\, i\, q_1\cdot q_2\gamma^5\varepsilon^{\mu\nu\alpha\beta}Q_\alpha\gamma_\beta,\\
\rho_{12}^{\mu\nu} &= -\frac{q_1^2}{2}\, P^\mu P\nu + \frac{q_1\cdot P}{2}\, P^\nu q_1^\mu + m_N\, q_1^2 P^\mu\gamma^\nu - m_N\, q_1\cdot P q_1^\mu\gamma^\nu\\
&\quad - \frac{i}{4}\, q_1^2\left(P^\mu\sigma^{\nu\alpha}Q_\alpha + P^\nu\sigma^{\mu\alpha}Q_\alpha\right) + \frac{i}{2}\, q_1\cdot P q_1^\mu\sigma^{\nu\alpha}Q_\alpha + \frac{i}{2}\, q_1^2 q_1\cdot P\sigma^{\mu\nu}
\end{aligned}$$

$$+\frac{i}{2}\, m_N\, q_1^2 \gamma^5 \varepsilon^{\mu\nu\alpha\beta} Q_\alpha \gamma_\beta. \tag{B.2}$$

We use the conventions of Bjorken and Drell [BD 64], in particular $\sigma_{\mu\nu} = i[\gamma_\mu, \gamma_\nu]/2$ and the sign of the Levi-Cività symbol is fixed by $\varepsilon_{0123} = -\varepsilon^{0123} = 1$.

The VCS tensor $\mathcal{M}^{\mu\nu}$ can be written as

$$\mathcal{M}^{\mu\nu} = \sum_{i=1}^{12} f_i\left(Q^2, \nu, t\right)\, \rho_i^{\mu\nu}, \tag{B.3}$$

where the basis in Eq. (B.2) is such that not only the $\rho_i^{\mu\nu}$ but also the coefficients f_i are free of kinematical poles. Moreover as the basis of Eq. (B.2) is a particularly suitable linear combination of the tensors in Eq. (B.1) the f_i are either even or odd functions with respect to nucleon crossing combined with charge conjugation:

$$\begin{aligned} f_i\left(Q^2, \nu, t\right) &= +\, f_i\left(Q^2, -\nu, t\right), \ (i = 1, 2, 5, 6, 7, 9, 11, 12), \\ f_i\left(Q^2, \nu, t\right) &= -\, f_i\left(Q^2, -\nu, t\right), \ (i = 3, 4, 8, 10). \end{aligned} \tag{B.4}$$

B.1 Extraction of the f_i

Extracting the f_i from the calculated diagrams using the exact linear combinations of tensors spelled out in Eq. (B.2) is a cumbersome task. We therefore use a more convenient set of *easy-to-identify* basis tensors $\widetilde{K}_i^{\mu\nu}$:

$$\begin{aligned}
\widetilde{K}_1^{\mu\nu} &= g^{\mu\nu}, & \widetilde{K}_{13}^{\mu\nu} &= P^\nu q_2^\mu, & \widetilde{K}_{25}^{\mu\nu} &= q_1^\mu \gamma^\nu, \\
\widetilde{K}_2^{\mu\nu} &= \not{q}_1 g^{\mu\nu}, & \widetilde{K}_{14}^{\mu\nu} &= q_1^\mu q_2^\nu \not{q}_1, & \widetilde{K}_{26}^{\mu\nu} &= q_2^\mu \gamma^\nu, \\
\widetilde{K}_3^{\mu\nu} &= \gamma^\mu \gamma^\nu \not{q}_1, & \widetilde{K}_{15}^{\mu\nu} &= q_1^\nu q_2^\mu \not{q}_1, & \widetilde{K}_{27}^{\mu\nu} &= q_1^\nu \gamma^\mu, \\
\widetilde{K}_4^{\mu\nu} &= \gamma^\mu \gamma^\nu, & \widetilde{K}_{16}^{\mu\nu} &= q_1^\mu q_1^\nu \not{q}_1, & \widetilde{K}_{28}^{\mu\nu} &= q_2^\nu \gamma^\mu, \\
\widetilde{K}_5^{\mu\nu} &= q_1^\mu q_2^\nu, & \widetilde{K}_{17}^{\mu\nu} &= q_2^\mu q_2^\nu \not{q}_1, & \widetilde{K}_{29}^{\mu\nu} &= \gamma^\nu \not{q}_1 P^\mu, \\
\widetilde{K}_6^{\mu\nu} &= q_1^\nu q_2^\mu, & \widetilde{K}_{18}^{\mu\nu} &= P^\mu P^\nu \not{q}_1, & \widetilde{K}_{30}^{\mu\nu} &= \gamma^\mu \not{q}_1 P^\nu, \\
\widetilde{K}_7^{\mu\nu} &= q_1^\mu q_1^\nu, & \widetilde{K}_{19}^{\mu\nu} &= P^\mu q_1^\nu \not{q}_1, & \widetilde{K}_{31}^{\mu\nu} &= \gamma^\nu \not{q}_1 q_1^\mu, \\
\widetilde{K}_8^{\mu\nu} &= q_2^\mu q_2^\nu, & \widetilde{K}_{20}^{\mu\nu} &= P^\mu q_2^\nu \not{q}_1, & \widetilde{K}_{32}^{\mu\nu} &= \gamma^\mu \not{q}_1 q_2^\nu, \\
\widetilde{K}_9^{\mu\nu} &= P^\mu P^\nu, & \widetilde{K}_{21}^{\mu\nu} &= P^\nu q_1^\mu \not{q}_1, & \widetilde{K}_{33}^{\mu\nu} &= \gamma^\nu \not{q}_1 q_2^\mu, \\
\widetilde{K}_{10}^{\mu\nu} &= P^\mu q_1^\nu, & \widetilde{K}_{22}^{\mu\nu} &= P^\nu q_2^\mu \not{q}_1, & \widetilde{K}_{34}^{\mu\nu} &= \gamma^\mu \not{q}_1 q_1^\nu. \\
\widetilde{K}_{11}^{\mu\nu} &= P^\mu q_2^\nu, & \widetilde{K}_{23}^{\mu\nu} &= P^\mu \gamma^\nu & & \\
\widetilde{K}_{12}^{\mu\nu} &= P^\nu q_1^\mu, & \widetilde{K}_{24}^{\mu\nu} &= P^\nu \gamma^\mu, & &
\end{aligned} \tag{B.5}$$

The relation to the original basis of Eq. (B.1) is given by

$$\begin{aligned}
&K_1^{\mu\nu} = \widetilde{K}_1^{\mu\nu}, \quad K_2^{\mu\nu} = \widetilde{K}_5^{\mu\nu}, \quad K_3^{\mu\nu} = \widetilde{K}_6^{\mu\nu}, \quad K_4^{\mu\nu} = \widetilde{K}_7^{\mu\nu} + \widetilde{K}_8^{\mu\nu}, \\
&K_5^{\mu\nu} = \widetilde{K}_7^{\mu\nu} - \widetilde{K}_8^{\mu\nu}, \quad K_6^{\mu\nu} = \widetilde{K}_9^{\mu\nu}, \quad K_7^{\mu\nu} = \widetilde{K}_{10}^{\mu\nu} + \widetilde{K}_{13}^{\mu\nu}, \quad K_8^{\mu\nu} = \widetilde{K}_{10}^{\mu\nu} - \widetilde{K}_{13}^{\mu\nu},
\end{aligned}$$

$$
\begin{aligned}
&K_9^{\mu\nu} = \widetilde{K}_{11}^{\mu\nu} + \widetilde{K}_{12}^{\mu\nu}, \quad K_{10}^{\mu\nu} = \widetilde{K}_{11}^{\mu\nu} - \widetilde{K}_{12}^{\mu\nu}, \quad K_{11}^{\mu\nu} = 2\widetilde{K}_{2}^{\mu\nu}, \quad K_{12}^{\mu\nu} = 2\widetilde{K}_{14}^{\mu\nu}, \quad K_{13}^{\mu\nu} = 2\widetilde{K}_{15}^{\mu\nu},\\
&K_{14}^{\mu\nu} = 2\left(\widetilde{K}_{16}^{\mu\nu} + \widetilde{K}_{17}^{\mu\nu}\right), \quad K_{15}^{\mu\nu} = 2\left(\widetilde{K}_{16}^{\mu\nu} - \widetilde{K}_{17}^{\mu\nu}\right), \quad K_{16}^{\mu\nu} = 2\widetilde{K}_{18}^{\mu\nu},\\
&K_{17}^{\mu\nu} = 2\left(\widetilde{K}_{19}^{\mu\nu} + \widetilde{K}_{22}^{\mu\nu}\right), \quad K_{18}^{\mu\nu} = 2\left(\widetilde{K}_{19}^{\mu\nu} - \widetilde{K}_{22}^{\mu\nu}\right),\\
&K_{19}^{\mu\nu} = 2\left(\widetilde{K}_{20}^{\mu\nu} + \widetilde{K}_{21}^{\mu\nu}\right), \quad K_{20}^{\mu\nu} = 2\left(\widetilde{K}_{20}^{\mu\nu} - \widetilde{K}_{21}^{\mu\nu}\right),\\
&K_{21}^{\mu\nu} = \widetilde{K}_{23}^{\mu\nu} + \widetilde{K}_{24}^{\mu\nu}, \quad K_{22}^{\mu\nu} = \widetilde{K}_{23}^{\mu\nu} - \widetilde{K}_{24}^{\mu\nu},\\
&K_{23}^{\mu\nu} = \widetilde{K}_{25}^{\mu\nu} + \widetilde{K}_{28}^{\mu\nu}, \quad K_{24}^{\mu\nu} = \widetilde{K}_{25}^{\mu\nu} - \widetilde{K}_{28}^{\mu\nu},\\
&K_{25}^{\mu\nu} = \widetilde{K}_{26}^{\mu\nu} + \widetilde{K}_{27}^{\mu\nu}, \quad K_{26}^{\mu\nu} = \widetilde{K}_{26}^{\mu\nu} - \widetilde{K}_{27}^{\mu\nu},\\
&K_{27}^{\mu\nu} = 4\left(-\widetilde{K}_{10}^{\mu\nu} - \widetilde{K}_{12}^{\mu\nu} + \widetilde{K}_{29}^{\mu\nu} + \widetilde{K}_{30}^{\mu\nu} - \widetilde{K}_{9}^{\mu\nu} + \widetilde{K}_{23}^{\mu\nu}\, m_N + \widetilde{K}_{24}^{\mu\nu}\, m_N\right),\\
&K_{28}^{\mu\nu} = 4\left(-\widetilde{K}_{10}^{\mu\nu} + \widetilde{K}_{12}^{\mu\nu} + \widetilde{K}_{29}^{\mu\nu} - \widetilde{K}_{30}^{\mu\nu} + \widetilde{K}_{23}^{\mu\nu}\, m_N - \widetilde{K}_{24}^{\mu\nu}\, m_N\right),\\
&K_{29}^{\mu\nu} = 2\left(-\widetilde{K}_{11}^{\mu\nu} - \widetilde{K}_{12}^{\mu\nu} + 2\left(\widetilde{K}_{31}^{\mu\nu} + \widetilde{K}_{32}^{\mu\nu} - \widetilde{K}_{5}^{\mu\nu} - \widetilde{K}_{7}^{\mu\nu} + \widetilde{K}_{25}^{\mu\nu}\, m_N + \widetilde{K}_{28}^{\mu\nu}\, m_N\right)\right),\\
&K_{30}^{\mu\nu} = 2\left(\widetilde{K}_{11}^{\mu\nu} - \widetilde{K}_{12}^{\mu\nu} + 2\left(\widetilde{K}_{31}^{\mu\nu} - \widetilde{K}_{32}^{\mu\nu} + \widetilde{K}_{5}^{\mu\nu} - \widetilde{K}_{7}^{\mu\nu} + \widetilde{K}_{25}^{\mu\nu}\, m_N - \widetilde{K}_{28}^{\mu\nu}\, m_N\right)\right),\\
&K_{31}^{\mu\nu} = 2\left(-\widetilde{K}_{10}^{\mu\nu} - \widetilde{K}_{13}^{\mu\nu} + 2\left(\widetilde{K}_{33}^{\mu\nu} + \widetilde{K}_{34}^{\mu\nu} - \widetilde{K}_{6}^{\mu\nu} - \widetilde{K}_{7}^{\mu\nu} + \widetilde{K}_{26}^{\mu\nu}\, m_N + \widetilde{K}_{27}^{\mu\nu}\, m_N\right)\right),\\
&K_{32}^{\mu\nu} = 2\left(\widetilde{K}_{10}^{\mu\nu} - \widetilde{K}_{13}^{\mu\nu} + 2\left(\widetilde{K}_{33}^{\mu\nu} - \widetilde{K}_{34}^{\mu\nu} - \widetilde{K}_{6}^{\mu\nu} + \widetilde{K}_{7}^{\mu\nu} + \widetilde{K}_{26}^{\mu\nu}\, m_N - \widetilde{K}_{27}^{\mu\nu}\, m_N\right)\right),\\
&K_{33}^{\mu\nu} = 2\left(\widetilde{K}_{4}^{\mu\nu} - \widetilde{K}_{1}^{\mu\nu}\right),\\
&K_{34}^{\mu\nu} = 4\left(\widetilde{K}_{23}^{\mu\nu} - \widetilde{K}_{24}^{\mu\nu} + 2\left(-\widetilde{K}_{2}^{\mu\nu} + \widetilde{K}_{25}^{\mu\nu} - \widetilde{K}_{27}^{\mu\nu} + \widetilde{K}_{3}^{\mu\nu}\right)\right).
\end{aligned}
$$

Writing the Compton tensor as

$$\mathcal{M}^{\mu\nu} = \sum_{i=1}^{34} \kappa_i\, K_i^{\mu\nu} \tag{B.6}$$

and using the above relations we can extract the coefficients κ_i of the diagrams in terms of the basis in Eq. (B.1). Taking Eq. (B.3) and Eq. (B.6) to be equal and by comparison of coefficients, we find

$$
\begin{aligned}
f_1 &= \kappa_3,\\
f_2 &= \frac{-\kappa_{11} + (\kappa_7 + \kappa_8 - 2(\kappa_{31} - \kappa_{32}))\, m_N + (\kappa_{14} + \kappa_{15})\, Q^2}{2\nu\, m_N^2},\\
f_3 &= \frac{-2m_N(\kappa_8 - 2\,\kappa_{31}) - (\kappa_{14} + \kappa_{15})\, Q^2}{m_N Q^2},\\
f_4 &= \kappa_{16},\\
f_5 &= 4(\kappa_{19} - \kappa_{20}),\\
f_6 &= \frac{\kappa_{11} - 4m_N\,\kappa_{32} - (\kappa_{14} + \kappa_{15})\, Q^2}{4\nu m_N^2},\\
f_7 &= 4\kappa_{18},
\end{aligned}
$$

$$
\begin{aligned}
f_8 &= -\frac{2\left(\kappa_{14}+\kappa_{15}\right)}{m_N},\\
f_9 &= \frac{2\kappa_{31}}{\nu\, m_N},\\
f_{10} &= \frac{\kappa_{11}}{2m_N},\\
f_{11} &= \kappa_{17},\\
f_{12} &= -\frac{2\left(\kappa_{29}+\kappa_{30}\right)}{\nu\, m_N}.
\end{aligned}
$$

As the κ_i's are not independent this solution is not unique, however it has the practical advantage that all odd functions in ν ($i = 3, 4, 8, 10$) are not suppressed with an additional power of ν.

Appendix C

One-loop integrals

In this Appendix we give the basic definitions for the one-loop integrals needed in this work as well as explicit formulas for derivatives of one-loop integrals. For numerical evaluations of the one-loop integrals we use the LoopTools library [HPV 99] which is based on the FF library [OV 90]. Keeping this Appendix as self-contained as possible we recall some definitions of the LoopTools package for the one-loop integrals, further information can be found in [HPV 99] and the user manual.

C.1 Definitions of the one-loop integrals

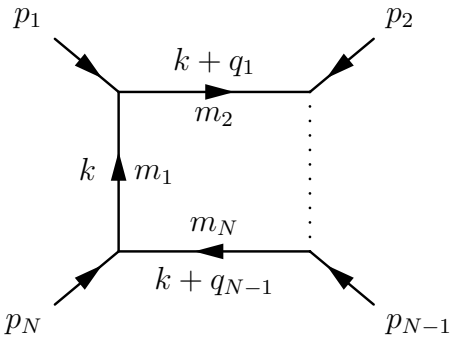

For a general N-point one-loop integral we write

$$T^N_{\mu_1,\ldots\mu_p} = \frac{\left(2\,\pi\mu\right)^{4-D}}{i\pi^2}\int d^Dk \frac{k_{\mu_1}\cdots k_{\mu_p}}{\left[k^2-m_1^2\right]\left[\left(k+q_1\right)^2-m_2^2\right]\ldots\left[\left(k+q_{N-1}\right)^2-m_N^2\right]},$$

where the momenta q_i are related to the external momenta p_i as

$$q_i = \sum_{j=1}^{i} p_j, \tag{C.1}$$

momentum conservation yields

$$\sum_{j=1}^{N} p_j = 0. \tag{C.2}$$

In the following we will use the abbreviation $p_{ij} = (p_i + p_j)$. The nomenclature for the scalar integrals is A_0 for T^1, B_0 for T^2, C_0 for T^3 and D_0 for T^4.

C.1.1 Scalar integrals

One-point function

$$A_0\big(m^2\big) = \frac{\big(2\,\pi\mu\big)^{4-D}}{i\pi^2}\int d^Dk\,\frac{1}{k^2-m^2}.$$

Two-point function

$$B_0\big(p_1^2,m_1^2,m_2^2\big) = \frac{\big(2\,\pi\mu\big)^{4-D}}{i\pi^2}\int d^Dk\,\frac{1}{\big[k^2-m_1^2\big]\big[\big(k+p_1\big)^2-m_2^2\big]}.$$

Three-point function

$$C_0\big(p_1^2,p_2^2,p_{12}^2,m_1^2,m_2^2,m_3^2\big) = \frac{\big(2\,\pi\mu\big)^{4-D}}{i\pi^2}\int d^Dk\,\frac{1}{\big[k^2-m_1^2\big]\big[\big(k+p_1\big)^2-m_2^2\big]\big[\big(k+p_1+p_2\big)^2-m_3^2\big]}.$$

Four-point function

$$D_0\big(p_1^2,p_2^2,p_3^2,p_4^2,p_{12}^2,p_{23}^2,m_1^2,m_2^2,m_3^2,m_4^2\big) = \frac{\big(2\,\pi\mu\big)^{4-D}}{i\pi^2}\int d^Dk\,\frac{1}{\big[k^2-m_1^2\big]\big[\big(k+p_1\big)^2-m_2^2\big]\big[\big(k+p_1+p_2\big)^2-m_3^2\big]\big[\big(k+p_4\big)^2-m_4^2\big]}.$$

C.1.2 Tensor Coefficients

In order to have a compact notation for the tensor decomposition we use the notation of Denner and Dittmaier [DD 06] in which curly brackets denote symmetrization with respect to Lorentz indices in such a way that all non-equivalent permutations of Lorentz indices on metric tensors g and momenta p contribute with weight 1. More specifically we have

$$\begin{aligned}\big\{gp\big\}_{i_1}^{\mu\nu\rho} &= g^{\mu\nu}p_{i_1}^{\rho} + g^{\nu\rho}p_{i_1}^{\mu} + g^{\mu\rho}p_{i_1}^{\nu},\\ \big\{gpp\big\}_{i_1i_2}^{\mu\nu\rho\sigma} &= g^{\mu\nu}p_{i_1}^{\rho}p_{i_2}^{\sigma} + g^{\mu\rho}p_{i_1}^{\nu}p_{i_2}^{\sigma} + g^{\mu\sigma}p_{i_1}^{\nu}p_{i_2}^{\rho} + g^{\nu\rho}p_{i_1}^{\sigma}p_{i_2}^{\mu} + g^{\rho\sigma}p_{i_1}^{\nu}p_{i_2}^{\mu} + g^{\sigma\nu}p_{i_1}^{\rho}p_{i_2}^{\mu},\end{aligned}$$

$$\{gg\}^{\mu\nu\rho\sigma} = g^{\mu\nu}g^{\rho\sigma} + g^{\mu\rho}g^{\nu\sigma} + g^{\mu\sigma}g^{\rho\nu}. \tag{C.3}$$

Using the above abbreviations we can write the tensor integrals as

$$\begin{aligned}
B^{\mu} &= q_1^{\mu} B_1, \\
B^{\mu\nu} &= g^{\mu\nu}\, B_{00} + q_1^{\mu} q_1^{\nu} B_1 1, \\
B^{\mu\nu\rho} &= \{gq\}_1^{\mu\nu\rho} B_{001} + q_1^{\mu} q_1^{\nu} q_1^{\rho}\, B_{111}, \\
C^{\mu} &= \sum_{i=1}^{2} q_i^{\mu} C_i, \\
C^{\mu\nu} &= g^{\mu\nu}\, C_{00} + \sum_{i,j=1}^{2} q_i^{\mu} q_j^{\nu} C_{ij}, \\
C^{\mu\nu\rho} &= \sum_{i=1}^{2} \{gq\}_i^{\mu\nu\rho} C_{00i} + \sum_{i,j,k=1}^{2} q_i^{\mu} q_j^{\nu} q_k^{\rho}\, C_{ijk}, \\
C^{\mu\nu\rho\sigma} &= \{gg\}^{\mu\nu\rho\sigma} C_{0000} + \sum_{i,j=1}^{2} \{gqq\}_{ij}^{\mu\nu\rho\sigma} C_{00ij} + \sum_{i,j,k,l=1}^{2} q_i^{\mu} q_j^{\nu} q_k^{\rho} q_l^{\sigma}\, C_{ijkl}, \\
D^{\mu} &= \sum_{i=1}^{3} q_i^{\mu} D_i, \\
D^{\mu\nu} &= g^{\mu\nu}\, D_{00} + \sum_{i,j=1}^{3} q_i^{\mu} q_j^{\nu} D_{ij}, \\
D^{\mu\nu\rho} &= \sum_{i=1}^{3} \{gq\}_i^{\mu\nu\rho} D_{00i} + \sum_{i,j,k=1}^{3} q_i^{\mu} q_j^{\nu} q_k^{\rho}\, D_{ijk}, \\
D^{\mu\nu\rho\sigma} &= \{gg\}^{\mu\nu\rho\sigma} D_{0000} + \sum_{i,j=1}^{3} \{gqq\}_{ij}^{\mu\nu\rho\sigma} D_{00ij} + \sum_{i,j,k,l=1}^{3} q_i^{\mu} q_j^{\nu} q_k^{\rho} q_l^{\sigma}\, D_{ijkl}.
\end{aligned}$$

The q_i are defined in Eq. (C.1).

C.2 Derivative of one-loop integrals

In this section we adapt the derivatives of the one-loop two- and three-point functions calculated by Devaraj and Stuart [DS 98] to our conventions. Furthermore we will give explicit formulas for the derivatives of the four-point function.

C.2.1 Derivative of the 2- and 3-point functions

Here we give explicit results for the derivatives of the 2-point functions in the notations of [HPV 99].

$$\frac{\partial}{\partial p^2} B_0\left(p^2, m_1^2, m_2^2\right) = \frac{1}{D}\Big[B_0\left(0, m_1^2, m_1^2\right)\left(-p^2 + m_1^2 - m_2^2\right) m_1^2$$

$$
\begin{aligned}
&- \left(p^2 + m_1^2 - m_2^2\right)\left(p^2 - m_1^2 + \left(B_0\left(0, m_2^2, m_2^2\right) + 1\right) m_2^2\right) \\
&+ B_0\left(p^2, m_1^2, m_2^2\right)\left(-m_1^4 + \left(p^2 + 2m_2^2\right) m_1^2 - m_2^4 + p^2 m_2^2\right)\Big], \\
&= \frac{1}{D}\Big[\Big(-p^2 + m_1^2 + m_2^2\Big)p^2 - A_0\big(m_2^2\big)\Big(p^2 + m_1^2 - m_2^2\Big) \\
&- A_0\big(m_1^2\big)\Big(p^2 - m_1^2 + m_2^2\Big) \\
&+ B_0\Big(p^2, m_1^2, m_2^2\Big)\Big(p^2\Big(m_1^2 + m_2^2\Big) - \Big(m_1^2 - m_2^2\Big)^2\Big)\Big],
\end{aligned}
$$

where

$$
D = p^2\left(m_1^4 - 2\left(p^2 + m_2^2\right) m_1^2 + \left(p^2 - m_2^2\right)^2\right).
$$

Some special cases read

$$
\frac{\partial}{\partial p^2} B_0\left(p^2, m_1^2, m_2^2\right)\Big|_{p^2=0} = \frac{m_1^4 - 2A_0\Big(m_2^2\Big)m_1^2 - m_2^4 + 2A_0\Big(m_1^2\Big)m_2^2}{2\Big(m_1^2 - m_2^2\Big)^3},
$$

$$
\frac{\partial}{\partial p^2} B_0\left(p^2, m_1^2, m_2^2\right)\Big|_{p^2=0, m_1^2=m_2^2=m^2} = \frac{1}{6m^2}.
$$

For the derivatives with respect to the masses we have

$$
\begin{aligned}
\frac{\partial}{\partial m_1^2} B_0\big(p^2, m_1^2, m_2^2\big) = \frac{1}{D}\Big[&-A_0\Big(m_1^2\Big)\Big(-p^2 + m_1^2 + m_2^2\Big) \\
&+ m_1^2\Big(2A_0\Big(m_2^2\Big) - \Big(B_0\Big(p^2, m_1^2, m_2^2\Big) - 1\Big)\Big(p^2 - m_1^2 + m_2^2\Big)\Big)\Big],
\end{aligned}
$$

where

$$
D = m_1^2\Big(m_1^4 - 2\Big(p^2 + m_2^2\Big)m_1^2 + \Big(p^2 - m_2^2\Big)^2\Big).
$$

Some special cases are given by

$$
\frac{\partial}{\partial m_1^2} B_0\Big(p^2, m_1^2, m_2^2\Big)\Big|_{p^2=0} = \frac{m_1^2\Big(-m_1^2 + m_2^2 + A_0\Big(m_2^2\Big)\Big) - A_0\Big(m_1^2\Big)m_2^2}{m_1^2\Big(m_1^2 - m_2^2\Big)^2},
$$

$$
\frac{\partial}{\partial m_1^2} B_0\Big(p^2, m_1^2, m_2^2\Big)\Big|_{p^2=0, m_1^2=m_2^2=m^2} = -\frac{1}{2m^2}.
$$

One can get the derivatives with respect to m_2 by exploiting the symmetry of the 2-point function under permutation of its mass arguments.

The derivatives of the 3-point function have been calculated in [DS 98]. They can be expressed as a sum over the scalar 3-point function C_0 and mass-derivatives of the 2-point function B_0. To see this it is advantageous to first express B_0 and C_0 in terms of Feynman parameters.

The Feynman parameter representation of B_0 reads

$$B_0\left(p^2, m_1^2, m_2^2\right) = \Delta - \int\limits_0^1 dx\, \ln\Big(m_1^2\,(x-1) - \left(m_2^2 + p^2\,(x-1)\right) x\Big),$$

and

$$\Delta = -\frac{2}{D-4} - \gamma_E + \ln 4\pi,$$

where D is the number of space-time dimension and $\gamma_E = -\Gamma'(1)$ is Euler's constant. The divergent part of B_0 is parameterized by Δ, which would be put equal to zero in the $\overline{\rm MS}$ scheme[1]. From this one easily obtains the Feynman parameter representation of the mass derivatives of B_0

$$\begin{aligned}
\frac{\partial}{\partial m_1^2} B_0\left(p^2, m_1^2, m_2^2\right) &= -\int\limits_0^1 dx\, \frac{1-x}{p^2\,x^2 + (m_2^2 - m_1^2 - p^2)\,x + m_1^2}, \\
\frac{\partial}{\partial m_2^2} B_0\left(p^2, m_1^2, m_2^2\right) &= -\int\limits_0^1 dx\, \frac{x}{p^2\,x^2 + (m_2^2 - m_1^2 - p^2)\,x - m_1^2}.
\end{aligned} \tag{C.4}$$

The Feynman parameter representation of C_0 reads

$$\begin{aligned}
C_0\left(p_1^2, p_2^2, p_{12}^2, m_1^2, m_2^2, m_3^2\right) &= \int\limits_0^1 dx \int\limits_0^x dy \frac{1}{a\,x^2 + b\,y^2 + c\,x\,y + d\,x + e\,y + f}, \\
&= \int\limits_0^1 dx \int\limits_0^x dy \frac{1}{D}.
\end{aligned} \tag{C.5}$$

The coefficients in Eq. (C.5) are given by

$$\begin{aligned}
&a = -p_1^2, && b = -p_2^2, && c = p_1^2 + p_2^2 - p_{12}^2, \\
&d = p_1^2 + m_1^2 - m_2^2, && e = p_{12}^2 - p_1^2 + m_2^2 - m_3^2, && f = -m_1^2.
\end{aligned}$$

The derivatives of C_0 with respect to any argument can be written as

$$C_0' = \int\limits_0^1 dx \int\limits_0^x dy \frac{\alpha_{x^2}\,x^2 + \alpha_{y^2}\,y^2 + \alpha_{xy}\,xy + \alpha_x\,x + \alpha_y\,y + \alpha_1}{D^2}, \tag{C.6}$$

where the coefficients α_i are summarized in Table C.1.

[1]The $\widetilde{\rm MS}$ scheme of chiral perturbation theory corresponds to $\Delta = -1$.

The task at hand is to find a basis of integrals which can be expressed as linear combinations of C_0 and mass-derivatives of B_0 and at the same time uniquely describe the polynomial in the numerator of Eq. (C.6). In [DS 98] such a basis has been constructed:

$$I_1 = \int_0^1 dx \int_0^x dy \, \frac{y\left(2\,by + cx + e\right)}{D^2}, \qquad I_2 = \int_0^1 dx \int_0^x dy \, \frac{y\left(2\,ax + cy + d\right)}{D^2},$$

$$I_3 = \int_0^1 dx \int_0^x dy \, \frac{x\left(2\,by + cx + e\right)}{D^2}, \qquad I_4 = \int_0^1 dx \int_0^x dy \, \frac{2\,ax + cy + d}{D^2},$$

$$I_5 = \int_0^1 dx \int_0^x dy \, \frac{2\,by + cx + e}{D^2}, \qquad I_6 = \int_0^1 dx \int_0^x dy \, \frac{dx + ey + 2f}{D^2}.$$

Using partial integration and the Feynman parametrization of Eq. (C.4) and (C.5) one can show that

$$\begin{aligned}
I_1 &= C_0 - \frac{\partial}{\partial m_3^2} B_0\left(p_{12}^2, m_1^2, m_3^2\right), \\
I_2 &= -\frac{\partial}{\partial m_3^2} B_0\left(p_2^2, m_2^2, m_3^2\right) + \frac{\partial}{\partial m_3^2} B_0\left(p_{12}^2, m_1^2, m_3^2\right), \\
I_3 &= -\frac{\partial}{\partial m_3^2} B_0\left(p_{12}^2, m_1^2, m_3^2\right) + \frac{\partial}{\partial m_2^2} B_0\left(p_1^2, m_1^2, m_2^2\right), \\
I_4 &= \Big(\frac{\partial}{\partial m_1^2} + \frac{\partial}{\partial m_3^2}\Big) B_0\left(p_{12}^2, m_1^2, m_3^2\right) - \Big(\frac{\partial}{\partial m_2^2} + \frac{\partial}{\partial m_3^2}\Big) B_0\left(p_2^2, m_2^2, m_3^2\right), \\
I_5 &= \Big(\frac{\partial}{\partial m_1^2} + \frac{\partial}{\partial m_2^2}\Big) B_0\left(p_1^2, m_1^2, m_2^2\right) - \Big(\frac{\partial}{\partial m_1^2} + \frac{\partial}{\partial m_3^2}\Big) B_0\left(p_{12}^2, m_1^2, m_3^2\right), \\
I_6 &= \Big(\frac{\partial}{\partial m_2^2} + \frac{\partial}{\partial m_3^2}\Big) B_0\left(p_2^2, m_2^2, m_3^2\right).
\end{aligned} \tag{C.7}$$

C_0' w.r.t.	α_{x^2}	α_{y^2}	α_{xy}	α_x	α_y	α_1
p_1^2	1	0	−1	−1	1	0
p_2^2	0	1	−1	0	0	0
p_{12}^2	0	0	1	0	−1	0
m_1^2	0	0	0	−1	0	1
m_2^2	0	0	0	1	−1	0
m_3^2	0	0	0	0	1	0

Table C.1: Numerator coefficients α_i in Eq. (C.6) for derivatives of C_0.

We can now perform the decomposition of C_0' in terms of the above basis

$$C_0' = \sum_{a=1}^{6} \beta_a \, I_a.$$

By comparison of coefficients we get a set of linear equations

$$\begin{pmatrix} 0 & 0 & c & 0 & 0 & 0 \\ 2b & c & 0 & 0 & 0 & 0 \\ c & 2a & 2b & 0 & 0 & \\ 0 & 0 & e & 2a & c & d \\ e & d & 0 & c & 2b & e \\ 0 & 0 & 0 & d & e & 2f \end{pmatrix} \begin{pmatrix} \beta_1 \\ \beta_2 \\ \beta_3 \\ \beta_4 \\ \beta_5 \\ \beta_6 \end{pmatrix} = \begin{pmatrix} \alpha_{x^2} \\ \alpha_{y^2} \\ \alpha_{xy} \\ \alpha_x \\ \alpha_y \\ \alpha_1 \end{pmatrix}.$$

From these equations we can solve the β_i and thus express C_0' as a sum over C_0 and mass-derivatives of B_0's. As noted in [DS 98] the derivatives of C_0 with respect to any of its mass arguments reduces to B_0's only.

C.2.2 Derivative of the 4-point function

We proceed in complete analogy to the derivation in the previous section. The four-point function in terms of Feynman parameters is given by

$$D_0(p_1^2, p_2^2, p_3^2, p_4^2, p_{12}^2, p_{23}^2, m_1^2, m_2^2, m_3^2, m_4^2) = \int_0^1 dx \int_0^x dy \int_0^y dz \frac{1}{D}, \qquad \text{(C.8)}$$

where

$$D = (a\,x^2 + b\,y^2 + c\,z^2 + d\,x\,y + e\,x\,z + f\,y\,z + g\,x + h\,y + i\,z + j)^2. \qquad \text{(C.9)}$$

The coefficients are given by

$$\begin{aligned} &a = -p_1^2, && b = -p_2^2, && c = -p_3^2, \\ &d = p_1^2 + p_2^2 - p_{12}^2, && e = p_{12}^2 + p_{23}^2 - p_2^2 - p_4^2, && f = p_2^2 + p_3^2 - p_{23}^2, \\ &g = p_1^2 + m_1^2 - m_2^2, && h = p_{12}^2 - p_1^2 + m_2^2 - m_3^2, && i = p_4^2 - p_{12}^2 + m_3^2 - m_4^2, \\ &j = -m_1^2. \end{aligned}$$

We define a set of basis integrals as follows,

$$I_1 = \int_0^1 dx \int_0^x dy \int_0^y dz\, z \frac{\partial}{\partial z} \frac{1}{D},$$

$$I_2 = \int_0^1 dx \int_0^x dy \int_0^y dz\, x \frac{\partial}{\partial z} \frac{1}{D},$$

$$
\begin{aligned}
I_3 &= \int_0^1 dx \int_0^x dy \int_0^y dz\, y\, \frac{\partial}{\partial z}\, \frac{1}{D},\\
I_4 &= \int_0^1 dx \int_0^x dy \int_0^y dz\, z\, \frac{\partial}{\partial y}\, \frac{1}{D},\\
I_5 &= \int_0^1 dx \int_0^x dy \int_0^y dz\, x\, \frac{\partial}{\partial y}\, \frac{1}{D},\\
I_6 &= \int_0^1 dx \int_0^x dy \int_0^y dz\, \frac{\partial}{\partial y}\, \frac{y}{D},\\
I_7 &= \int_0^1 dx \int_0^x dy \int_0^y dz\, \frac{\partial}{\partial y}\, \frac{1}{D},\\
I_8 &= \int_0^1 dx \int_0^x dy \int_0^y dz\, z\, \frac{\partial}{\partial x}\, \frac{1}{D},\\
I_9 &= \int_0^1 dx \int_0^x dy \int_0^y dz\, \frac{\partial}{\partial x}\, \frac{x}{D},\\
I_{10} &= \int_0^1 dx \int_0^x dy \int_0^y dz\, \frac{\partial}{\partial z} \left(z\, \frac{1}{D} \right).
\end{aligned}
\tag{C.10}
$$

The integrals in Eq. (C.10) can be expressed as functions of D_0 and derivatives of 3-point functions. First let us define the modified denominator $\widetilde{\boldsymbol{D}}$ obtained from D in (C.9) by performing the substitutions

$$\widetilde{\boldsymbol{D}} = D(z \to z'\, y, y \to y'\, x).$$

With this definition and using partial integration the basis integrals of (C.10) read

$$
\begin{aligned}
I_1 &= \int_0^1 dx \int_0^x dy \int_0^y dz\, z\, \frac{\partial}{\partial z}\, \frac{1}{D} \qquad (C.11)\\
&= \int_0^1 dx \int_0^x dy \left(\frac{z}{D}\Big|_0^y - \int_0^y dz\, \frac{1}{D} \right)\\
&= \int_0^1 dx \int_0^x dy \frac{z}{D}\Big|_0^y - \int_0^1 dx \int_0^x dy \int_0^y dz\, \frac{1}{D},
\end{aligned}
$$

$$I_2 = \int_0^1 dx \int_0^x dy \int_0^y dz\, x \frac{\partial}{\partial z} \frac{1}{D} \tag{C.12}$$
$$= \int_0^1 dx \int_0^x dy\, x \frac{1}{D}\Big|_0^y,$$

$$I_3 = \int_0^1 dx \int_0^x dy \int_0^y dz\, y \frac{\partial}{\partial z} \frac{1}{D} \tag{C.13}$$
$$= \int_0^1 dx \int_0^x dy\, y \frac{1}{D}\Big|_0^y,$$

$$I_4 = \int_0^1 dx \int_0^x dy \int_0^y dz\, z \frac{\partial}{\partial y} \frac{1}{D} \tag{C.14}$$
$$= \int_0^1 dx \int_0^1 dy' \int_0^1 dz'\, x^2\ y'^2\ z' \left(\frac{\partial}{\partial y'}\frac{1}{\widetilde{\boldsymbol{D}}} - \frac{z'}{y'}\frac{\partial}{\partial z'}\frac{1}{\widetilde{\boldsymbol{D}}}\right)$$
$$= \int_0^1 dx \int_0^1 dz'\, x^2\, z' \left(\frac{y'^2}{\widetilde{\boldsymbol{D}}}\Big|_0^1\right) - \int_0^1 dx \int_0^1 dy'\, x^2\, y' \left(\frac{z'^2}{\widetilde{\boldsymbol{D}}}\Big|_0^1\right),$$

$$I_5 = \int_0^1 dx \int_0^x dy \int_0^y dz\, x \frac{\partial}{\partial y} \frac{1}{D} \tag{C.15}$$
$$= \int_0^1 dx \int_0^1 dy' \int_0^1 dz'\ x^2 y' \left(\frac{\partial}{\partial y'}\frac{1}{\widetilde{\boldsymbol{D}}} - \frac{z'}{y'}\frac{\partial}{\partial z'}\frac{1}{\widetilde{\boldsymbol{D}}}\right)$$
$$= \int_0^1 dx \int_0^1 dz'\ x^2 \left(\frac{y'}{\widetilde{\boldsymbol{D}}}\Big|_0^1\right) - \int_0^1 dx \int_0^1 dy'\ x^2 \left(\frac{z'}{\widetilde{\boldsymbol{D}}}\Big|_0^1\right),$$

$$I_6 = \int_0^1 dx \int_0^x dy \int_0^y dz\ \frac{\partial}{\partial y} \frac{y}{D} \tag{C.16}$$
$$= \int_0^1 dx \int_0^x dy \int_0^y dz\, \frac{1}{D} + \int_0^1 dx \int_0^1 dy' \int_0^1 dz'\ x^2 y'^2 \left(\frac{\partial}{\partial y'}\frac{1}{\widetilde{\boldsymbol{D}}} - \frac{z'}{y'}\frac{\partial}{\partial z'}\frac{1}{\widetilde{\boldsymbol{D}}}\right)$$
$$= \int_0^1 dx \int_0^1 dz'\ x^2 \left(\frac{y'^2}{\widetilde{\boldsymbol{D}}}\Big|_0^1\right) - \int_0^1 dx \int_0^1 dy'\ x^2\, y' \left(\frac{z'}{\widetilde{\boldsymbol{D}}}\Big|_0^1\right),$$

$$I_7 = \int_0^1 dx \int_0^x dy \int_0^y dz \, \frac{\partial}{\partial y} \, \frac{1}{D} \tag{C.17}$$
$$= \int_0^1 dx \int_0^1 dy' \int_0^1 dz' \; xy' \left(\frac{\partial}{\partial y'} \frac{1}{\widetilde{\boldsymbol{D}}} - \frac{z'}{y'} \frac{\partial}{\partial z'} \frac{1}{\widetilde{\boldsymbol{D}}} \right)$$
$$= \int_0^1 dx \int_0^1 dz' \; x \left(\frac{y'}{\widetilde{\boldsymbol{D}}} \Big|_0^1 \right) - \int_0^1 dx \int_0^1 dy' \; x \left(\frac{z'}{\widetilde{\boldsymbol{D}}} \Big|_0^1 \right),$$

$$I_8 = \int_0^1 dx \int_0^x dy \int_0^y dz \, z \, \frac{\partial}{\partial x} \, \frac{1}{D} \tag{C.18}$$
$$= \int_0^1 dx \int_0^1 dy' \int_0^1 dz' \, x^3 \; y'^2 \; z' \left(\frac{\partial}{\partial x} \frac{1}{\widetilde{\boldsymbol{D}}} - \frac{y'}{x} \frac{\partial}{\partial y'} \frac{1}{\widetilde{\boldsymbol{D}}} \right)$$
$$= \int_0^1 dy' \int_0^1 dz' y'^2 \; z' \left(\frac{x^3}{\widetilde{\boldsymbol{D}}} \Big|_0^1 \right) - \int_0^1 dx \int_0^1 dz' \; x^2 \; z' \left(\frac{y'^3}{\widetilde{\boldsymbol{D}}} \Big|_0^1 \right),$$

$$I_9 = \int_0^1 dx \int_0^x dy \int_0^y dz \, \frac{\partial}{\partial x} \, \frac{x}{D} \tag{C.19}$$
$$= \int_0^1 dx \int_0^x dy \int_0^y dz \, \frac{1}{D} + \int_0^1 dx \int_0^1 dy' \int_0^1 dz' \, x^3 \; y' \; \left(\frac{\partial}{\partial x} \frac{1}{\widetilde{\boldsymbol{D}}} - \frac{y'}{x} \frac{\partial}{\partial y'} \frac{1}{\widetilde{\boldsymbol{D}}} \right)$$
$$= \int_0^1 dy' \int_0^1 dz' y' \; \left(\frac{x^3}{\widetilde{\boldsymbol{D}}} \Big|_0^1 \right) - \int_0^1 dx \int_0^1 dz' \; x^2 \; \left(\frac{y'^2}{\widetilde{\boldsymbol{D}}} \Big|_0^1 \right),$$

$$I_{10} = \int_0^1 dx \int_0^x dy \int_0^y dz \, \frac{\partial}{\partial z} \left(z \, \frac{1}{D} \right) \tag{C.20}$$
$$= \int_0^1 dx \int_0^x dy \; \frac{z}{D} \Big|_0^y .$$

We arrive at relations between the basis integrals of (C.10) and Feynman parameter representations of D_0 and derivatives of C_0 with respect to its mass arguments, more specifically

$$I_1 = \frac{\partial}{\partial m_4^2} C_0(1,2,4) - D_0,$$
$$I_2 = \frac{\partial}{\partial m_2^2} C_0(1,2,4) + \frac{\partial}{\partial m_4^2} C_0(1,2,4) - \frac{\partial}{\partial m_2^2} C_0(1,2,3) - \frac{\partial}{\partial m_3^2} C_0(1,2,3),$$

$$
\begin{aligned}
I_3 &= \frac{\partial}{\partial m_4^2} C_0(1,2,4) - \frac{\partial}{\partial m_3^2} C_0(1,2,3),\\
I_4 &= \frac{\partial}{\partial m_4^2} C_0(1,3,4) - \frac{\partial}{\partial m_4^2} C_0(1,2,4),\\
I_5 &= \frac{\partial}{\partial m_3^2} C_0(1,3,4) + \frac{\partial}{\partial m_4^2} C_0(1,3,4) - \frac{\partial}{\partial m_2^2} C_0(1,2,4) - \frac{\partial}{\partial m_4^2} C_0(1,2,4),\\
I_6 &= \frac{\partial}{\partial m_3^2} C_0(1,3,4) + \frac{\partial}{\partial m_4^2} C_0(1,3,4) - \frac{\partial}{\partial m_4^2} C_0(1,2,4),\\
I_7 &= \frac{\partial}{\partial m_1^2} C_0(1,3,4) + \frac{\partial}{\partial m_3^2} C_0(1,3,4) + \frac{\partial}{\partial m_4^2} C_0(1,3,4)\\
&\quad - \frac{\partial}{\partial m_1^2} C_0(1,2,4) - \frac{\partial}{\partial m_2^2} C_0(1,2,4) - \frac{\partial}{\partial m_4^2} C_0(1,2,4),\\
I_8 &= \frac{\partial}{\partial m_4^2} C_0(2,3,4) - \frac{\partial}{\partial m_4^2} C_0(1,3,4),\\
I_9 &= \frac{\partial}{\partial m_2^2} C_0(2,3,4) + \frac{\partial}{\partial m_3^2} C_0(2,3,4) + \frac{\partial}{\partial m_4^2} C_0(2,3,4)\\
&\quad - \frac{\partial}{\partial m_3^2} C_0(1,3,4) - \frac{\partial}{\partial m_4^2} C_0(1,3,4),\\
I_{10} &= \frac{\partial}{\partial m_4^2} C_0(1,2,4).
\end{aligned}
$$

The arguments of C_0 indicate the propagators, numbered according to their appearance in D_0, e.g. $C_0(1,2,3)$ represents D_0 with the fourth propagator omitted.

Using the Feynman parameter representation for D_0 in Eq. (C.8) any derivative of D_0 can be written as

$$
D_0' = \int_0^1 dx \int_0^x dy \int_0^y dz\\
\frac{\alpha_{x^2}\, x^2 + \alpha_{y^2}\, y^2 + \alpha_{z^2}\, z^2 + \alpha_{xy}\, x\, y\ + \alpha_{xz}\, x\, z + \alpha_{yz}\, y\, z + \alpha_x\, x + \alpha_y\, y + \alpha_z\, z + \alpha_1}{D^{3/2}},
\tag{C.21}
$$

where the α_i are given in Table C.2.

On the other hand the derivatives of D_0 can be decomposed into a sum over the basis integrals I_a of Eq. (C.10)

$$
D_0' = \sum_{a=1}^{10} \beta_a\, I_a.
$$

D_0' w.r.t.	α_{z^2}	α_{y^2}	α_{x^2}	α_{xy}	α_{xz}	α_{zy}	α_z	α_y	α_x	α_1
p_1^2	0	0	2	−2	0	0	0	2	−2	0
p_2^2	0	2	0	−2	2	−2	0	0	0	0
p_3^2	2	0	0	0	0	−2	0	0	0	0
p_4^2	0	0	0	0	2	0	−2	0	0	0
$(p_1+p_2)^2$	0	0	0	0	2	−2	0	2	−2	0
$(p_2+p_3)^2$	0	0	0	0	−2	2	0	0	0	0
m_1^2	0	0	0	0	0	0	0	0	−2	2
m_2^2	0	0	0	0	0	0	0	−2	2	0
m_3^2	0	0	0	0	0	0	−2	2	0	0
m_4^2	0	0	0	0	0	0	2	0	0	0

Table C.2: Numerator coefficients α_i in Eq. (C.21) for derivatives of D_0.

Thus by comparison of coefficients one gets a set of linear equations

$$\begin{pmatrix} -4c & 0 & 0 & -2f & 0 & c & 0 & -2e & c & -3c \\ 0 & 0 & -2f & 0 & 0 & -3b & 0 & 0 & b & b \\ 0 & -2e & 0 & 0 & -2d & a & 0 & 0 & -3a & a \\ 0 & -2f & -2e & 0 & -4b & -d & 0 & 0 & -d & d \\ -2e & -4c & 0 & -2d & -2f & e & 0 & -4a & -e & -e \\ -2f & 0 & -4c & -4b & 0 & -f & 0 & -2d & f & -f \\ -2i & 0 & 0 & -2h & 0 & i & -2f & -2g & i & -i \\ 0 & 0 & -2i & 0 & 0 & -h & -4b & 0 & h & h \\ 0 & -2i & 0 & 0 & -2h & g & -2d & 0 & -g & g \\ 0 & 0 & 0 & 0 & 0 & j & -2h & 0 & j & j \end{pmatrix} \begin{pmatrix} \beta_1 \\ \beta_2 \\ \beta_3 \\ \beta_4 \\ \beta_5 \\ \beta_6 \\ \beta_7 \\ \beta_8 \\ \beta_9 \\ \beta_{10} \end{pmatrix} = \begin{pmatrix} \alpha_{z^2} \\ \alpha_{y^2} \\ \alpha_{x^2} \\ \alpha_{xy} \\ \alpha_{xz} \\ \alpha_{yz} \\ \alpha_z \\ \alpha_y \\ \alpha_x \\ \alpha_1 \end{pmatrix}.$$

As the solutions for the β_i are quite lengthy we refrain form displaying them here.

Given the above considerations we can calculate the derivatives of D_0 as a sum over D_0 and mass derivatives of C_0. Furthermore the mass derivatives of C_0 can be expressed by B_0's thus leading to a closed form expression for D_0'.

Appendix D

Subtraction terms

We use the infrared regularization of Becher and Leutwyler [BL 99] in its reformulated version of Ref. [SGS 04]. The reformulated version of IR is a prescription of how to obtain the terms, analytic in quark masses and small momenta, which violate power counting to a given order. Essentially the power-counting-violating terms are calculated by expanding the integrand of a one-loop integral, parameterized either using Feynman or Schwinger parameters, in small quantities to a given order. Upon interchange of summation and integration the individual terms in the expansion allow for an easy calculation. This procedure is consistent with the IR of Becher and Leutwyler up to terms of higher order in the expansion of the integrand. Thus the difference between IR by Becher and Leutwyler and the reformulated version is shifted to terms, which are beyond the accuracy of a given calculation. The big advantage of the reformulated version is that one can use the standard definition of the one-loop integrals. The infrared regulated integrals are constructed by subtracting the power-counting-violating terms from the original integral, hence these terms are called subtraction terms.

In order to calculate the subtraction terms we first perform the Schwinger parametrization of one-loop integrals, see [Dav 91] and references therein. To that end we rewrite the denominators using the identity

$$\frac{1}{\left(q^2 - M^2 + i\varepsilon\right)^\alpha} = \frac{i^{-\alpha}}{\Gamma(\alpha)} \int\limits_0^\infty dx_1\, x_1^{\alpha-1}\, e^{ix_1\left(q^2-M^2\right)-\varepsilon\, x_1}. \tag{D.1}$$

Using the above trick the integration over the loop momentum amounts to a gaussian integral in D dimensions, for which we may write

$$\int d^D k\, \exp\bigl[i\,A\,k^2 - 2i\,B\,k\bigr] = i^{1-D/2}\pi^{D/2}A^{-D/2}\exp\bigl[-i\frac{B^2}{A}\bigr]. \tag{D.2}$$

For a general N-point one-loop integral A is a function of the sum of the x_i. The remaining exponential can be eliminated by appropriate substitutions of the x_i. By choosing the substitution to be such that $\sum_i x_i = \lambda$ and using

$$\int\limits_0^\infty d\lambda\, \lambda^\alpha e^{-i\beta\lambda} = i^{-\alpha-1}\Gamma(\alpha+1)\beta^{-\alpha-1}, \tag{D.3}$$

one can always eliminate one parameter in the representation of a one-loop integral. Thus any N-point one-loop integral can be parameterized by $N-1$ parameters. Let us illustrate the above considerations by a simple example[1].

$$
\begin{aligned}
I(p,m_1,m_2) &= i\int\frac{d^Dk}{(2\pi)^n}\frac{1}{\left[k^2-m_1^2\right]\left[\left(k+p\right)^2-m_2^2\right]},\\
&\overset{(D.1)}{=}\frac{i\,i^{-2}}{\Gamma(1)^2}\int\frac{d^Dk}{(2\pi)^D}\int\limits_0^\infty dx_1\int\limits_0^\infty dx_2\,\exp\Big[ik^2\big(x_1+x_2\big)+2i\,k\cdot p\,x_2\\
&\quad -i(x_1\,m_1^2+x_2\,(m_2^2-p^2))\Big],\\
&\overset{(D.2)}{=}-i^{2-D/2}\int\limits_0^\infty dx_1\int\limits_0^\infty dx_2\,\frac{\pi^{D/2}}{(2\pi)^D}\big(x_1+x_2\big)^{-D/2}\exp\Big[-i\frac{p^2x_2^2}{(x_1+x_2)}\Big]\\
&\quad\times\exp[-i(x_1\,m_1^2+x_2\,(m_2^2-p^2))],\\
&=-i^{2-D/2}\frac{\pi^{D/2}}{(2\pi)^D}\int\limits_0^\infty d\lambda\int\limits_0^1 d\xi\,\lambda^{1-D/2}\exp\Big[-i\,\frac{\lambda^2(1-\xi)^2p^2}{\lambda}\Big]\\
&\quad\times\exp[-i(\lambda\xi\,m_1^2+\lambda(1-\xi)\,(m_2^2-p^2))],\\
&=-i^{2-D/2}\frac{\pi^{D/2}}{(2\pi)^D}\int\limits_0^\infty d\lambda\int\limits_0^1 d\xi\,\lambda^{1-D/2}\\
&\quad\times\exp\Big[-i\,\lambda\Big\{(1-\xi)^2p^2+\xi\,m_1^2+(1-\xi)\,(m_2^2-p^2)\Big\}\Big],\\
&\overset{(D.3)}{=}-\frac{\pi^{D/2}}{(2\pi)^D}\int\limits_0^1 d\xi\;\Gamma(2-D/2)\left[(1-\xi)^2p^2+\xi\,m_1^2+(1-\xi)\,(m_2^2-p^2)\right]^{2-D/2},
\end{aligned}
\tag{D.4}
$$

where the substitutions $x_1=\lambda\xi$ and $x_2=\lambda(1-\xi)$ were made. The divergence of the integral for $D\to 4$ is encoded in the Γ-function. A possible scenario for the above example would be the nucleon self-energy. We set $m_1=M_\pi$, $p=p_i$ and $m_2=m_N$, where p_i is the momentum of the nucleon. The expression thus reads

$$
\begin{aligned}
I(p_i,M_\pi,m_N) &= -\frac{\pi^{D/2}}{(2\pi)^D}\int\limits_0^1 d\xi\;\Gamma(2-D/2)\\
&\quad\times\left[(1-\xi)^2p_i^2+\xi\,M_\pi^2+(1-\xi)\,(m_N^2-p_i^2)\right]^{2-D/2}.
\end{aligned}
\tag{D.5}
$$

Now we rescale all expressions according to their chiral order, note that the nucleon is almost on-shell, i.e. $p_i^2\approx m_N^2$,

$$
M_\pi\mapsto\aleph M_\pi,\quad (p_i^2-m_N^2)\equiv\Delta_N\mapsto\aleph\Delta_N.
$$

[1]For the sake of readability we drop the $i\varepsilon$ prescription.

For the rescaled integral we obtain

$$I(p_i, M_\pi, m_N) = -\frac{\pi^{D/2}}{(2\pi)^D} \int_0^1 d\xi\ \Gamma(2 - D/2) \times \Big[(1-\xi)^2(\Delta_N \aleph + m_N^2) + \xi\, M_\pi^2\, \aleph^2 - (1-\xi)\,\Delta_N \aleph\Big]^{2-D/2}. \quad \text{(D.6)}$$

The expansion of the integrand around the small quantities up to first order reads

$$I(p_i, M_\pi, m_N) = -\frac{\pi^{D/2}}{(2\pi)^D} \int_0^1 d\xi\ \Gamma(2 - D/2) \times \Big[\big(m_N^2\xi^2\big)^{D/2-2} - \frac{\aleph}{2}\big(D-4\big)\big(m_N^2\xi^2\big)^{D/2-3}\Delta_N\,\xi(1-\xi) + \mathcal{O}(\aleph^2)\Big] \quad \text{(D.7)}$$

We exchange integration and summation and use the identity

$$\int_0^1 dx\, x^{\alpha-1}(1-x)^{\beta-1} = \frac{\Gamma(\alpha)\,\Gamma(\beta)}{\Gamma(\alpha+\beta)}, \quad \text{(D.8)}$$

and obtain[2]

$$I^{\mathrm{ST}}(p_i, M_\pi, m_N) = -\frac{\pi^{D/2}}{(2\pi)^D}\Gamma(2 - D/2)\Big[\big(m_N^2\big)^{D/2-2}\frac{\Gamma(D-3)}{\Gamma(D-2)} - \frac{\aleph}{2}\big(D-4\big)\big(m_N^2\big)^{D/2-3}\Delta_N\,\frac{\Gamma(D-4)}{\Gamma(D-2)} + \mathcal{O}(\aleph^2)\Big]. \quad \text{(D.9)}$$

The integral is subsequently expanded around $D = 4$, and the divergences are discarded according to the $\widetilde{\mathrm{MS}}$ scheme. Note that the term linear in $\aleph$ generates an additional contribution to the divergent part, not present in the original integral. This additional divergence is compensated by the according divergence in the infrared singular part.

The infrared regulated integrals are obtained by subtracting the so-obtained terms form the original integrals.

We have written a Mathematica program implementing the above algorithm for integrals with up to four denominators and up to tensor rank 4. There is no restriction on the chiral order of the subtraction terms, except for computational boundaries of Mathematica. The program expects the integrals in LoopTools notation and the order to which subtraction terms should be calculated as input. The maximum chiral order of the 2-point integrals in our calculation was 4, for the 3-point integrals 3, and for the 4-point integrals we needed subtraction terms up to order 2.

[2]The superscript ST stands for subtraction term. $I^{\mathrm{ST}}(p_i, M_\pi, m_N)$ is the power counting violating part of the integral to a specific order.

Appendix E

Results

Most of our results are too large to be displayed in this work. The most compact results we obtained are the invariant amplitudes $\bar{F}_i(Q^2)$ at the real photon point $Q^2 = 0$. We used these expressions to check against the heavy-baryon results in previous works. The coupling constants c_6 and c_7 (e_{105} and e_{106}) can be related to the magnetic moments $\kappa_{p/n}$ of the proton and neutron according to

$$c_6 = \frac{\kappa_v}{4m_N}, \quad c_7 = \frac{\kappa_s}{2m_N}, \tag{E.1}$$

where

$$\kappa_p = \frac{1}{2}\big(\kappa_s + \kappa_v\big), \quad \kappa_n = \frac{1}{2}\big(\kappa_s - \kappa_v\big). \tag{E.2}$$

For a more extensive discussion of the coupling constants see Chapter 5.

The explicit expressions for the one-loop part read

$$\begin{aligned}
\bar{F}_1(Q^2=0) = {} & \frac{1}{576m_N^7\big(M_\pi^3 - 4m_N^2M_\pi\big)^2\pi^2F_\pi^2}\Big[48g_A^2m_N^{12} \\
& + 48M_\pi^2\big[-3\big(15\tau^3 + \big(8\tau^3+6\big)\kappa_s + 2\big(\tau^3+2\big)\kappa_v + 13\big)g_A^2 \\
& + 16m_Nc_1 - 4m_N\big(c_2+2c_3\big)\big]m_N^{10} + 4M_\pi^4\big[\big(36\tau^3 + 12\big(4\tau^3+15\big)\kappa_s \\
& + 6\big(11\tau^3-72\big)\kappa_v - 1079\big)g_A^2 + 24m_N\big(-4c_1+c_2+2c_3\big)\big]m_N^8 \\
& + M_\pi^6\big[\big(2256\tau^3 + 27\big(57\tau^3+25\big)\kappa_s + 3\big(321\tau^3+469\big)\kappa_v + 4420\big)g_A^2 \\
& + 48m_Nc_1 - 12m_N\big(c_2+2c_3\big)\big]m_N^6 - M_\pi^8g_A^2\big[1071\tau^3 + \big(861\tau^3+459\big)\kappa_s \\
& + \big(435\tau^3+357\big)\kappa_v + 1340\big]m_N^4 + 3M_\pi^{10}g_A^2\big[44\big(\tau^3+1\big) + 3\big(16\tau^3+7\big)\kappa_s \\
& + \big(7\tau^3+10\big)\kappa_v\big]m_N^2 + 6M_\pi^{12}\tau^3g_A^2\big(\kappa_v-\kappa_s\big)\Big] \\
& + \frac{g_A^2\,A_0\big(m_N^2\big)}{384m_N^3\big(M_\pi^3 - 4m_N^2M_\pi\big)^2\pi^2F_\pi^2}\Big[32m_N^6 \\
& + 16M_\pi^2\big[-90\tau^3 - 3\big(19\tau^3+9\big)\kappa_s - 3\big(\tau^3+7\big)\kappa_v - 85\big]m_N^4 \\
& + 8M_\pi^4\big[158\big(\tau^3+1\big) + 9\big(11\tau^3+9\big)\kappa_s + 3\big(9\tau^3+13\big)\kappa_v\big]m_N^2 \\
& - 3M_\pi^6\big[72\big(\tau^3+1\big) + \big(45\tau^3+39\big)\kappa_s + \big(15\tau^3+17\big)\kappa_v\big]\Big]
\end{aligned}$$

$$
\begin{aligned}
&+\frac{A_0\big(M_\pi^2\big)}{192m_N^3\big(M_\pi^3-4m_N^2M_\pi\big)^2\pi^2F_\pi^2}\big[64c_2m_N^7-8\big(24\tau^3+47\big)g_A^2m_N^6\\
&-192\tau^3g_A^2\kappa_sm_N^6+8M_\pi^2\big[\big(155\tau^3+\big(93\tau^3+63\big)\kappa_s+3\big(9\tau^3+11\big)\kappa_v\\
&+158\big)g_A^2+20m_Nc_2\big]m_N^4+4M_\pi^4\big[-\big(185\big(\tau^3+1\big)+9\big(12\tau^3+11\big)\kappa_s\\
&+\big(42\tau^3+45\big)\kappa_v\big)g_A^2-23m_Nc_2\big]m_N^2+3M_\pi^6\big[3\big(\tau^3+1\big)\big(7\kappa_s+3\big(\kappa_v+4\big)\big)g_A^2\\
&+4m_Nc_2\big]\big]\\
&+\frac{g_A^2\,B_0\big(m_N^2,M_\pi^2,m_N^2\big)}{192m_N^3\big(M_\pi^3-4m_N^2M_\pi\big)^2\pi^2F_\pi^2}\big[-16m_N^8+48M_\pi^2\big[19\tau^3+6\big(2\tau^3+1\big)\kappa_s\\
&+2\big(\tau^3+2\big)\kappa_v+22\big]m_N^6-24M_\pi^4\big[78\tau^3+\big(46\tau^3+36\big)\kappa_s\\
&+3\big(5\tau^3+6\big)\kappa_v+79\big]m_N^4-M_\pi^6\big[-848\big(\tau^3+1\big)-9\big(55\tau^3+51\big)\kappa_s\\
&-3\big(65\tau^3+69\big)\kappa_v\big]m_N^2-9M_\pi^8\big(\tau^3+1\big)\big[7\kappa_s+3\big(\kappa_v+4\big)\big]\big], \qquad \text{(E.3)}\\
\bar{F}_2(Q^2=0)=&\frac{1}{9216m_N^7M_\pi^2\big(4m_N^2-M_\pi^2\big)^3\pi^2F_\pi^2}\Big[-8448g_A^2m_N^{12}\\
&+192M_\pi^2\big[\big(239\tau^3+24\big(7\tau^3+3\big)\kappa_s+24\big(\tau^3+1\big)\kappa_v+73\big)g_A^2\\
&+32m_Nc_2\big]m_N^{10}-64M_\pi^4\big[72m_Nc_2-g_A^2\big(936\tau^3+6\big(16\tau^3-57\big)\kappa_s\\
&+12\big(12-13\tau^3\big)\kappa_v+2543\big)\big]m_N^8+48M_\pi^6\big[24m_Nc_2\\
&-g_A^2\big(5\big(361\tau^3+425\big)+2\big(614\tau^3+63\big)\kappa_s+12\big(24\tau^3-11\big)\kappa_v\big)\big]m_N^6\\
&-12M_\pi^8\big[8m_Nc_2-g_A^2\big(3030\tau^3+9\big(347\tau^3+107\big)\kappa_s+3\big(381\tau^3-239\big)\kappa_v\\
&+1238\big)\big]m_N^4-M_\pi^{10}g_A^2\big[8\big(819\tau^3-167\big)+\big(8691\tau^3+3519\big)\kappa_s\\
&+3\big(1241\tau^3-819\big)\kappa_v\big]m_N^2+3M_\pi^{12}g_A^2\big[21\big(7\tau^3-5\big)+4\big(58\tau^3+27\big)\kappa_s\\
&+36\big(3\tau^3-2\big)\kappa_v\big]\Big]\\
&+\frac{g_A^2\,A_0\big(m_N^2\big)}{384m_N^5M_\pi^2\big(4m_N^2-M_\pi^2\big)^3\pi^2F_\pi^2}\Big[-352m_N^8\\
&-24M_\pi^2\big[-85\tau^3-8\big(7\tau^3+3\big)\kappa_s-8\big(\tau^3+1\big)\kappa_v-89\big]m_N^6\\
&-4M_\pi^4\big[557\tau^3+6\big(59\tau^3+45\big)\kappa_s+90\big(\tau^3+1\big)\kappa_v+559\big]m_N^4\\
&+2M_\pi^6\big[9\big(25\tau^3+23\big)\kappa_s+\big(\tau^3+1\big)\big(69\kappa_v+358\big)\big]m_N^2\\
&-3M_\pi^8\big(\tau^3+1\big)\big(15\kappa_s+5\kappa_v+24\big)\Big]\\
&+\frac{A_0\big(M_\pi^2\big)}{384m_N^5M_\pi^2\big(4m_N^2-M_\pi^2\big)^3\pi^2F_\pi^2}\Big[-16\big(16m_Nc_2\\
&-g_A^2\big(24\kappa_s\tau^3+48\tau^3+85\big)\big)m_N^8-4M_\pi^2\big[g_A^2\big(913\tau^3+72\big(8\tau^3+5\big)\kappa_s\\
&+120\big(\tau^3+1\big)\kappa_v+971\big)-48m_Nc_2\big]m_N^6\\
&-12M_\pi^4\big[4m_Nc_2-g_A^2\big(239\tau^3+\big(151\tau^3+123\big)\kappa_s+41\big(\tau^3+1\big)\kappa_v+241\big)\big]m_N^4\\
&-M_\pi^6\big[g_A^2\big(9\big(55\tau^3+51\big)\kappa_s+\big(\tau^3+1\big)\big(153\kappa_v+788\big)\big)-4m_Nc_2\big]m_N^2\\
&+3M_\pi^8\big(\tau^3+1\big)g_A^2\big(15\kappa_s+5\kappa_v+24\big)\Big]
\end{aligned}
$$

$$
\begin{aligned}
&+\frac{g_A^2\,B_0\big(m_N^2,M_\pi^2,m_N^2\big)}{384m_N^5M_\pi^2\big(4m_N^2-M_\pi^2\big)^3\pi^2F_\pi^2}\Big[352m_N^{10}\\
&+8M_\pi^2\big[-351\tau^3-72\big(3\tau^3+1\big)\kappa_s-24\big(\tau^3+1\big)\kappa_v-437\big]m_N^8\\
&+120M_\pi^4g_A^2\big[49\tau^3+\big(31\tau^3+21\big)\kappa_s+7\big(\tau^3+1\big)\kappa_v+51\big]m_N^6\\
&-2M_\pi^6\big[4\big(448\tau^3+451\big)+3\big(377\tau^3+315\big)\kappa_s+315\big(\tau^3+1\big)\kappa_v\big]m_N^4\\
&+4M_\pi^8\big[9\big(15\tau^3+14\big)\kappa_s+\big(\tau^3+1\big)\big(42\kappa_v+215\big)\big]m_N^2\\
&-3M_\pi^{10}\big(\tau^3+1\big)\big(15\kappa_s+5\kappa_v+24\big)\Big],
\end{aligned}
\tag{E.4}
$$

$$
\begin{aligned}
\bar{F}_4(Q^2=0)=&\frac{g_A^2}{768m_N^5M_\pi^2\big(4m_N^2-M_\pi^2\big)^3\pi^2F_\pi^2}\Big[64\big(\kappa_s\tau^3+6\tau^3+3\kappa_v+7\big)m_N^{10}\\
&-8M_\pi^2\big[402\tau^3+3\big(129\tau^3+89\big)\kappa_s+3\big(69\tau^3+77\big)\kappa_v+82\big]m_N^8\\
&+8M_\pi^4\big[154\tau^3-3\big(421\tau^3-65\big)\kappa_s+\big(179\tau^3-915\big)\kappa_v-568\big]m_N^6\\
&+2M_\pi^6\big[-30\big(\tau^3-55\big)+\big(4199\tau^3-381\big)\kappa_s+\big(2971-353\tau^3\big)\kappa_v\big]m_N^4\\
&+M_\pi^8\big[-2\big(7\tau^3+387\big)-3\big(707\tau^3-69\big)\kappa_s+\big(179\tau^3-1493\big)\kappa_v\big]m_N^2\\
&+M_\pi^{10}\big[7\big(25\tau^3-3\big)\kappa_s+\big(123-17\tau^3\big)\kappa_v+60\big]\Big]\\
&+\frac{g_A^2\,A_0\big(m_N^2\big)}{192m_N^5M_\pi^2\big(4m_N^2-M_\pi^2\big)^3\pi^2F_\pi^2}\Big[16\big(\kappa_s\tau^3+3\big(2\tau^3+\kappa_v+5\big)\big)m_N^8\\
&-2M_\pi^2\big[602\tau^3+\big(463\tau^3+267\big)\kappa_s+\big(207\tau^3+331\big)\kappa_v+630\big]m_N^6\\
&+M_\pi^4\big[2\big(593\tau^3+597\big)+21\big(51\tau^3+43\big)\kappa_s+\big(627\tau^3+731\big)\kappa_v\big]m_N^4\\
&+M_\pi^6\big[-366\big(\tau^3+1\big)-\big(353\tau^3+333\big)\kappa_s-3\big(75\tau^3+79\big)\kappa_v\big]m_N^2\\
&+12M_\pi^8\big(\tau^3+1\big)\big(3\kappa_s+2\kappa_v+3\big)\Big]\\
&+\frac{g_A^2\,A_0\big(M_\pi^2\big)}{192m_N^5M_\pi^2\big(4m_N^2-M_\pi^2\big)^3\pi^2F_\pi^2}\Big[-8\big(82\tau^3+\big(43\tau^3+12\big)\kappa_s\\
&+\big(12\tau^3+41\big)\kappa_v+105\big)m_N^8+M_\pi^2\big[\big(1709\tau^3+1197\big)\kappa_s\\
&+3\big(698\tau^3+\big(291\tau^3+403\big)\kappa_v+722\big)\big]m_N^6-4M_\pi^4\big[379\tau^3+\big(347\tau^3+300\big)\kappa_s\\
&+\big(207\tau^3+236\big)\kappa_v+381\big]m_N^4+M_\pi^6\big[402\big(\tau^3+1\big)+\big(389\tau^3+369\big)\kappa_s\\
&+3\big(83\tau^3+87\big)\kappa_v\big]m_N^2-12M_\pi^8\big(\tau^3+1\big)\big(3\kappa_s+2\kappa_v+3\big)\Big]\\
&+\frac{g_A^2\,B_0\big(m_N^2,M_\pi^2,m_N^2\big)}{192m_N^5M_\pi^2\big(4m_N^2-M_\pi^2\big)^3\pi^2F_\pi^2}\Big[-16\big(\kappa_s\tau^3+3\big(2\tau^3+\kappa_v+5\big)\big)m_N^{10}\\
&+10M_\pi^2\big[\big(127\tau^3+63\big)\kappa_s+3\big(62\tau^3+\big(17\tau^3+33\big)\kappa_v+70\big)\big]m_N^8\\
&-20M_\pi^4\big[4\big(41\tau^3+42\big)+\big(139\tau^3+105\big)\kappa_s+\big(75\tau^3+97\big)\kappa_v\big]m_N^6\\
&+M_\pi^6\big[2\big(941\tau^3+945\big)+\big(1741\tau^3+1533\big)\kappa_s+\big(1053\tau^3+1181\big)\kappa_v\big]m_N^4\\
&-M_\pi^8\big[438\big(\tau^3+1\big)+5\big(85\tau^3+81\big)\kappa_s+3\big(91\tau^3+95\big)\kappa_v\big]m_N^2\\
&+12M_\pi^{10}\big(\tau^3+1\big)\big(3\kappa_s+2\kappa_v+3\big)\Big],
\end{aligned}
\tag{E.5}
$$

$$
\begin{aligned}
\bar{F}_6(Q^2=0) = {} & \frac{g_A^2}{18432 m_N^7 M_\pi^2 \big(4m_N^2 - M_\pi^2\big)^3 \pi^2 F_\pi^2} \Big[-768 \big(\big(3\tau^3 - 1\big) - 2\tau^3 \kappa_s + 2\kappa_v \big) m_N^{12} \\
& - 96 M_\pi^2 \big[42\tau^3 + 9\big(17\tau^3 + 7\big)\kappa_s + 3\big(25\tau^3 + 59\big)\kappa_v + 214 \big] m_N^{10} \\
& - 32 M_\pi^4 \big[-906\tau^3 + 9\big(99\tau^3 - 245\big)\kappa_s + 3\big(53 - 847\tau^3\big)\kappa_v - 46 \big] m_N^8 \\
& - 8 M_\pi^6 \big[-1038\tau^3 + \big(2853 - 4069\tau^3\big)\kappa_s + \big(1917\tau^3 + 299\big)\kappa_v + 1746 \big] m_N^6 \\
& - 12 M_\pi^8 \big[6\big(227\tau^3 - 181\big) + \big(967\tau^3 + 735\big)\kappa_s + \big(1531\tau^3 - 497\big)\kappa_v \big] m_N^4 \\
& + 8 M_\pi^{10} \big[612\tau^3 + 3\big(74\tau^3 + 183\big)\kappa_s + 3\big(296\tau^3 - 79\big)\kappa_v - 448 \big] m_N^2 \\
& - M_\pi^{12} \big[63\big(7\tau^3 - 5\big) + \big(101\tau^3 + 459\big)\kappa_s + \big(699\tau^3 - 175\big)\kappa_v \big] \Big] \\
& + \frac{g_A^2 \, A_0\big(m_N^2\big)}{384 m_N^5 M_\pi^2 \big(4m_N^2 - M_\pi^2\big)^3 \pi^2 F_\pi^2} \Big[-16 \big(\big(3\tau^3 + 7\big) + 2\tau^3 \kappa_s - 2\kappa_v \big) m_N^8 \\
& - 2 M_\pi^2 \big[-26\tau^3 + \big(113\tau^3 + 63\big)\kappa_s + \big(75\tau^3 + 217\big)\kappa_v - 46 \big] m_N^6 \\
& + M_\pi^4 \big[-6\big(3\tau^3 + 5\big) + \big(265\tau^3 + 219\big)\kappa_s + \big(287\tau^3 + 409\big)\kappa_v \big] m_N^4 \\
& - 2 M_\pi^6 \big[-\tau^3 + \big(44\tau^3 + 42\big)\kappa_s + \big(55\tau^3 + 62\big)\kappa_v - 1 \big] m_N^2 \\
& + 3 M_\pi^8 \big(\tau^3 + 1\big)\big(3\kappa_s + 4\kappa_v\big) \Big] \\
& + \frac{g_A^2 \, A_0\big(M_\pi^2\big)}{384 m_N^5 M_\pi^2 \big(4m_N^2 - M_\pi^2\big)^3 \pi^2 F_\pi^2} \Big[8 \big(\big(13\tau^3 + 25\big) + 6\tau^3 \kappa_s - 30\kappa_v \big) m_N^8 \\
& + M_\pi^2 \big[-2\big(41\tau^3 + 55\big) + \big(375\tau^3 + 321\big)\kappa_s + \big(373\tau^3 + 751\big)\kappa_v \big] m_N^6 \\
& + 2 M_\pi^4 \big[11\tau^3 - 17\big(10\tau^3 + 9\big)\kappa_s - \big(195\tau^3 + 262\big)\kappa_v + 13 \big] m_N^4 \\
& + M_\pi^6 \big[-2\big(\tau^3 + 1\big) + \big(97\tau^3 + 93\big)\kappa_s + 2\big(61\tau^3 + 68\big)\kappa_v \big] m_N^2 \\
& - 3 M_\pi^8 \big(\tau^3 + 1\big)\big(3\kappa_s + 4\kappa_v\big) \Big] \\
& + \frac{g_A^2 \, B_0\big(m_N^2, M_\pi^2, m_N^2\big)}{384 m_N^5 M_\pi^2 \big(4m_N^2 - M_\pi^2\big)^3 \pi^2 F_\pi^2} \Big[16 \big(\big(3\tau^3 + 7\big) + 2\tau^3 \kappa_s - 2\kappa_v \big) m_N^{10} \\
& + 2 M_\pi^2 \big[-2\big(39\tau^3 + 73\big) + \big(89\tau^3 + 63\big)\kappa_s + \big(75\tau^3 + 337\big)\kappa_v \big] m_N^8 \\
& + 20 M_\pi^4 \big[5\tau^3 - \big(32\tau^3 + 27\big)\kappa_s - \big(33\tau^3 + 58\big)\kappa_v + 7 \big] m_N^6 \\
& + 2 M_\pi^6 \big(\big(214\tau^3 + 195\big)\kappa_s + 2\big(-6\tau^3 + \big(125\tau^3 + 162\big)\kappa_v - 7 \big) \big) m_N^4 \\
& + 2 M_\pi^8 \big[\tau^3 - \big(53\tau^3 + 51\big)\kappa_s - \big(67\tau^3 + 74\big)\kappa_v + 1 \big] m_N^2 \\
& + 3 M_\pi^{10} \big(\tau^3 + 1\big)\big(3\kappa_s + 4\kappa_v\big) \Big], \qquad \text{(E.6)}
\end{aligned}
$$

$$
\begin{aligned}
\bar{F}_{10}(Q^2=0) = {} & \frac{g_A^2}{6144 m_N^6 M_\pi^2 \big(4m_N^2 - M_\pi^2\big)^3 \pi^2 F_\pi^2} \Big[-1024 \big(\big(3\tau^3 + 4\big) + 3\tau^3 \kappa_s + \kappa_v \big) m_N^{12} \\
& + 256 M_\pi^2 \big[187\tau^3 + \big(84\tau^3 + 75\big)\kappa_s + 9\big(7\tau^3 + 2\big)\kappa_v + 98 \big] m_N^{10} \\
& + 64 M_\pi^4 \big[1110\tau^3 + \big(1129\tau^3 + 927\big)\kappa_s + \big(1411\tau^3 + 2209\big)\kappa_v + 2102 \big] m_N^8 \\
& - 64 M_\pi^6 \big[728\tau^3 + 3\big(457\tau^3 + 102\big)\kappa_s + \big(347\tau^3 + 1647\big)\kappa_v + 1844 \big] m_N^6 \\
& + 32 M_\pi^8 \big[78\tau^3 + \big(1142\tau^3 - 297\big)\kappa_s + \big(809 - 601\tau^3\big)\kappa_v + 1120 \big] m_N^4 \\
& - 4 M_\pi^{10} \big[-544\tau^3 + \big(1675\tau^3 - 1101\big)\kappa_s + \big(519 - 1961\tau^3\big)\kappa_v + 1152 \big] m_N^2
\end{aligned}
$$

$$
\begin{aligned}
&- M_\pi^{12}\big[42\big(7\tau^3-5\big)+\big(447-461\tau^3\big)\kappa_s+\big(779\tau^3+7\big)\kappa_v\big]\Big]\\
&+\frac{g_A^2\,A_0\big(m_N^2\big)}{192m_N^4M_\pi^2\big(4m_N^2-M_\pi^2\big)^3\pi^2F_\pi^2}\Big[-32\big(\big(3\tau^3+8\big)+3\tau^3\kappa_s+\kappa_v\big)m_N^8\\
&+8M_\pi^2\big[229\tau^3+3\big(42\tau^3+25\big)\kappa_s+\big(63\tau^3+64\big)\kappa_v+238\big]m_N^6\\
&-2M_\pi^4\big[2\big(532\tau^3+537\big)+\big(635\tau^3+555\big)\kappa_s+335\big(\tau^3+1\big)\kappa_v\big]m_N^4\\
&-M_\pi^6\big[-\big(433\tau^3+411\big)\kappa_s-\big(\tau^3+1\big)\big(229\kappa_v+704\big)\big]m_N^2\\
&-3M_\pi^8\big(\tau^3+1\big)\big(15\kappa_s+8\big(\kappa_v+3\big)\big)\Big]\\
&+\frac{g_A^2\,A_0\big(M_\pi^2\big)}{192m_N^4M_\pi^2\big(4m_N^2-M_\pi^2\big)^3\pi^2F_\pi^2}\Big[16\big(\big(49\tau^3+68\big)\\
&+3\big(11\tau^3+4\big)\kappa_s+3\big(4\tau^3+5\big)\kappa_v\big)m_N^8\\
&+4M_\pi^2\big[-853\tau^3-5\big(100\tau^3+69\big)\kappa_s-5\big(49\tau^3+50\big)\kappa_v-878\big]m_N^6\\
&+M_\pi^4\big[2762\tau^3+15\big(111\tau^3+97\big)\kappa_s+\big(867\tau^3+869\big)\kappa_v+2774\big]m_N^4\\
&+M_\pi^6\big[-2\big(239\tau^3+228\big)\kappa_s-\big(\tau^3+1\big)\big(253\kappa_v+776\big)\big]m_N^2\\
&+3M_\pi^8\big(\tau^3+1\big)\big(15\kappa_s+8\big(\kappa_v+3\big)\big)\Big]\\
&+\frac{g_A^2\,B_0\big(m_N^2,M_\pi^2,m_N^2\big)}{192m_N^4M_\pi^2\big(4m_N^2-M_\pi^2\big)^3\pi^2F_\pi^2}\Big[32\big(\big(3\tau^3+8\big)+3\tau^3\kappa_s+\kappa_v\big)m_N^{10}\\
&-8M_\pi^2\big[327\tau^3+3\big(64\tau^3+33\big)\kappa_s+\big(87\tau^3+94\big)\kappa_v+374\big]m_N^8\\
&+10M_\pi^4\big[554\tau^3+3\big(109\tau^3+83\big)\kappa_s+\big(165\tau^3+167\big)\kappa_v+566\big]m_N^6\\
&-2M_\pi^6\big[1733\tau^3+\big(1049\tau^3+933\big)\kappa_s+\big(548\tau^3+549\big)\kappa_v+1739\big]m_N^4\\
&+M_\pi^8\big[\big(523\tau^3+501\big)\kappa_s+\big(\tau^3+1\big)\big(277\kappa_v+848\big)\big]m_N^2\\
&-3M_\pi^{10}\big(\tau^3+1\big)\big(15\kappa_s+8\big(\kappa_v+3\big)\big)\Big],
\end{aligned}
\tag{E.7}
$$

$$
\begin{aligned}
\bar{F}_{11}(Q^2=0)=&\frac{g_A^2}{3072m_N^6\big(M_\pi^3-4m_N^2M_\pi\big)^2\pi^2F_\pi^2}\Big[64\big(\big(2\tau^3-3\big)+2\tau^3\kappa_s-2\kappa_v\big)m_N^{10}\\
&+32M_\pi^2\big[45\kappa_s\tau^3+26\tau^3+3\big(8\tau^3+9\big)\kappa_v+20\big]m_N^8\\
&+8M_\pi^4\big[-34\tau^3+3\big(53\tau^3-29\big)\kappa_s+\big(167-127\tau^3\big)\kappa_v+178\big]m_N^6\\
&+16M_\pi^6\big[\tau^3-\big(136\tau^3+57\big)\kappa_s-\big(59\tau^3+131\big)\kappa_v-48\big]m_N^4\\
&+M_\pi^8\big[\big(787\tau^3+639\big)\kappa_s+31\big(21\tau^3+25\big)\kappa_v+96\big]m_N^2\\
&+M_\pi^{10}\big[-2\big(43\tau^3+45\big)\kappa_s-2\big(45\tau^3+43\big)\kappa_v\big]\Big]\\
&+\frac{g_A^2\,A_0\big(m_N^2\big)}{768m_N^4\big(M_\pi^3-4m_N^2M_\pi\big)^2\pi^2F_\pi^2}\Big[16\big(\big(2\tau^3+1\big)+2\tau^3\kappa_s-2\kappa_v\big)m_N^6\\
&+8M_\pi^2\big[31\kappa_s\tau^3+12\tau^3+\big(24\tau^3+41\big)\kappa_v+9\big]m_N^4\\
&+2M_\pi^4\big[-50\big(\tau^3+1\big)-5\big(25\tau^3+21\big)\kappa_s-\big(121\tau^3+137\big)\kappa_v\big]m_N^2\\
&+9M_\pi^6\big(\tau^3+1\big)\big(5\kappa_s+5\kappa_v+2\big)\Big]
\end{aligned}
$$

$$
\begin{aligned}
&+\frac{g_A^2\,A_0\big(M_\pi^2\big)}{768m_N^4\big(M_\pi^3-4m_N^2M_\pi\big)^2\pi^2F_\pi^2}\Big[-8\big(3\big(2\tau^3-3\big)-10\tau^3\kappa_s+34\kappa_v\big)m_N^6\\
&-4M_\pi^2\big[42\tau^3+\big(107\tau^3+60\big)\kappa_s+\big(100\tau^3+149\big)\kappa_v+46\big]m_N^4\\
&+M_\pi^4\big[118\big(\tau^3+1\big)+5\big(59\tau^3+51\big)\kappa_s+\big(287\tau^3+319\big)\kappa_v\big]m_N^2\\
&-9M_\pi^6\big(\tau^3+1\big)\big(5\kappa_s+5\kappa_v+2\big)\Big]\\
&+\frac{g_A^2\,B_0\big(m_N^2,M_\pi^2,m_N^2\big)}{768m_N^4\big(M_\pi^3-4m_N^2M_\pi\big)^2\pi^2F_\pi^2}\Big[-16\big(\big(2\tau^3+1\big)+2\tau^3\kappa_s-2\kappa_v\big)m_N^8\\
&-24M_\pi^2\big[7\kappa_s\tau^3+2\tau^3+\big(8\tau^3+25\big)\kappa_v+6\big]m_N^6\\
&+2M_\pi^4\big[2\big(67\tau^3+71\big)+3\big(113\tau^3+75\big)\kappa_s+\big(321\tau^3+435\big)\kappa_v\big]m_N^4\\
&-4M_\pi^6\big[34\big(\tau^3+1\big)+\big(85\tau^3+75\big)\kappa_s+\big(83\tau^3+91\big)\kappa_v\big]m_N^2\\
&+9M_\pi^8\big(\tau^3+1\big)\big(5\kappa_s+5\kappa_v+2\big)\Big]. \qquad \text{(E.8)}
\end{aligned}
$$

Appendix F

Diagrams for VCS

Here we display all diagrams contributing to VCS at $\mathcal{O}(q^4)$ in BχPT. We group the diagrams according to their symmetry with respect to nucleon crossing and charge conjugation.
One-loop diagrams marked with an asterisk have a symmetry factor of $\frac{1}{2}$.
The one-loop diagrams have been generated using the FeynArts [Hah 01] package. We modified the counter term routines of the FeynArts package to account for vertices of different chiral order.
Taking into account the crossed diagrams we have a total of 43 diagrams at order $\mathcal{O}(q^3)$ and 57 additional diagrams at order $\mathcal{O}(q^4)$.

F.1 Tree-order diagrams

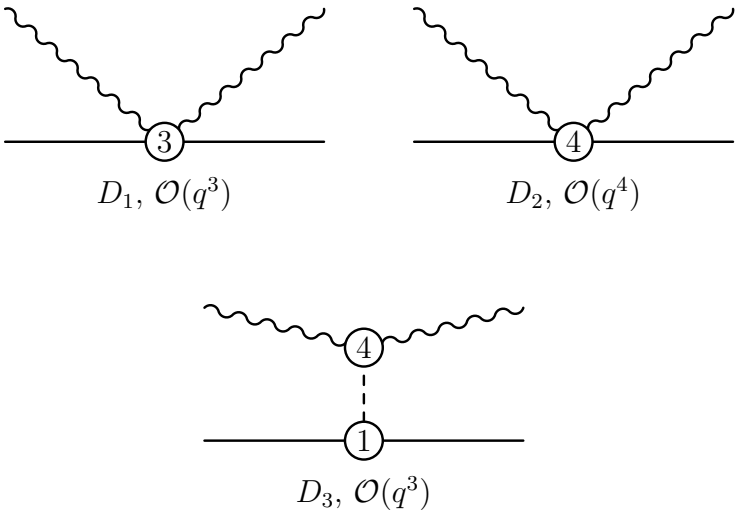

D_1, $\mathcal{O}(q^3)$ D_2, $\mathcal{O}(q^4)$

D_3, $\mathcal{O}(q^3)$

Form factor type diagrams

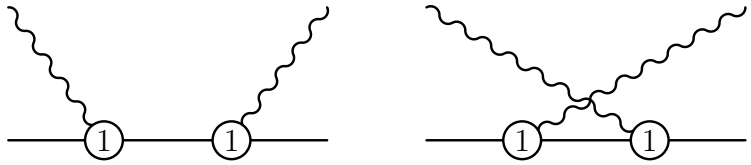

D_4, $\mathcal{O}(q^1)$

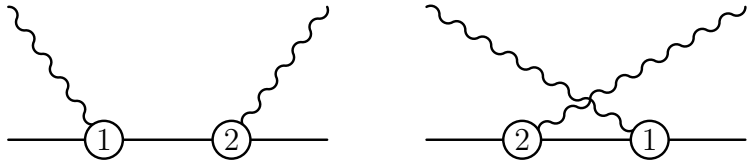

D_5, $\mathcal{O}(q^2)$

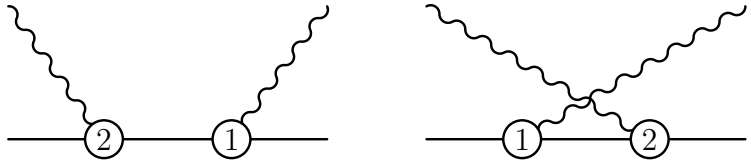

D_6, $\mathcal{O}(q^2)$

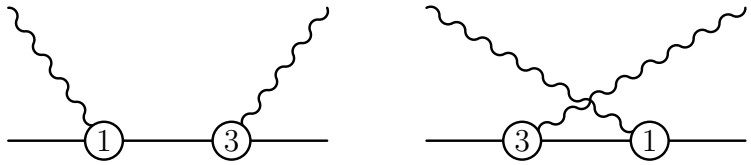

D_7, $\mathcal{O}(q^3)$

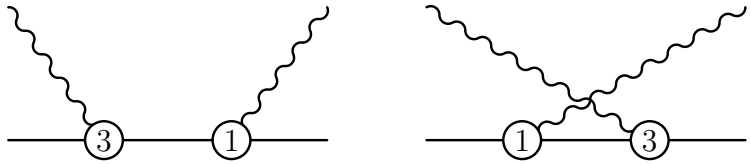

D_8, $\mathcal{O}(q^3)$

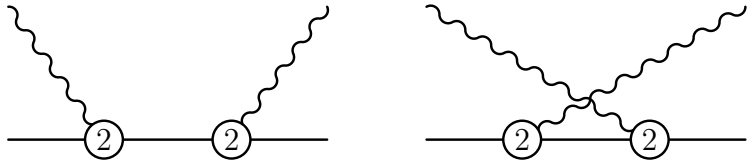

D_9, $\mathcal{O}(q^3)$

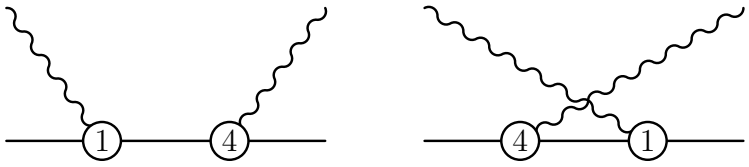

D_{10}, $\mathcal{O}(q^4)$

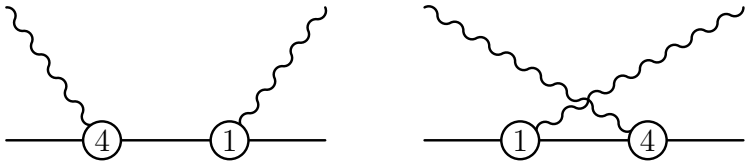

D_{11}, $\mathcal{O}(q^4)$

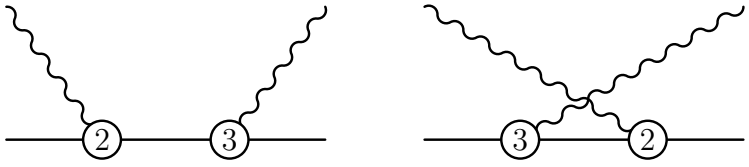

D_{12}, $\mathcal{O}(q^4)$

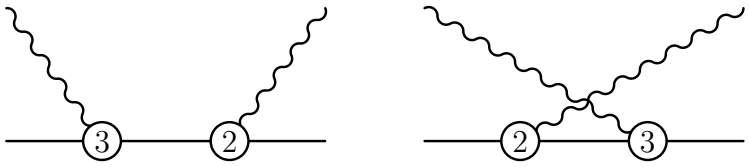

D_{13}, $\mathcal{O}(q^4)$

F.2 One-loop diagrams

Four denominators

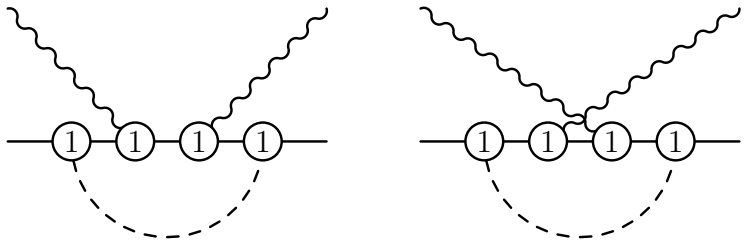

D_{14}, $\mathcal{O}(q^3)$

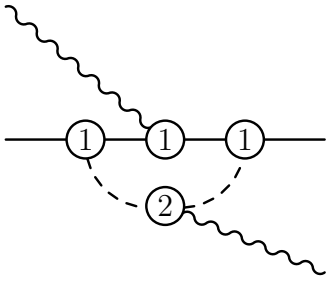

D_{15}, $\mathcal{O}(q^4)$

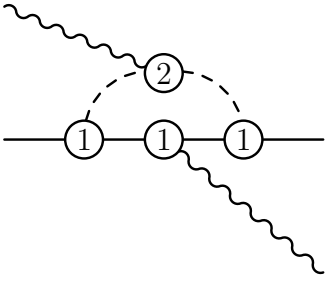

D_{16}, $\mathcal{O}(q^4)$

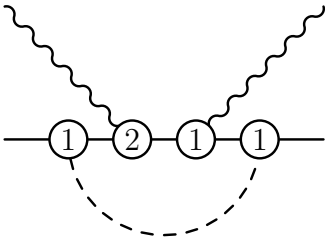

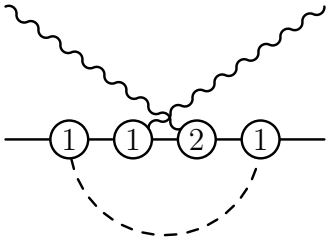

D_{17}, $\mathcal{O}(q^4)$

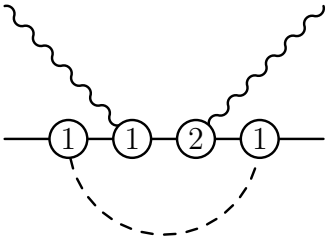

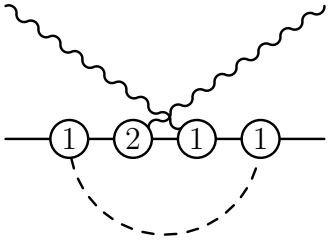

D_{18}, $\mathcal{O}(q^4)$

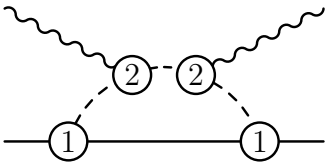

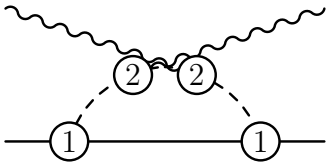

D_{19}, $\mathcal{O}(q^4)$

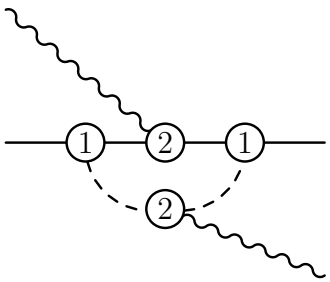

D_{20}, $\mathcal{O}(q^4)$

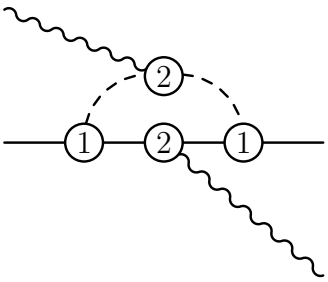

D_{21}, $\mathcal{O}(q^4)$

Three denominators

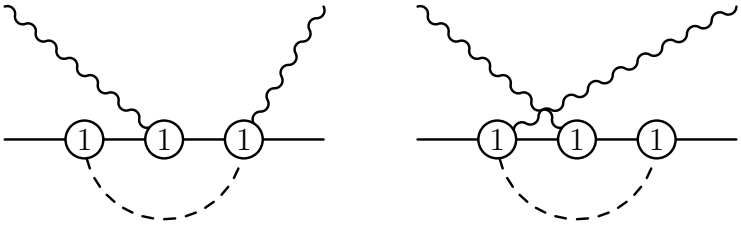

D_{22}, $\mathcal{O}(q^3)$

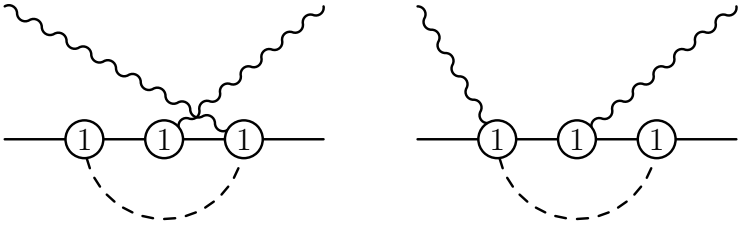

D_{23}, $\mathcal{O}(q^3)$

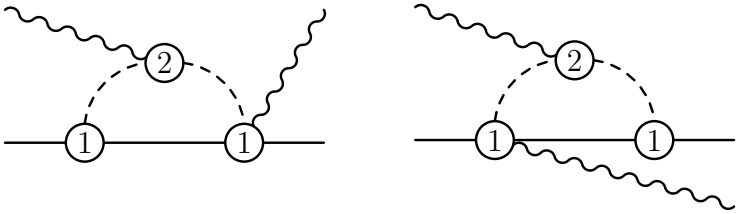

D_{24}, $\mathcal{O}(q^3)$

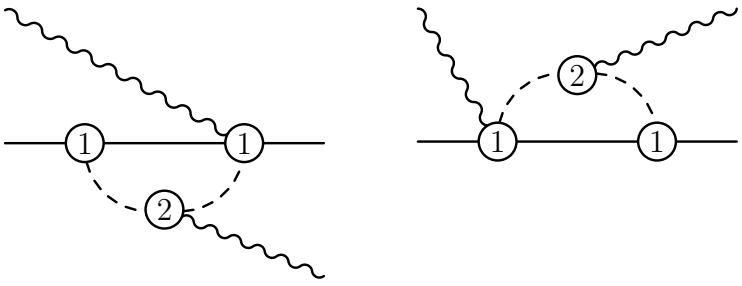

D_{25}, $\mathcal{O}(q^3)$

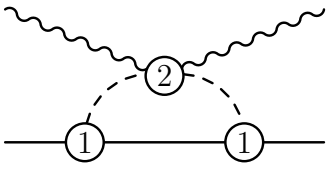

D_{26}, $\mathcal{O}(q^3)$

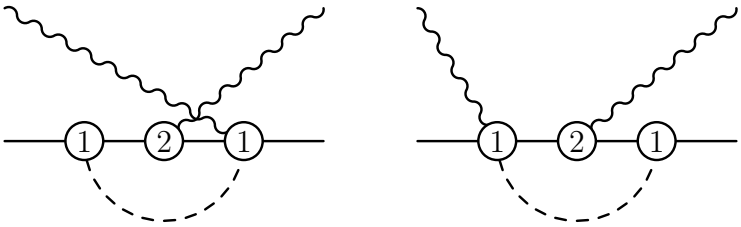

D_{27}, $\mathcal{O}(q^4)$

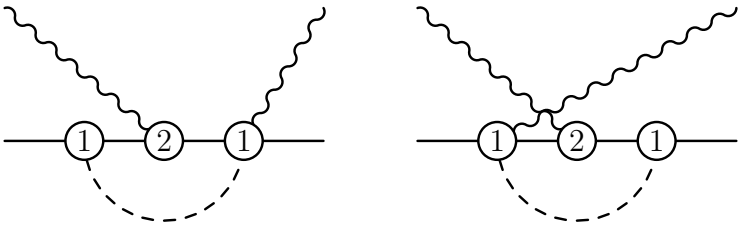

D_{28}, $\mathcal{O}(q^4)$

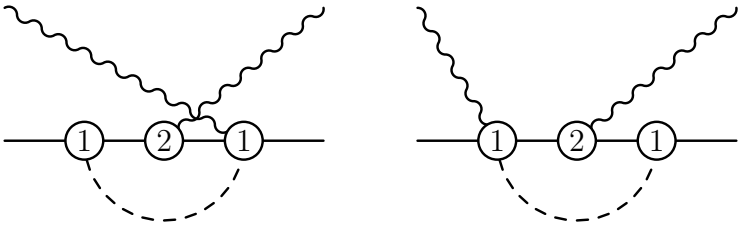

D_{29}, $\mathcal{O}(q^4)$

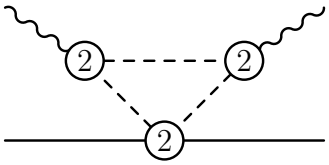

D_{30}, $\mathcal{O}(q^4)$

Form factor type diagrams

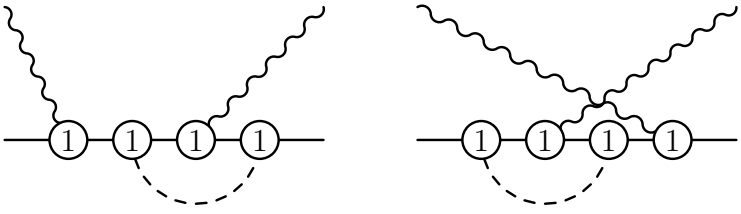

D_{31}, $\mathcal{O}(q^3)$

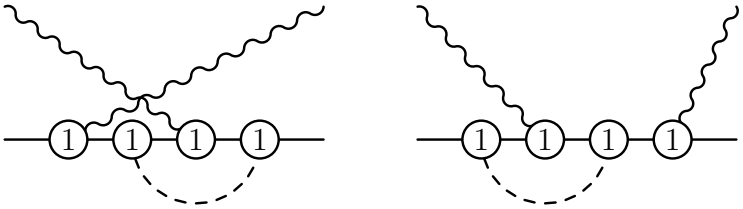

D_{32}, $\mathcal{O}(q^3)$

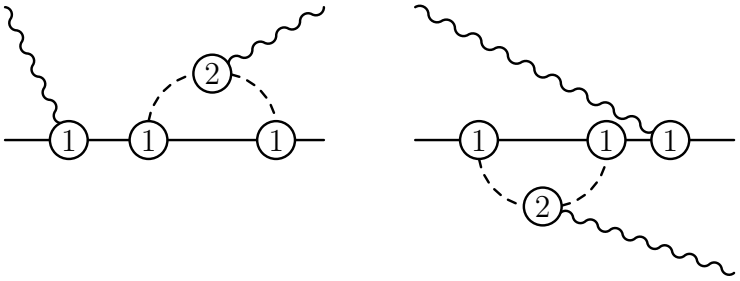

D_{33}, $\mathcal{O}(q^3)$

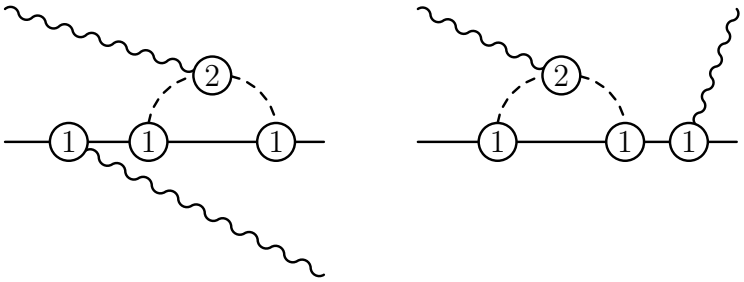

D_{34}, $\mathcal{O}(q^3)$

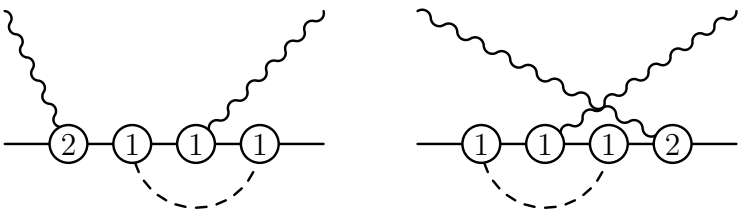

D_{35}, $\mathcal{O}(q^4)$

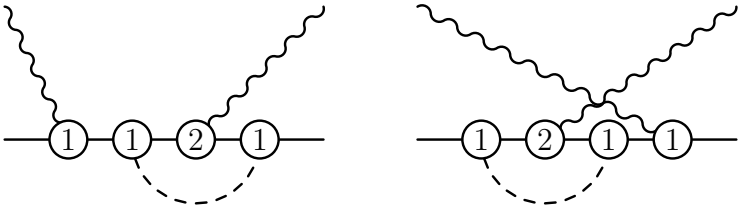

D_{36}, $\mathcal{O}(q^4)$

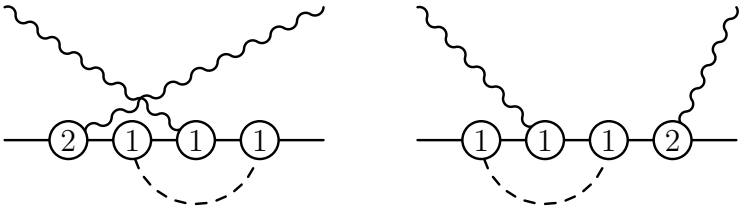

D_{37}, $\mathcal{O}(q^4)$

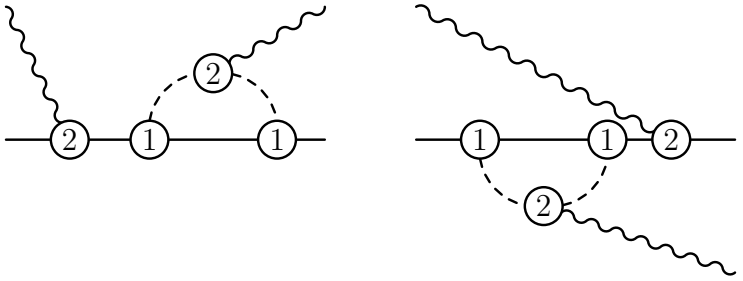

D_{38}, $\mathcal{O}(q^4)$

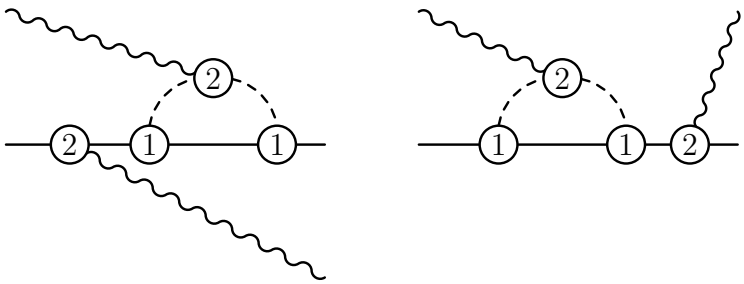

D_{39}, $\mathcal{O}(q^4)$

Two denominators

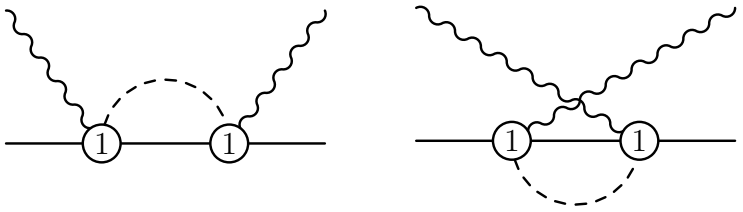

D_{40}, $\mathcal{O}(q^3)$

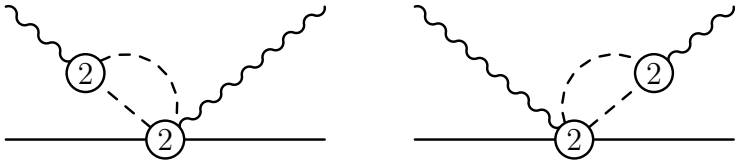

D^*_{41}, $\mathcal{O}(q^4)$ D^*_{42}, $\mathcal{O}(q^4)$

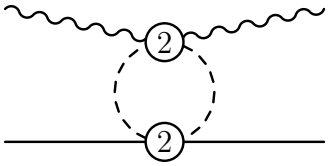

D^*_{43}, $\mathcal{O}(q^4)$

Form factor type diagrams

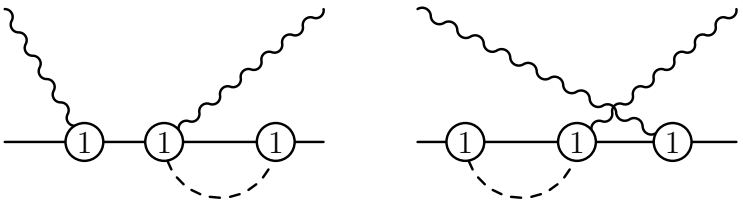

D_{44}, $\mathcal{O}(q^3)$

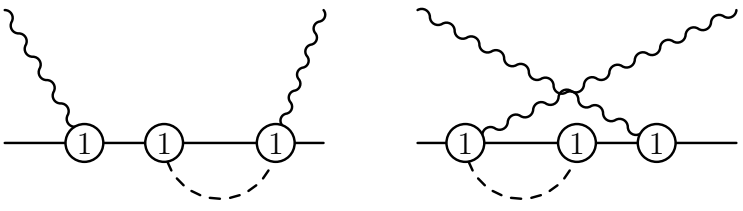

D_{45}, $\mathcal{O}(q^3)$

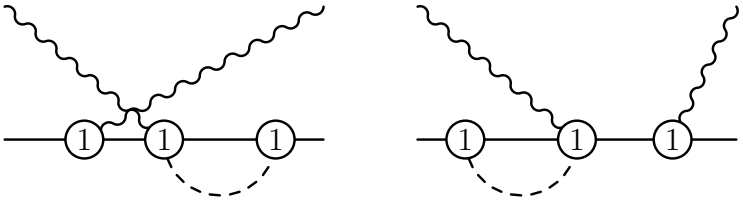

D_{46}, $\mathcal{O}(q^3)$

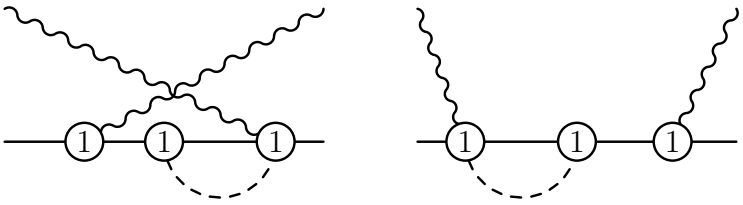

D_{47}, $\mathcal{O}(q^3)$

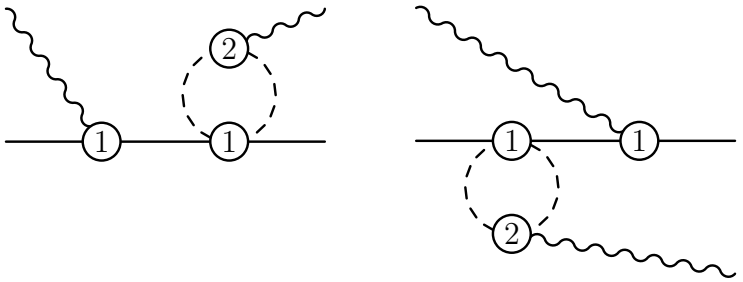

D^*_{48}, $\mathcal{O}(q^3)$

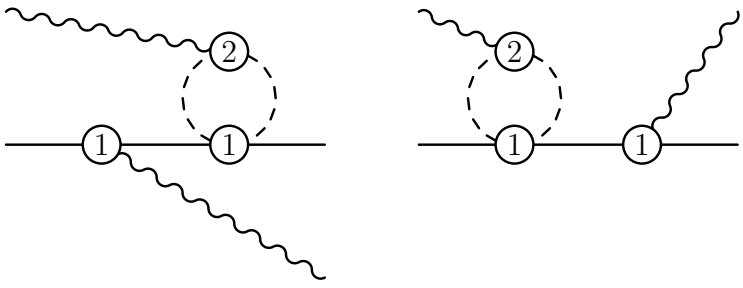

D^*_{49}, $\mathcal{O}(q^3)$

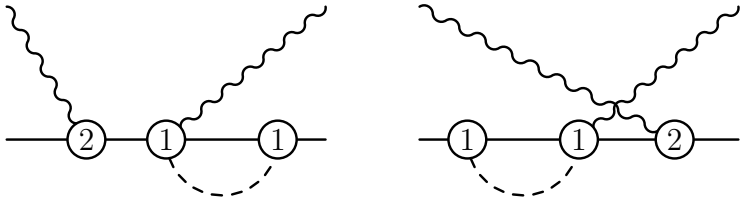

D_{50}, $\mathcal{O}(q^4)$

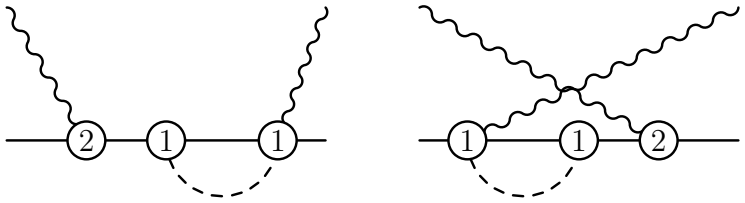

D_{51}, $\mathcal{O}(q^4)$

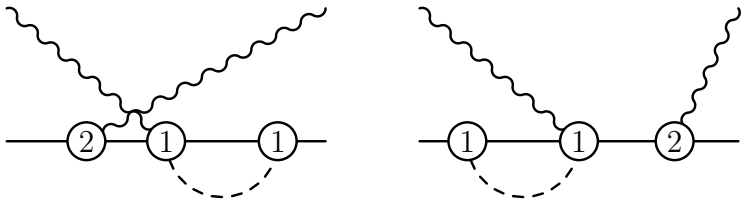

D_{52}, $\mathcal{O}(q^4)$

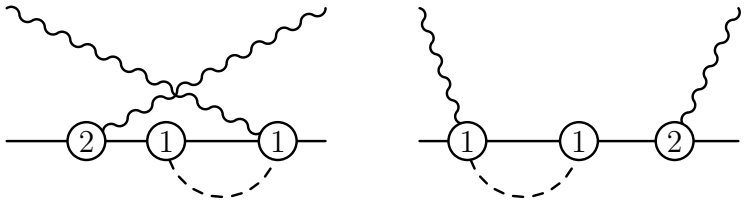

D_{53}, $\mathcal{O}(q^4)$

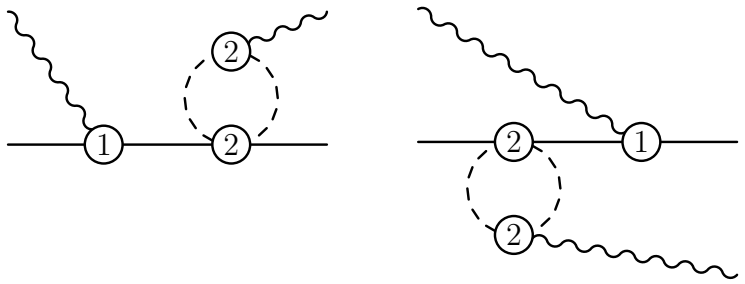

D^*_{54}, $\mathcal{O}(q^4)$

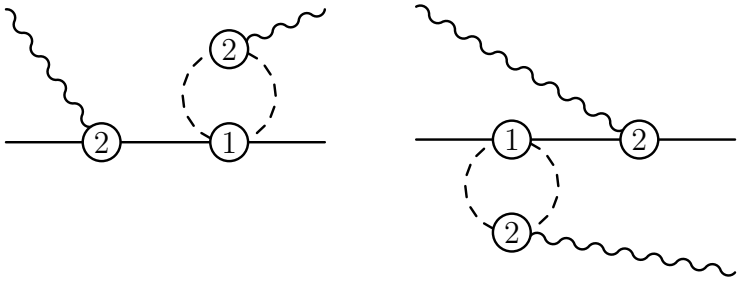

D^*_{55}, $\mathcal{O}(q^4)$

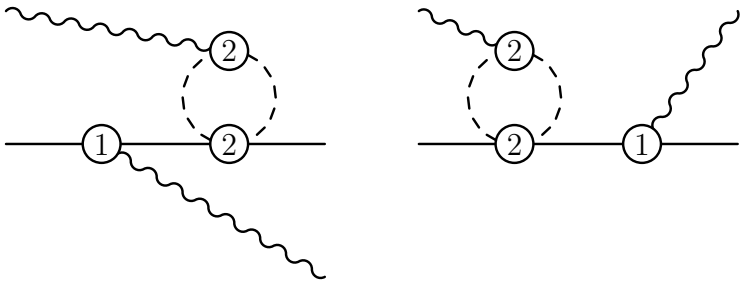

D^*_{56}, $\mathcal{O}(q^4)$

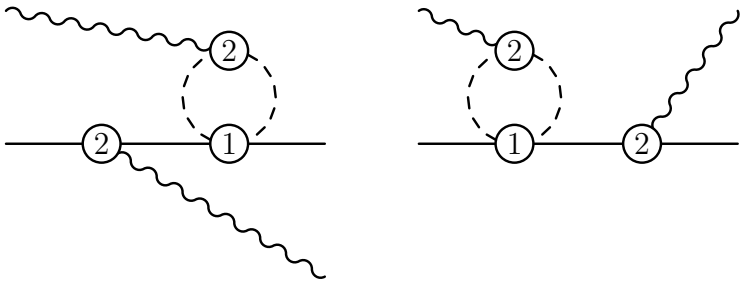

D^*_{57}, $\mathcal{O}(q^4)$

One denominator

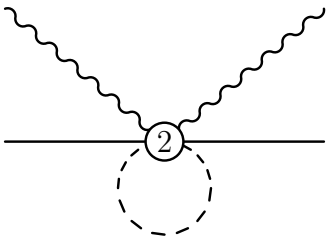

D^*_{58}, $\mathcal{O}(q^4)$

Form factor type

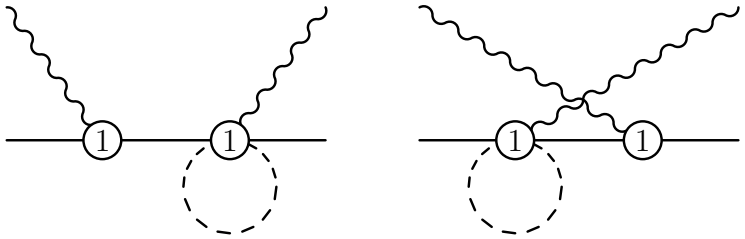

D^*_{59}, $\mathcal{O}(q^3)$

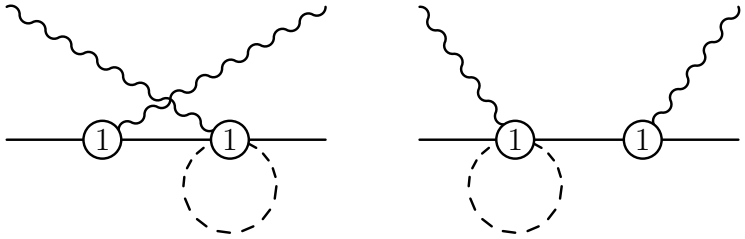

D^*_{60}, $\mathcal{O}(q^3)$

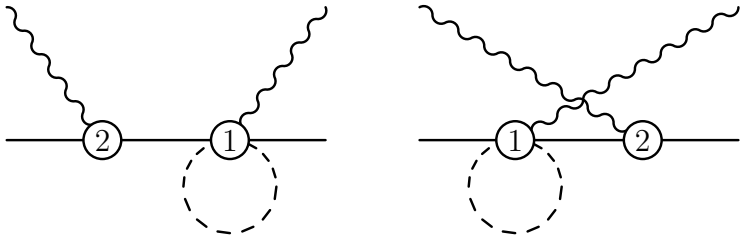

D^*_{61}, $\mathcal{O}(q^4)$

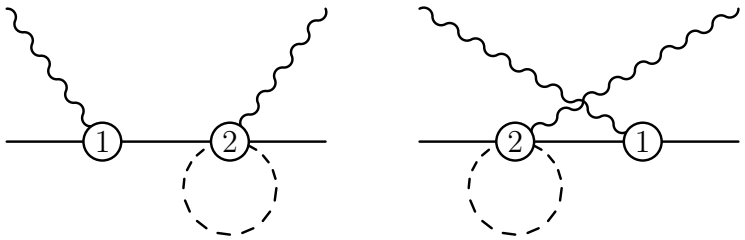

D^*_{62}, $\mathcal{O}(q^4)$

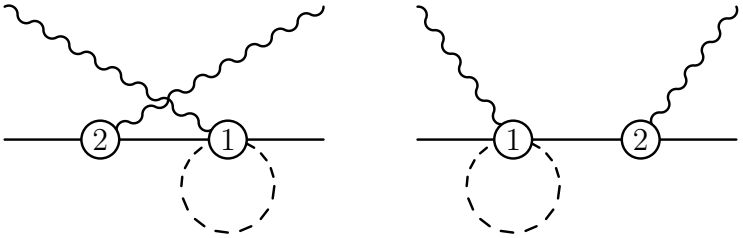

D^*_{63}, $\mathcal{O}(q^4)$

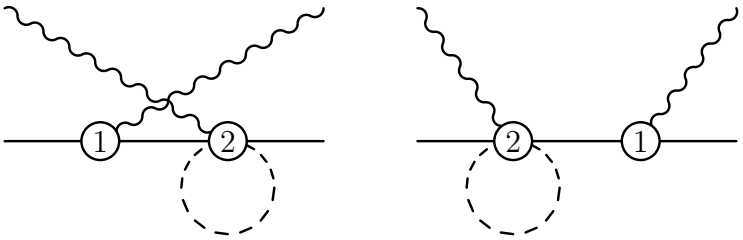

D^*_{64}, $\mathcal{O}(q^4)$

Self energy type diagrams

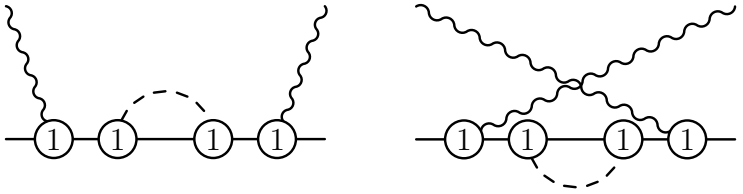

D_{65}, $\mathcal{O}(q^3)$

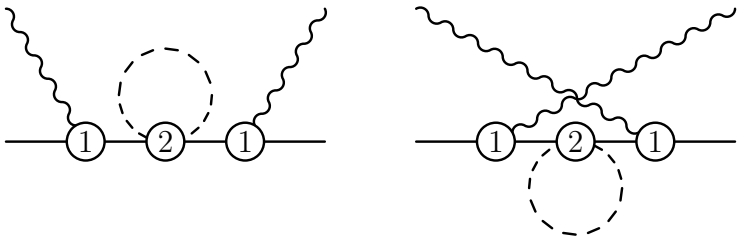

D^*_{66}, $\mathcal{O}(q^4)$

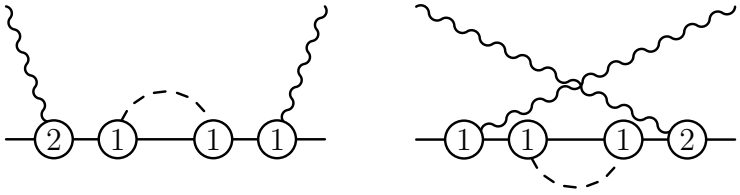

D_{67}, $\mathcal{O}(q^4)$

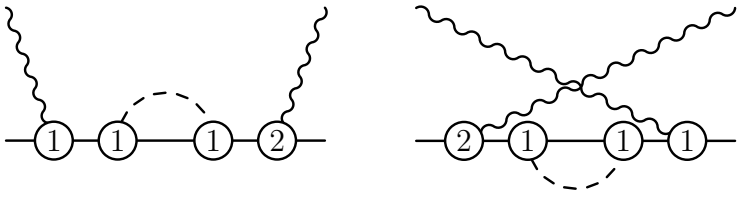

D_{68}, $\mathcal{O}(q^4)$

Bibliography

[Bab+ 98] D. Babusci, G. Giordano, A. I. L'vov, G. Matone, and A. M. Nathan, *Low-energy Compton scattering of polarized photons on polarized nucleons*, Phys. Rev. **C58** (1998), 1013–1041.

[Bal 60] A.M. Baldin, *Polarizability of Nucleons* , Nucl. Phys. **18** (1960), 310.

[Bar+ 01] P. S. Baranov, A. I. Lvov, V. A. Petrunkin, and L. N. Shtarkov, *Experimental status of the electric and magnetic polarizabilities of a proton*, Phys. Part. Nucl. **32** (2001), 376–394.

[BD 64] J. D. Bjorken and S. D. Drell, *Relativistic quantum mechanics*, vol. 1, McGraw-Hill Book Company, New York, 1964.

[BD 02] C. Bauer and H. S. Do, *One-loop integrals with XLOOPS-GiNaC*, Comput. Phys. Commun. **144** (2002), 154–168.

[Bea+ 03] S. R. Beane, M. Malheiro, J. A. McGovern, D. R. Phillips, and U. van Kolck, *Nucleon polarizabilities from low-energy Compton scattering*, Phys. Lett. **B567** (2003), 200–206.

[Ber+ 92] Veronique Bernard, Norbert Kaiser, Joachim Kambor, and Ulf G. Meißner, *Chiral structure of the nucleon*, Nucl. Phys. **B388** (1992), 315–345.

[Ber+ 93] Veronique Bernard, Norbert Kaiser, Armin Schmidt, and Ulf G. Meißner, *Consistent calculation of the nucleon electromagnetic polarizabilities in chiral perturbation theory beyond next- to-leading order*, Phys. Lett. **B319** (1993), 269–275.

[BFK 00] Christian W. Bauer, Alexander Frink, and Richard Kreckel, *Introduction to the GiNaC Framework for Symbolic Computation within the C++ Programming Language*.

[BHM 03] Veronique Bernard, Thomas R. Hemmert, and Ulf-G. Meißner, *Spin structure of the nucleon at low energies*, Phys. Rev. **D67** (2003), 076008.

[BKM 95] V. Bernard, Norbert Kaiser, and Ulf-G. Meißner, *Chiral dynamics in nucleons and nuclei*, Int. J. Mod. Phys. **E4** (1995), 193–346.

[BL 99] Thomas Becher and H. Leutwyler, *Baryon chiral perturbation theory in manifestly Lorentz invariant form*, Eur. Phys. J. **C9** (1999), 643–671.

[BM 00] Paul Buettiker and Ulf-G. Meissner, *Pion nucleon scattering inside the Mandelstam triangle*, Nucl. Phys. **A668** (2000), 97–112.

[Bou+ 06] P. Bourgeois et al., *Measurements of the generalized electric and magnetic polarizabilities of the proton at low Q**2 using the VCS reaction*, Phys. Rev. Lett. **97** (2006), 212001.

[BT 68] William A. Bardeen and W. K. Tung, *Invariant amplitudes for photon processes*, Phys. Rev. **173** (1968), 1423–1433.

[Cal+ 69] Jr. Callan, Curtis G., Sidney R. Coleman, J. Wess, and Bruno Zumino, *Structure of phenomenological Lagrangians. 2*, Phys. Rev. **177** (1969), 2247–2250.

[CWZ 69] Sidney R. Coleman, J. Wess, and Bruno Zumino, *Structure of phenomenological Lagrangians. 1*, Phys. Rev. **177** (1969), 2239–2247.

[Dav 91] Andrei I. Davydychev, *A Simple formula for reducing Feynman diagrams to scalar integrals*, Phys. Lett. **B263** (1991), 107–111.

[DD 06] Ansgar Denner and S. Dittmaier, *Reduction schemes for one-loop tensor integrals*, Nucl. Phys. **B734** (2006), 62–115.

[DH 66] S. D. Drell and Anthony C. Hearn, *Exact Sum Rule for Nucleon Magnetic Moments*, Phys. Rev. Lett. **16** (1966), 908–911.

[DKT 07] D. Drechsel, S. S. Kamalov, and L. Tiator, *Unitary Isobar Model - MAID2007*, Eur. Phys. J. **A34** (2007), 69–97.

[DPV 03] D. Drechsel, B. Pasquini, and M. Vanderhaeghen, *Dispersion relations in real and virtual Compton scattering*, Phys. Rept. **378** (2003), 99–205.

[DR 84] D. Drechsel and A. Russo, *Nucleon structure effects in photon scattering by nuclei*, Phys. Lett. **B137** (1984), 294–298.

[Dre+ 97] D. Drechsel, G. Knöchlein, A. Metz, and S. Scherer, *Generalized polarizabilities and the spin-averaged amplitude in virtual Compton scattering off the nucleon*, Phys. Rev. **C55** (1997), 424–430.

[Dre+ 98] D. Drechsel, G. Knöchlein, A. Yu. Korchin, A. Metz, and S. Scherer, *Structure analysis of the virtual Compton scattering amplitude at low energies*, Phys. Rev. **C57** (1998), 941–952.

[DS 98] Ganesh Devaraj and Robin G. Stuart, *Reduction of one-loop tensor form-factors to scalar integrals: A general scheme*, Nucl. Phys. **B519** (1998), 483–513.

[DT 92] D. Drechsel and L. Tiator, *Threshold pion photoproduction on nucleons*, J. Phys. **G18** (1992), 449–497.

[DW 07] Dieter Drechsel and Thomas Walcher, *Hadron structure at low Q^2*, hep-ph/0711.3396 (2007).

[Eck 95] G. Ecker, *Chiral perturbation theory*, Prog. Part. Nucl. Phys. **35** (1995), 1–80.

[EM 96] G. Ecker and M. Mojzis, *Low-energy expansion of the pion - nucleon Lagrangian*, Phys. Lett. **B365** (1996), 312–318.

[ET 98] Paul J. Ellis and Hua-Bin Tang, *Pion nucleon scattering in a new approach to chiral perturbation theory*, Phys. Rev. **C57** (1998), 3356–3375.

[Fed+ 91] F. J. Federspiel et al., *The Proton Compton effect: A Measurement of the electric and magnetic polarizabilities of the proton*, Phys. Rev. Lett. **67** (1991), 1511–1514.

[Fer+ 03] Andrea Ferroglia, Massimo Passera, Giampiero Passarino, and Sandro Uccirati, *All-purpose numerical evaluation of one-loop multi-leg Feynman diagrams*, Nucl. Phys. **B650** (2003), 162–228.

[Fet+ 00] Nadia Fettes, Ulf-G. Meißner, Martin Mojzis, and Sven Steininger, *The chiral effective pion nucleon Lagrangian of order p^4*, Ann. Phys. **283** (2000), 273–302.

[FMS 98] Nadia Fettes, Ulf-G. Meißner, and Sven Steininger, *Pion nucleon scattering in chiral perturbation theory. I: Isospin-symmetric case*, Nucl. Phys. **A640** (1998), 199–234.

[Fra 55] E. S. Fradkin, *Concerning some general relations of quantum electrodynamics*, Zh. Eksp. Teor. Fiz. **29** (1955), 258–261.

[FS 33] R. Frisch and O. Stern, *Über die magnetische Ablenkung von Wasserstoffmolekülen und das magnetische Moment des Protons. I*, Z. Phys. **85** (1933), no. 1, 4–16.

[FS 98] H. W. Fearing and S. Scherer, *Virtual Compton scattering off spin-zero particles at low energies*, Few Body Syst. **23** (1998), 111–126.

[Fuc+ 03] T. Fuchs, J. Gegelia, G. Japaridze, and S. Scherer, *Renormalization of relativistic baryon chiral perturbation theory and power counting*, Phys. Rev. **D68** (2003), 056005.

[Ger 66] S. B. Gerasimov, *A Sum rule for magnetic moments and the damping of the nucleon magnetic moment in nuclei*, Sov. J. Nucl. Phys. **2** (1966), 430–433.

[GHM 00] George C. Gellas, Thomas R. Hemmert, and Ulf-G. Meißner, *Complete one-loop analysis of the nucleon's spin polarizabilities*, Phys. Rev. Lett. **85** (2000), 14–17.

[GJ 99] J. Gegelia and G. Japaridze, *Matching heavy particle approach to relativistic theory*, Phys. Rev. **D60** (1999), 114038.

[GL 84] J. Gasser and H. Leutwyler, *Chiral Perturbation Theory to One Loop*, Ann. Phys. **158** (1984), 142.

[GL 85] J. Gasser and H. Leutwyler, *Chiral Perturbation Theory: Expansions in the Mass of the Strange Quark*, Nucl. Phys. **B250** (1985), 465.

[GLT 95] P. A. M. Guichon, G. Q. Liu, and Anthony William Thomas, *Virtual Compton scattering and generalized polarizabilities of the proton*, Nucl. Phys. **A591** (1995), 606–638.

[GMG 54] Murray Gell-Mann and M. L. Goldberger, *Scattering of low-energy photons by particles of spin 1/2*, Phys. Rev. **96** (1954), 1433–1438.

[GMGT 54] Murray Gell-Mann, M. L. Goldberger, and Walter E. Thirring, *Use of causality conditions in quantum theory*, Phys. Rev. **95** (1954), 1612–1627.

[GMN 64] Murray Gell-Mann and Yuval Neemam, *The eightfold way: a review with a collection of reprints*, Benjamin, New York, 1964.

[Goi+ 01] J. L. Goity, D. Lehmann, G. Prezeau, and J. Saez, *Regularization for effective field theory with two heavy particles*, Phys. Lett. **B504** (2001), 21–27.

[GSS 88] J. Gasser, M. E. Sainio, and A. Svarc, *Nucleons with Chiral Loops*, Nucl. Phys. **B307** (1988), 779.

[GV 98] P. A. M. Guichon and M. Vanderhaeghen, *Virtual Compton scattering off the nucleon*, Prog. Part. Nucl. Phys. **41** (1998), 125–190.

[GW 73] D. J. Gross and Frank Wilczek, *Ultraviolet behavior of non-abelian gauge theories*, Phys. Rev. Lett. **30** (1973), 1343–1346.

[Hah 01] Thomas Hahn, *Generating Feynman diagrams and amplitudes with FeynArts 3*, Comput. Phys. Commun. **140** (2001), 418–431.

[HBY 58] R. Hofstadter, F. Bumiller, and M. R. Yearian, *Electromagnetic structure of the proton and neutron*, Rev. Mod. Phys. **30** (1958), no. 2, 482–497.

[Hem+ 97a] Thomas R. Hemmert, Barry R. Holstein, Germar Knöchlein, and Stefan Scherer, *Generalized polarizabilities and the chiral structure of the nucleon*, Phys. Rev. Lett. **79** (1997), 22–25.

[Hem+ 97b] Thomas R. Hemmert, Barry R. Holstein, Germar Knöchlein, and Stefan Scherer, *Virtual Compton scattering off the nucleon in chiral perturbation theory*, Phys. Rev. **D55** (1997), 2630–2643.

[Hem+ 98] Thomas R. Hemmert, Barry R. Holstein, Joachim Kambor, and Germar Knöchlein, *Compton scattering and the spin structure of the nucleon at low energies*, Phys. Rev. **D57** (1998), 5746–5754.

[Hem+ 00] Thomas R. Hemmert, Barry R. Holstein, Germar Knöchlein, and Dieter Drechsel, *Generalized polarizabilities of the nucleon in chiral effective theories*, Phys. Rev. **D62** (2000), 014013.

[Hol+ 00] Barry R. Holstein, D. Drechsel, B. Pasquini, and M. Vanderhaeghen, *Higher order polarizabilities of the proton*, Phys. Rev. **C61** (2000), 034316.

[HPV 99] T. Hahn and M. Perez-Victoria, *Automatized one-loop calculations in four and D dimensions*, Comput. Phys. Commun. **118** (1999), 153–165.

[JM 91] Elizabeth Ellen Jenkins and Aneesh V. Manohar, *Chiral corrections to the baryon axial currents*, Phys. Lett. **B259** (1991), 353–358.

[KBD 90] J. Kublbeck, M. Bohm, and Ansgar Denner, *FeynArts: Computer algebraic generation of Feynman graphs and amplitudes* , Comput. Phys. Commun. **60** (1990), 165–180.

[KPV 04] Chung-Wen Kao, Barbara Pasquini, and Marc Vanderhaeghen, *New predictions for generalized spin polarizabilities from heavy baryon chiral perturbation theory*, Phys. Rev. **D70** (2004), 114004.

[KV 02] Chung Wen Kao and Marc Vanderhaeghen, *Generalized spin polarizabilities of the nucleon in heavy baryon chiral perturbation theory at next-to-leading order*, Phys. Rev. Lett. **89** (2002), 272002.

[Leh 07] Björn C. Lehnhart, *Elektromagnetische Pionproduktion in manifest Lorentz-invarianter baryonischer chiraler Störungstheorie*, Ph.D. thesis, http://archimed.uni-mainz.de (2007).

[Leo+ 01] V. Olmos de Leon et al., *Low-energy Compton scattering and the polarizabilities of the proton*, Eur. Phys. J. **A10** (2001), 207–215.

[Low 54] F. E. Low, *Scattering of light of very low frequency by systems of spin 1/2*, Phys. Rev. **96** (1954), 1428–1432.

[LR 06] Alejandro Lorca and Tord Riemann, *An integrated tool for loop calculations: aITALC*, Comput. Phys. Commun. **174** (2006), 71–82.

[LSZ 55] H. Lehmann, K. Symanzik, and W. Zimmermann, *On the formulation of quantized field theories*, Nuovo Cim. **1** (1955), 205–225.

[L'v+ 01] A. I. L'vov, S. Scherer, B. Pasquini, C. Unkmeir, and D. Drechsel, *Generalized dipole polarizabilities and the spatial structure of hadrons*, Phys. Rev. **C64** (2001), 015203.

[Mac+ 95] B. E. MacGibbon et al., *Measurement of the electric and magnetic polarizabilities of the proton*, Phys. Rev. **C52** (1995), 2097–2109.

[MBD 91] R. Mertig, M. Bohm, and Ansgar Denner, *FeynCalc: Computer algebraic calculation of Feynman amplitudes*, Comput. Phys. Commun. **64** (1991), 345–359.

[MD 96] A. Metz and D. Drechsel, *Generalized polarizabilities of the nucleon studied in the linear sigma model*, Z. Phys. **A356** (1996), 351–357.

[Mei 06] Ulf-G. Meißner, *Quark mass dependence of baryon properties*, PoS **LAT2005** (2006), 009.

[Nog 93] P. Nogueira, *Automatic Feynman graph generation*, J. Comput. Phys. **105** (1993), 279–289.

[OV 90] G. J. van Oldenborgh and J. A. M. Vermaseren, *New Algorithms for One Loop Integrals*, Z. Phys. **C46** (1990), 425–438.

[Pas+ 00] B. Pasquini, D. Drechsel, M. Gorchtein, A. Metz, and M. Vanderhaeghen, *Dispersion relation formalism for virtual Compton scattering and the generalized polarizabilities of the nucleon*, Phys. Rev. **C62** (2000), 052201.

[Pas+ 01] B. Pasquini, M. Gorchtein, D. Drechsel, A. Metz, and M. Vanderhaeghen, *Dispersion relation formalism for virtual Compton scattering off the proton*, Eur. Phys. J. **A11** (2001), 185–208.

[Pas 05] Barbara Pasquini, *Compton scattering observables*, private communication (2005).

[Pol 73] H. David Politzer, *Reliable perturbative results for strong interactions?*, Phys. Rev. Lett. **30** (1973), 1346–1349.

[PV 79] G. Passarino and M. J. G. Veltman, *One Loop Corrections for e+ e- Annihilation Into mu+ mu- in the Weinberg Model*, Nucl. Phys. **B160** (1979), 151.

[Rag 93] S. Ragusa, *Third order spin polarizabilities of the nucleon*, Phys. Rev. **D47** (1993), 3757–3767.

[Rag 94] S. Ragusa, *Third order spin polarizabilities of the nucleon. 2*, Phys. Rev. **D49** (1994), 3157–3159.

[Roc+ 00] J. Roche et al., *The first determination of generalized polarizabilities of the proton by a virtual Compton scattering experiment*, Phys. Rev. Lett. **85** (2000), 708.

[Sch+ 84] A. Schafer, R. Muller, D. Vasak, and W. Greiner, *Electric and magnetic polarizability of the nucleon in the MIT bag model* , Phys. Lett. **B143** (1984), 323–325.

[Sch 03] Stefan Scherer, *Introduction to chiral perturbation theory*, Adv. Nucl. Phys. **27** (2003), 277.

[SGS 04] Matthias R. Schindler, Jambul Gegelia, and Stefan Scherer, *Infrared regularization of baryon chiral perturbation theory reformulated*, Phys. Lett. **B586** (2004), 258–266.

[SGS 05] Matthias R. Schindler, Jambul Gegelia, and Stefan Scherer, *Electromagnetic form factors of the nucleon in chiral perturbation theory including vector mesons*, Eur. Phys. J. **A26** (2005), 1–5.

[Sie 37] A. J. F. Siegert, *Note on the interaction between nuclei and electromagnetic radiation*, Phys. Rev. **52** (1937), 787–789.

[SKK 96] S. Scherer, A. Yu. Korchin, and J. H. Koch, *Virtual Compton scattering off the nucleon at low energies*, Phys. Rev. **C54** (1996), 904–919.

[SM 92] S. Scherer and P. J. Mulders, *Electromagnetic polarizabilities of the nucleon and the Delta in the Skyrme model*, Nucl. Phys. **A549** (1992), 521–536.

[Tak 57] Y. Takahashi, *On the generalized Ward identity*, Nuovo Cim. **6** (1957), 371.

[Tar 75] R. Tarrach, *Invariant Amplitudes for Virtual Compton Scattering Off Polarized Nucleons Free from Kinematical Singularities, Zeros and Constraints*, Nuovo Cim. **A28** (1975), 409.

[TF 00] M. Tentyukov and J. Fleischer, *A Feynman diagram analyser DIANA*, Comput. Phys. Commun. **132** (2000), 124–141.

[Thi 50] Walter E. Thirring, *Radiative corrections in the non-relativistic limit*, Phil. Mag. **41** (1950), 1193–1194.

[Van+ 00] M. Vanderhaeghen et al., *QED radiative corrections to virtual Compton scattering*, Phys. Rev. **C62** (2000), 025501.

[Ver 00] J. A. M. Vermaseren, *New features of FORM, math-ph/0010025.*

[VKMB 00] K. B. Vijaya Kumar, Judith A. McGovern, and Michael C. Birse, *Spin polarisabilities of the nucleon at NLO in the chiral expansion*, Phys. Lett. **B479** (2000), 167–172.

[VW 84] C. Vafa and Edward Witten, *Restrictions on Symmetry Breaking in Vector-Like Gauge Theories*, Nucl. Phys. **B234** (1984), 173.

[War 50] John Clive Ward, *An Identity in Quantum Electrodynamics*, Phys. Rev. **78** (1950), 182.

[Wei 79] Steven Weinberg, *Phenomenological Lagrangians*, Physica **A96** (1979), 327.

[Wit 83] Edward Witten, *Global Aspects of Current Algebra*, Nucl. Phys. **B223** (1983), 422–432.

[WZ 71] J. Wess and B. Zumino, *Consequences of anomalous Ward identities*, Phys. Lett. **B37** (1971), 95.

[Yao+ 06] W. M. Yao et al., *Review of particle physics*, J. Phys. **G33** (2006), 1–1232.

[Zie+ 92] A. Zieger et al., *180-degrees Compton scattering by the proton below the pion threshold*, Phys. Lett. **B278** (1992), 34–38.